PERFORMANCE EVALUATION OF W-BEAM GUARDRAILS ON SLOPED MEDIANS USING NONLINEAR FINITE ELEMENT SIMULATIONS

by

Ryan M. Baker

A thesis submitted to the faculty of
The University of North Carolina at Charlotte
in partial fulfillment of the requirements
for the degree of Master of Science in
Mechanical Engineering

Charlotte

2014

Approved by:

_____
Dr. Howie Fang

_____
Dr. Ronald E. Smelser

_____
Dr. David C. Weggel

ABSTRACT

RYAN M. BAKER. Performance evaluation of W-beam guardrails on sloped medians using nonlinear finite element simulations. (Under the direction of DR. HOWIE FANG)

This thesis presents the research using finite element (FE) modeling and simulations to evaluate the performance of single-faced and double-faced W-beam guardrails for different heights under MASH Test Level 3 (TL-3) impact conditions.

The modeling and simulation work was conducted on single-faced and double-faced W-beam guardrails with 29- and 31-inch rail heights and impacted by a 1996 Dodge Neon and a 2006 Ford F250. For the double-faced W-beam guardrail, the modeling and simulation work also included one with a lowered backside rail. Both single- and double-faced guardrails were evaluated under impacts of both vehicles at an impact speed of 62 mph (100 km/h) and a 25° angle.

The simulation results showed the effects of guardrail heights on the vehicle's post-impact responses such as redirection, snagging, and spin-out. The use of FE simulations was shown to be both effective and efficient because of their inexpensive repeatability and adaptability. Furthermore, the FE simulations were extremely economical compared to conducting physical crash tests and thus recommended for future investigations of other roadside safety research issues.

ACKNOWLEDGEMENTS

I would like to start by thanking my graduate advisor, Dr. Howie Fang, for allowing me the opportunity to work in his research lab during my graduate and undergraduate work. He constantly motivated me to do my best and this thesis would not have come to fruition without his support. I would also like to thank my committee members, Drs. Ronald Smelser and Dave Weggel, for their valuable reviews, comments, and advice on my thesis.

My thanks also go to the North Carolina Department of Transportation (NCDOT) for their financial support to me as a research assistant in NCDOT Project 2014-14. I would also like to thank my research colleagues, Matthew Gutowski, Ning Li, Emre Palta, and Daniil Kuvila, for all the help and advice on modeling and post-processing.

Last, but not least, I would like to thank my family, friends, and especially my loving wife Erin Baker for her unending support and devotion. Without her encouragement to change my career and go back to college, this thesis work would never have been possible, and I will never forget how much that means to me.

TABLE OF CONTENTS

CHAPTER 1: INTRODUCTION 1

1.1 Performance Evaluation of W-beam Guardrails 1

1.2 Finite Element Simulations of Vehicular Crashes 16

CHAPTER 2: CONTACT THEORY AND METHODS 29

2.1 Contact Analysis and Methods 29

2.2 Contact Handling in LS-DYNA 32

CHAPTER 3: FINITE ELEMENT MODELING 36

3.1 FE Models of Testing Vehicles 37

3.2 FE Models of the W-Beam Guardrails 39

3.3 FE Simulation Setup 42

CHAPTER 4: PERFORMANCE EVALUATION OF W-BEAM GUARDRAILS 46

4.1 Single-faced Guardrails 48

4.2 Double-faced Guardrails 60

4.2.1 Front-side Impacts on the Double-faced Guardrail 61

4.2.2 Backside Impacts on the Double-faced Guardrail 71

4.3 Double-faced Guardrails with Lowered Backside Rails 82

4.3.1 Front-side Impacts on the Double-faced Guardrail with Lowered Backside Rails 83

4.3.2 Backside Impacts on the Double-faced Guardrail with Lowered Backside Rails 95

CHAPTER 5: CONCLUSIONS 106

REFERENCES 110

LIST OF TABLES

TABLE 3.1: Categories of simulation work. 37

TABLE 4.1: Exit box dimensions for test vehicles. 48

TABLE 4.2: Simulation results for single-faced guardrails. 49

TABLE 4.3: Simulation results for double-faced guardrails. 60

TABLE 4.4: Simulation results for double-faced guardrails with lowered backside rails. 83

LIST OF FIGURES

FIGURE 1.1: Strong-post W-beam guardrail with wood blockout. 1

FIGURE 2.1: Master and slave surfaces. 30

FIGURE 2.2: Imaginary normal interface springs. 30

FIGURE 2.3: Tied-nodes-to-surface contact. 33

FIGURE 2.4: Automatic-surface-to-surface contact. 33

FIGURE 2.5: Self-contact checking for automatic-single-surface contact. 34

FIGURE 2.6: Shell edge-to-edge contact for automatic-general-interior. 35

FIGURE 3.1: 2.5H:1V sloped median. 36

FIGURE 3.2: FE models of the two vehicles used in crash simulations. 38

FIGURE 3.3: The FE models for different splice locations. 40

FIGURE 3.4: The FE models for double-faced guardrails. 41

FIGURE 3.5: The full FE model for single-faced guardrail. 42

FIGURE 3.6: The full FE model for double-faced guardrail. 42

FIGURE 3.7: FE model for single-faced front-side impact. 43

FIGURE 3.8: FE model for double-faced front-side impact. 43

FIGURE 3.9: FE model for double-faced backside impact. 44

FIGURE 3.10: FE model for double-faced, lowered backside rail, front-side impact. 44

FIGURE 3.11: FE model for double-faced, lowered backside rail, backside impact. 45

FIGURE 4.1: Definition of yaw, pitch, and roll angles. 47

FIGURE 4.2: Exit Box criterion in MASH. 48

FIGURE 4.3: Displacement path and exit box for Neon impacting 29-inch single-faced guardrail. 50

FIGURE 4.4: Yaw, pitch, and roll angles for Neon impacting 29-inch single-faced guardrail 50

FIGURE 4.5: Maximum deflection of W-beam for Neon impacting 29-inch single-faced guardrail. 51

FIGURE 4.6: Transverse displacements and speeds for Neon impacting 29-inch single-faced guardrail. 51

FIGURE 4.7: Displacement path and exit box for F250 impacting 29-inch single-faced guardrail. 52

FIGURE 4.8: Yaw, pitch, and roll angles for F250 impacting 29-inch single-faced guardrail. 53

FIGURE 4.9: Maximum deflection of W-beam for F250 impacting 29-inch single-faced guardrail. 54

FIGURE 4.10: Transverse displacements and speeds for F250 impacting 29-inch single-faced guardrail. 54

FIGURE 4.11: Displacement path and exit box for Neon impacting 31-inch single-faced guardrail. 55

FIGURE 4.12: Yaw, pitch, and roll angles for Neon impacting 31-inch single-faced guardrail. 55

FIGURE 4.13: Maximum deflection of W-beam for Neon impacting 31-inch single-faced guardrail. 56

FIGURE 4.14: Transverse displacements and speeds for Neon impacting 31-inch single-faced guardrail. 57

FIGURE 4.15: Displacement path and exit box for F250 impacting 31-inch single-faced guardrail. 58

FIGURE 4.16: Yaw, pitch, and roll angles for F250 impacting 31-inch single-faced guardrail. 58

FIGURE 4.17: Maximum deflection of W-beam for F250 impacting 31-inch single-faced guardrail. 59

FIGURE 4.18: Transverse displacements and speeds for F250 impacting 31-inch single-faced guardrail. 59

FIGURE 4.19: Displacement path and exit box for Neon impacting front-side of 29-inch double-faced guardrail. 61

FIGURE 4.20: Yaw, pitch, and roll angles for Neon impacting front-side of 29-inch double-faced guardrail. 62

FIGURE 4.21: Maximum deflection of W-beam for Neon impacting front-side of 29-inch double-faced guardrail. 63

FIGURE 4.22: Transverse displacements and speeds for Neon impacting front-side of 29-inch double-faced guardrail. 63

FIGURE 4.23: Displacement path and exit box for F250 impacting front-side of 29-inch double-faced guardrail. 64

FIGURE 4.24: Yaw, pitch, and roll angles for F250 impacting front-side of 29-inch double-faced guardrail. 64

FIGURE 4.25: Maximum deflection of W-beam for F250 impacting front-side of 29-inch double-faced guardrail. 65

FIGURE 4.26: Transverse displacements and speeds for F250 impacting front-side of 29-inch double-faced guardrail. 65

FIGURE 4.27: Displacement path and exit box for Neon impacting front-side of 31-inch double-faced guardrail. 66

FIGURE 4.28: Yaw, pitch, and roll angles for Neon impacting front-side of 31-inch double-faced guardrail. 67

FIGURE 4.29: Maximum deflection of W-beam for Neon impacting front-side of 31-inch double-faced guardrail. 68

FIGURE 4.30: Transverse displacements and speeds for Neon impacting front-side of 31-inch double-faced guardrail. 68

FIGURE 4.31: Displacement path and exit box for F250 impacting front-side of 31-inch double-faced guardrail. 69

FIGURE 4.32: Yaw, pitch, and roll angles for F250 impacting front-side of 31-inch double-faced guardrail. 70

FIGURE 4.33: Maximum deflection of W-beam for F250 impacting front-side of 31-inch double-faced guardrail. 71

FIGURE 4.34: Transverse displacements and speeds for F250 impacting front-side of 31-inch double-faced guardrail. 71

FIGURE 4.35: Displacement path and exit box for Neon impacting backside of 29-inch double-faced guardrail. 72

FIGURE 4.36: Yaw, pitch, and roll angles for Neon impacting backside of 29-inch double-faced guardrail. 72

FIGURE 4.37: Maximum deflection of W-beam for Neon impacting backside of 29-inch double-faced guardrail. 73

FIGURE 4.38: Transverse displacements and speeds for Neon impacting backside of 29-inch double-faced guardrail. 74

FIGURE 4.39: Displacement path and exit box for F250 impacting backside of 29-inch double-faced guardrail. 75

FIGURE 4.40: Yaw, pitch, and roll angles for F250 impacting backside of 29-inch double-faced guardrail. 75

FIGURE 4.41: Maximum deflection of W-beam for F250 impacting backside of 29-inch double-faced guardrail. 76

FIGURE 4.42: Transverse displacements and speeds for F250 impacting backside of 29-inch double-faced guardrail. 76

FIGURE 4.43: Displacement path and exit box for Neon impacting backside of 31-inch double-faced guardrail. 77

FIGURE 4.44: Yaw, pitch, and roll angles for Neon impacting backside of 31-inch double-faced guardrail. 78

FIGURE 4.45: Maximum deflection of W-beam for Neon impacting backside of 31-inch double-faced guardrail. 79

FIGURE 4.46: Transverse displacements and speeds for Neon impacting backside of 31-inch double-faced guardrail. 79

FIGURE 4.47: Displacement path and exit box for F250 impacting backside of 31-inch double-faced guardrail. 80

FIGURE 4.48: Yaw, pitch, and roll angles for F250 impacting backside of 31-inch double-faced guardrail. 81

FIGURE 4.49: Maximum deflection of W-beam for F250 impacting backside of 31-inch double-faced guardrail. 82

FIGURE 4.50: Transverse displacements and speeds for F250 impacting backside of 31-inch double-faced guardrail. 82

FIGURE 4.51: Displacement path and exit box for Neon impacting front-side of 29-inch double-faced guardrail with lowered backside rail. 84

FIGURE 4.52: Yaw, pitch, and roll angles for Neon impacting front-side of 29-inch double-faced guardrail with lowered backside rail. 85

FIGURE 4.53: Maximum deflection of W-beam for Neon impacting front-side of 29-inch double-faced guardrail with lowered backside rail. 86

FIGURE 4.54: Transverse displacements and speeds for Neon impacting front-side of 29-inch double-faced guardrail with lowered backside rail. 86

FIGURE 4.55: Displacement path and exit box for F250 impacting front-side of 29-inch double-faced guardrail with lowered backside rail. 87

FIGURE 4.56: Yaw, pitch, and roll angles for F250 impacting front-side of 29-inch double-faced guardrail with lowered backside rail. 88

FIGURE 4.57: Maximum deflection of W-beam for F250 impacting front-side of 29-inch double-faced guardrail with lowered backside rail. 89

FIGURE 4.58: Transverse displacements and speeds for F250 impacting front-side of 29-inch double-faced guardrail with lowered backside rail. 89

FIGURE 4.59: Displacement path and exit box for Neon impacting front-side of 31-inch double-faced guardrail with lowered backside rail. 90

FIGURE 4.60: Yaw, pitch, and roll angles for Neon impacting front-side of 31-inch double-faced guardrail with lowered backside rail. 90

FIGURE 4.61: Maximum deflection of W-beam for Neon impacting front-side of 31-inch double-faced guardrail with lowered backside rail. 91

FIGURE 4.62: Transverse displacements and speeds for Neon impacting front-side of 31-inch double-faced guardrail with lowered backside rail. 92

FIGURE 4.63: Displacement path and exit box for F250 impacting front-side of 31-inch double-faced guardrail with lowered backside rail. 93

FIGURE 4.64: Yaw, pitch, and roll angles for F250 impacting front-side of 31-inch double-faced guardrail with lowered backside rail. 93

FIGURE 4.65: Maximum deflection of W-beam for F250 impacting front-side of 31-inch double-faced guardrail with lowered backside rail. 94

FIGURE 4.66: Transverse displacements and speeds for F250 impacting front-side of 31-inch double-faced guardrail with lowered backside rail. 95

FIGURE 4.67: Displacement path and exit box for Neon impacting backside of 29-inch double-faced guardrail with lowered backside rail. 96

FIGURE 4.68: Yaw, pitch, and roll angles for Neon impacting backside of 29-inch double-faced guardrail with lowered backside rail. 96

FIGURE 4.69: Maximum deflection of W-beam for Neon impacting backside of 29-inch double-faced guardrail with lowered backside rail. 97

FIGURE 4.70: Transverse displacements and speeds for Neon impacting backside of 29-inch double-faced guardrail with lowered backside rail. 98

FIGURE 4.71: Displacement path and exit box for F250 impacting backside of 29-inch double-faced guardrail with lowered backside rail. 98

FIGURE 4.72: Yaw, pitch, and roll angles for F250 impacting backside of 29-inch double-faced guardrail with lowered backside rail. 99

FIGURE 4.73: Maximum deflection of W-beam for F250 impacting backside of 29-inch double-faced guardrail with lowered backside rail. 100

FIGURE 4.74: Transverse displacements and speeds for F250 impacting backside of 29-inch double-faced guardrail with lowered backside rail. 100

FIGURE 4.75: Displacement path and exit box for Neon impacting backside of 31-inch double-faced guardrail with lowered backside rail. 101

FIGURE 4.76: Yaw, pitch, and roll angles for Neon impacting backside of 31-inch double-faced guardrail with lowered backside rail. 101

FIGURE 4.77: Maximum deflection of W-beam for Neon impacting backside of 31-inch double-faced guardrail with lowered backside rail. 102

FIGURE 4.78: Transverse displacements and speeds for Neon impacting backside of 31-inch double-faced guardrail with lowered backside rail. 102

FIGURE 4.79: Displacement path and exit box for F250 impacting backside of 31-inch double-faced guardrail with lowered backside rail. 103

FIGURE 4.80: Yaw, pitch, and roll angles for F250 impacting backside of 31-inch double-faced guardrail with lowered backside rail. 104

FIGURE 4.81: Maximum deflection of W-beam for F250 impacting backside of 31-inch double-faced guardrail with lowered backside rail. 105

FIGURE 4.82: Transverse displacements and speeds for F250 impacting backside of 31-inch double-faced guardrail with lowered backside rail. 105

CHAPTER 1: INTRODUCTION

Median barriers have been developed and used on U.S. highways for decades, including concrete barriers, W-beam and Thrie-beam guardrails, and cable barriers. Presently, the strong-post W-beam guardrails, as shown by the example in Figure 1.1 (Mid-Park web1), are the most commonly used barriers across the U.S. This section will provide a comprehensive summary of studies related to W-beam guardrails. The topics cover performance evaluation (in-service and crash testing) and the application of finite element (FE) modeling and simulations for highway safety research.

Figure 1.1: Strong-post W-beam guardrail with wood blockout.

1.1 Performance Evaluation of W-beam Guardrails

In the early 1960s, New York State pioneered the development of weak-post barrier systems through analytical models and full-scale vehicle crash testing. In 1965,

the state's guardrail and median barrier standards were changed to include only weak-post barriers. In the early 1970s, a study by Zweden and Bryden (1977) was conducted to evaluate the field performance of the older strong-post barriers and newly-developed weak-post barriers based on New York State accident data collected from 1967 to 1970. A statistical analysis was performed to compare the performance of the investigated barrier systems based on occupant injury, vehicular response, and after impact maintenance. This study generated a number of significant conclusions on the performance of weak- and strong-post barriers. Although there was no significant difference in fatality rates between the two barrier systems, weak-post barriers exhibited a combined fatality/serious injury rate significantly lower than that for strong-post barriers. The resulting occupant injury appeared to be linked to barrier stiffness since both barrier systems had lower injury severity rates than other stiffer median barriers. With respect to barrier penetrations, the weak-post barriers demonstrated a lower penetration rate than the strong-post barriers, which might be due to the lack of consistency between early strong-post barrier designs. The study also indicated that barrier penetrations on the weak-post systems were typically due to the low rail heights, and that barrier end terminals (i.e., the first and the last 50 feet of the barrier) had higher rates of penetration and serious injury than the midsections. The study also related barrier damage to their stiffness. It was found that stiffer barriers (e.g., strong-post barriers) had less damage or shorter damaged sections than weaker barriers (e.g., weak-post barriers). The study also determined that despite their longer damage lengths, weak-post barriers were on average less expensive to repair than strong-post barriers.

Ross et al. (1984) investigated the impact performance of longitudinal barriers when placed on sloped terrain using both crash tests and the Highway-Vehicle-Object Simulation Model (HVOSM) computer program. In the study, they determined typical conditions to place longitudinal barriers on sloped terrain and evaluated the impact behavior of widely used barrier systems. Guidelines were developed for the selection and placement of barriers on sloped terrain. It was found from the study that W-beam guardrails were more sensitive to the terrain slopes than cable barriers.

In the study conducted by Ross et al. (1993), uniform procedures were developed for evaluating the safety performance of candidate roadside hardware systems, including longitudinal barriers, crash cushions, breakaway supports, truck-mounted attenuators, and work zone traffic control devices. The report from this study, the National Cooperative Highway Research Program (NCHRP) Report 350, was adopted as the standard guideline for evaluating the safety performance of roadside safety devices until it was replaced by the new standard, Manual for Assessing Safety Hardware (MASH), in 2009. The evaluation of devices in NCHRP 350 was facilitated through three main criteria: structural adequacy, occupant risk, and post-impact vehicle trajectory. Structural adequacy referred to how well the device performed its intended task (i.e. a guardrail preventing a vehicle from striking a shielded object). The occupant risk criteria attempted to quantify the probability of severe occupant injury. The post-impact vehicle trajectory was adopted to ensure that the device would not cause subsequent harm (i.e. a vehicle being unsafely redirected back into traffic). The guidelines recognized the infinite number of roadside hardware installations and crash configurations. Therefore, standardized installation configurations and practical high-frequency impact scenarios

were used to provide a basis for comparing the performance of similar devices. A matter of particular note was the multi-service level concept that provided six different test levels (TLs) to allow for more or less stringent performance evaluation (ideally depending on the ultimate usage/placement of the hardware).

Although the NCHRP Report 350 specified six different test levels, the warrants for devices satisfying an individual test level was outside the scope of the document and was left to the judgment of the transportation agency implementing the hardware. Generally speaking, devices tested to the lower test levels, i.e., TL-1 and TL-2, were mostly used on roadways with a smaller traffic volume and lower travel speeds, and devices tested to the higher levels, i.e., TL-3 to TL-6, were typically used on roadways with a larger volume and higher speeds.

In the NCHRP Project 22-14, "Improvement of the Procedures for the Safety Performance Evaluation of Roadside Features," updates were incorporated to the NCHRP Report 350 based on assessments at TL-3 conditions, which was the basic level used for devices on the *National Highway System*. In the report published by Mak and Bligh (2002), the effects of higher impact speeds and additional impact angles were considered for TL-3 conditions. These additional parameters were considered due to the fact that a number of states had changed maximum speed limits on some of their highways to 75 mph (121 km/hour) and not all crashes were occurring at an impact angle of 25° or less. These parameters often caused a concern on the stability of the test vehicle instead of containment capability. The report determined that increasing the impact speed to 68.4 mph (110 km/hour) would have significant effects on many of the existing roadside safety devices. Although some barriers could be modified to accommodate the higher impact

speed with minor modifications, some other barriers would require major changes and yet some barriers might never be able to accommodate the higher impact speed due to other design constraints. Increasing the impact speed could result in a whole new generation of roadside safety hardware. In return, the higher impact speed would only cover an additional 2.8% of the crashes and increase the percentage of covered crashes (i.e., crashes with impact speeds equal to or less than the design test speed) from approximately 90% to 92.7%. The reduction of the impact angle from 25° to 20° created controversial arguments including the possibility for existing W-beam guardrail systems to have difficulty containing vehicles at the higher impact speeds. It was emphasized that the selection of impact conditions was more of a policy decision than a technical issue to be resolved when updating the NCHRP Report 350 guidelines.

In the early 1990s, the Traffic Engineering Branch of the North Carolina Department of Transportation (NCDOT) conducted a study of accidents on North Carolina's interstate highways in which vehicles crossed the median and entered the opposing travel lanes (Lynch et al. 1993). The study analyzed accidents that occurred during the time period from April 1, 1988 through October 31, 1991. The objectives of this study were to identify interstate locations with unusually high cross-median accidents, to determine possible safety improvements, to develop a priority listing of these locations with recommended improvements, and to develop a model for identifying potentially dangerous locations on North Carolina interstate highways. Data collected in the study showed that 751 cross-median crashes took place in North Carolina, resulting in 105 fatalities. These crashes represented three percent of total crashes but 32% of total fatalities on interstate highways during the study period. One of the outcomes of this

study was the recommendation to construct median barriers at 24 sections of interstate highways in North Carolina.

Using data collected from Connecticut, Iowa, and North Carolina from 1997 to 1999, Ray and Weir (2001) performed an in-service performance evaluation of four guardrail systems: the G1 cable guiderail, G2 weak-post W-beam guardrail, and the G4(1S) and G4(1W) strong-post W-beam guardrails. The study particularly focused on estimating the number of unreported collisions and the true distribution of occupant injuries. The collision performance was measured in terms of collision characteristics, occupant injury, and barrier damage. Within the sample size limitations of the data collected in the study, no statistically significant difference was found on the performance of the guardrails in the three states, and there was no difference between the performance of G1 and G2 guardrails and between G1 and G4(1W) guardrails.

Ray et al. (2003) reviewed literature on in-service evaluations and identified previously found effective methods. The in-service performance of common barriers and terminals was examined by collecting data in the following three areas: crash, maintenance, and inventory information. A procedure manual for planning and conducting in-service evaluations of roadside hardware was developed based on the methods used and the lessons learned in the evaluation study. The manual was subsequently used as a guide for an in-service evaluation project performed in Washington State by a different research team and modified based on their experiences and recommendations.

A new median barrier guideline was developed for Texas to assist highway engineers in the evaluation of median barrier needs, with the intention of achieving the

highest practical level of median safety (Miaou et al. 2005; Bligh et al. 2006). In this work, statistical crash models for various types of median-related crashes were developed based on an analysis of crash data in Texas. Using estimates from the frequency and severity models and crash costs used by Texas Department of Transportation, an economic analysis of the median barrier need was performed. Guidelines for installing median barriers on divided, access-controlled freeways were developed as a function of average annual daily traffic and median width. Guidance to assist engineers evaluating median barriers needed on existing highway facilities was also developed based on the mean cross-median crash rate.

Under the guidelines of NCHRP Project 22-9, "Improved Methods for the Cost-Effectiveness Evaluation of Roadside Safety Features," Mak and Sicking (2003) developed the Roadside Safety Analysis Program (RSAP). The main objective of Project 22-9 was to develop an improved cost effective analysis procedure for assessing roadside safety improvements. The RSAP incorporated two integrated programs: the Main Analysis Program, which contained the cost-effectiveness procedure and algorithms, and the User Interface Program, which provided a user friendly environment for data input and review of program results. The cost-effectiveness procedure incorporated in RSAP was based on the concept of incremental benefit/cost analysis. In 2009, NCHRP Project 22-27, "Roadside Safety Analysis Program (RSAP) Update," was started to assist the American Association of State Highway and Transportation Officials (AASHTO) Technical Committee on Roadside Safety to develop the next edition of the AASHTO *Roadside Design Guide*. The objectives of this project were to rewrite the

software, update the manuals, improve the user interface, and update the embedded default data tables of the RSAP (NCHRP 22-27).

Donnell et al. (2002) reviewed the methods used to assess median safety on interstates and expressways in Pennsylvania, upon observations of cross-median collisions (CMCs) on highways where median barriers were not warranted by the Pennsylvania DOT design policy. A critical literature review and assessment of median safety practices for various state DOTs were conducted, and qualitatively assessed median safety practices were used to provide input for quantitative data collection. Negative binomial regression models were used to model CMC frequencies on earth-divided highways. The qualitative results from the study suggested that three-strand cable barriers, strong-post W-beam guardrails, or concrete barriers were recommended as median barriers and were warranted by site conditions. The quantitative results showed that CMCs were rare events and that nearly 15% involved fatalities. Additional findings concluded that CMC rates at earth-divided highways decreased as the median width increased, that CMCs appeared more likely to occur downstream of interchange entrance ramps, and that CMCs were more likely to involve adverse pavement surface conditions (e.g., wet or icy) than other crashes.

In a project funded by the New Jersey DOT, Gabler et al. (2005) evaluated the post-impact performance of two median barrier systems: a three-strand cable median barrier system and a modified thrie-beam median barrier system. FE modeling was adopted as a major means of the investigation. The project also included field investigation of crashes into the subject barriers and a survey of the median barrier experience of other state DOTs. This study concluded that thrie-beam median barrier was

capable of containing and redirecting passenger vehicles, as well as a limited number of heavy vehicles. The thrie-beam median barrier also reduced the incidence of higher severity cross-median collisions but increased the number of less severe collisions.

In a subsequent study also funded by the New Jersey DOT, Gabler and Gabauer (2006) investigated the fatalities and injuries in accidents involving W-beam guardrails on New Jersey highways. The study found that the guardrails generally performed well in vehicular crashes and only accounted for 1.5% of total highway fatalities. This study also found that occupant injuries in guardrail crashes were not a major issue unless the vehicle had a rollover; three-fourths of all occupants exposed to guardrail crashes suffered no injuries. Some of the issues related to the guardrail performance were also identified. For example, the study found that over half of all the fatal collisions with guardrails involved secondary events, i.e., either a second impact or a rollover. It was also found that 14% of all fatal crashes on guardrails resulted in a rollover and that light trucks had a significantly greater chance of vaulting and/or rollover than other vehicles when colliding with the guardrail.

The placement of median barriers on sloped medians imposed a significant challenge to retaining the desired performance as seen on flat terrains. The performance tests specified by NCHRP Report 350 and MASH were all based on flat terrain conditions, though terrain conditions can have a significant effect on the barrier's impact performance (AASHTO 2011). Median slopes can affect the performance of the barrier, because the vehicle may engage the barrier in a significantly different manner than on flat terrain. In NCHRP Project 17-14, "Improved Guidelines for Median Safety," researchers attempted to develop guidelines for using a median barrier and selecting median

widths/slopes (BMI-SG 2004). Unfortunately, the collection of data needed for this project proved to be very expensive and the data limitations hampered the strength of the recommendations. The project results have not been incorporated into practice, but should be very beneficial to future research.

To avoid some of the obstacles that NCHRP Project 17-14 faced, NCHRP Project 22-21 focused on typical cross-section designs for a construction or reconstruction project rather than on the exact cross-section design at a particular point. The typical cross-section designs were determined early in the design process before adjustments were made to account for variations along the alignment (e.g., horizontal and vertical curves, interchanges and intersections, and special drainage requirements). Project 22-21 was started on January 2006 and was completed in April 2011. However, the Midwest Research Institute has yet to release the final report including the research findings (expected fall of 2014). It is anticipated that the final report of Project 22-21 would contain guidance that practitioners can use to evaluate the safety implications of various median cross-section designs, including barrier type and placement guidelines (based on the NCHRP Project 22-22), so that a cost-effective design can be achieved. The NCHRP Project 22-22, "Placement of Traffic Barriers on Roadside and Median Slopes," has been extended to NCHRP Project 22-22(02) "Effectiveness of Traffic Barriers on Non-Level Terrain" to conduct simulation modeling in accordance with the approved plan developed in NCHRP Project 22-22 and verify the results by conducting crash testing. The results of NCHRP Project 22-22(02) are to be incorporated into the final product of NCHRP Project 22-21.

In 2009, MASH was published to supersede the old roadside safety standard, NCHRP Report 350. MASH presents uniform guidelines for crash testing permanent and temporary highway safety features and recommends evaluation criteria to assess test results. MASH does not supersede any guidelines for the design of roadside safety hardware, which are contained within the AASHTO *Roadside Design Guide*. As of January 1, 2011, the Federal Highway Administration (FHWA) has required that all new product designs be tested using MASH test criteria for use on the National Highway System. A few of the significant changes from NCHRP Report 350 to MASH include:

- The weight of the small car test vehicle was increased from 1,800 lbs. (820C) to 2,420 lbs. (1100C)
- The impact angle of the small test vehicle was increased from 20° to 25°
- The weight of the pickup truck test vehicle was increased from 4,400 lbs. (2000P) to 5,000 lbs. (2270P)
- The mass of the single unit truck in TL-4 was increased from 18,000 lbs. (8,000 kg) to 22,000 lbs. (10,000 kg) and the impact speed was increased from 50 mph (80 km/hour) to 56 mph (90 km/hour).

Recently, a study was conducted to analyze the severity of median barrier crashes using five years of data from rural divided highways in North Carolina (Hu and Donnell 2010). The criteria used for the analysis included median barrier type, the barrier's offset distance from the edge of the travel lane, roadway segment characteristics, roadway surface conditions, driver and vehicle characteristics, median barrier placement, and median cross-slope data. The major conclusion of this study was that less severe crash outcomes pertained to those on cable median barriers when compared to concrete barriers

and W-beam guardrails. It was also observed that the barrier's offset distance from the travel lane was associated with a lower probability of severe crashes.

In 2010, Hampton et al. (2010) conducted crash tests and finite element analysis (FEA) on already damaged sections of the G4(1S) W-beam guardrails, which had not previously been conducted. The FEA work will be discussed in depth in the following section. Two crash tests were performed by the MGA Research Corporation for the NCHRP Project 22-23, "Criteria for Restoration of Longitudinal Barriers," to evaluate the performance of guardrails with prescribed rail and post deflections. The first crash test was conducted at 30 mph (48.3 km/hour) with an impact angle of 25° and resulted in a 36-ft (10.97-m) damaged section of barrier with a maximum deflection of 1.21-ft (0.37-m). The second crash test was performed in the damaged location with undesirable results. The barrier provided minimal resistance to the impacting vehicle as it vaulted over the barrier. These results were due to a failed link present in the barrier that separated the post from the rail. The study concluded that a deflection of 0.92-ft (0.279-m) or more on the post and rail would result in vehicle vaulting over the median barrier.

Gabauer et al. (2010) also conducted research on the G4(1S) guardrail performance with minor damage already done to sections. There were five types of damage that were assessed using pendulum impact tests: vertical tear, horizontal tear, splice damage, twisted blockout, and missing blockout. W-beam rupture was observed in tests with vertical tear damage due to the tear causing a stress concentrator and was recommended to be repaired with high priority. There was no evidence of rail rupture near the location of a horizontal tear, but there was an observed splice failure at the higher speed test of 20 mph (32.2 km/hr). The recommendation for a horizontal tear was that tears less than 12

inches in length and .5 inches in width would not significantly affect the performance of the barrier and should be repaired with medium priority. The splice damage was simulated with one of the bolts having lost all bearing capacity and had a performance indistinguishable from the undamaged barrier. The recommended repair priority for a single compromised bolt is medium with a high priority for more than one bolt. A twisted blockout had little to no effect on the performance of the barrier and was recommended to have a low repair priority. The performance of the barrier with a missing blockout was marginal to unacceptable for the higher speed tests with a medium priority for repair. Further investigations with full-scale crashes would help evaluate vehicle trajectory and stability due to the limitations of the pendulum tests.

Ochoa and Ochoa (2011) completed a study to optimize guardrail barriers for rural roadways in the United States, Europe, and some developing countries. In order to optimize the W-beam guardrail, the main methods for identifying failures had to be defined and considered. In the conventional strong-post W-beam guardrails, the relatively high release load varied by approximately 360% and was further compounded by another 40% due to variations in the yield strength of guardrail panels. A physics-based guardrail analysis was performed to determine the solution of optimizing the release load in relation to post section properties. This optimization was accomplished by introducing an improved fastening system that incorporated a separate deformable release member to consistently provide a predefined release load of around 1,700 lbs. (7,565 N) with a maximum variation of 20%. The versatile W-beam guardrail incorporating these improvements was successfully crash tested and accepted by FHWA at NCHRP Report 350 and MASH TL-3 conditions.

In 2011, AASHTO published the new *Roadside Design Guide*, which presented a synthesis of current information and operating practices related to roadside safety. The guide was intended to be used as a resource document from which individual highway agencies could develop standards and policies. It was focused on safety treatments that could minimize the likelihood of serious injuries when a motorist leaves the roadway. The 2011 edition was updated to include hardware systems that had been tested to meet the evaluation criteria contained in NCHRP Report 350. It also included an outline of the most current evaluation criteria contained in MASH.

In 2012, Findley et al. (2012) conducted a statewide structural and safety investigation on the performance of weathered steel beam guardrails (WSBG) in North Carolina. This research was performed at the Institute of Transportation Research and Education at North Carolina State University. This study was prompted when New Hampshire found that the WSBG deteriorates at a much faster rate compared to the galvanized steel guardrail (GSG) in the northeast due to the harsher weather conditions. The study concluded that in all test sites across North Carolina, there were no structural concerns about using WSBG. Additionally, the research suggested a lower percentage of injury collisions associated with WSBG installations than the GSG installations at comparable sites. However, this study used a small sample size, and further investigation would need to be made for a more robust comparison.

Alluri et al. (2012) evaluated the safety performance of the G4(1S) guardrail system installed on both limited and non-limited access facilities in Florida. The effectiveness of the guardrail was measured by the percentage of vehicles prevented from crossing the guardrail during a crash. During the years 2006-2010, there were a total of

7,290 crashes involving the G4(1S) guardrail on limited access facilities and 1,384 on non-limited access facilities. For the limited access facilities, 95.3% of the vehicles were prevented from crossing over the guardrail, which broke down into 97.5% for cars and 91.6% for light trucks (included vans and trucks with four rear tires). For guardrails installed at median and roadside locations, 95.5% of all vehicles were prevented from crossing over at median locations and 94.5% at roadside locations. Medium and heavy trucks were found to have a significantly lower crossover prevention percentage of 78% due to the fact that the safety requirement of the guardrail system was not for these vehicle types. The severity of crossover crashes was found to be higher than that of non-crossover crashes, with over-rides being the most severe cases. Similar findings were observed on the non-limited access facilities that had a higher percentage of preventing vehicular penetrations at median locations than at roadside locations.

Researchers at the Midwest Roadside Safety Facility (MwRSF) performed a study on the safety performance of the Midwest Guardrail System (MGS) with no blockout. This revised design could possibly be used at locations where the required 12-inch blockout would not work well and an alternative was required. They successfully crash tested the non-proprietary design of the MGS with a rail height of 31 inches using a passenger car and a pickup truck under MASH TL-3 conditions (Schrum et al. 2013). The results of this report suggested that the MGS with no blockout could be used on roadways where the width of the blockout was a limiting factor and the standard MGS with blockouts was recommended for other locations.

1.2 Finite Element Simulations of Vehicular Crashes

Mackerle (2003) provided a bibliography that included 271 references published between 1998 and 2002 on crash simulations using FEA and on impact-induced injuries. This bibliography categorized the references into four different topic areas: 1) Crash and impact simulations where occupants were not included; 2) Impact-induced injuries; 3) Human surrogates; and 4) Injury protection. Topics in the first area included crashworthiness of aircrafts and helicopters, automobiles, and vehicle rail structures. The second area of research utilized two major types of models for humans, the crash dummy and real human body models. Research topics in this area were mainly on biomechanics and impact analyses for various human injuries. Topics on human surrogates focused on the development FE models of hybrid and other types of human dummies. These dummy models were used to obtain dynamic responses of the whole human body during impacts, which were difficult to measure experimentally. In the area of injury protection, FEA were utilized to simulate and analyze injury protection systems such as seat belts, air bags, and collapsible structures to reduce serious or fatal injuries. The references included in Mackerle's bibliography were generally useful to the work on FE crash simulations; however, only a few references under injury protection were related to roadside safety.

Most publicly available FE models of vehicles and roadside safety structures were developed at the FHWA National Crash Analysis Center (NCAC) at George Washington University. Since the 1990s, significant efforts have been put on the development of FE models for crash analysis. Most of these models are available as LS-DYNA input files from NCAC's website (NCAC web1). A list of references on these modeling efforts and

the simulation work performed at NCAC is also available from NCAC's website (NCAC web2).

The modeling and simulation efforts from NCAC can be found in several representative works. Marzougui et al. (2000) developed the FE model of an F-shaped portable concrete barrier (PCB) and validated the model with full-scale crash test data. With the proven fidelity and accuracy of the modeling methodology, models for two modified PCB designs were created and used in FE simulations to evaluate their safety performance. A third design was then developed based on the simulation results. In the work by Zaouk et al. (2000a, 2000b), a detailed FE model of a 1996 Plymouth Neon was developed. The three dimensional geometric data of each component was obtained by using a passive digitizing arm and then imported into a preprocessor for mesh generation, part connections, and material properties assignment. Tensile tests were conducted on specimens to obtain the material properties of the various sheet metal components. The body-in-white model was used in the simulation of a frontal impact and the results were compared with test data to evaluate the accuracy and validity of the model.

Kan et al. (2001) developed an integrated FE model that included the vehicular structure, interior components, occupant (Hybrid III dummy), and airbag for crashworthiness evaluation. The integrated model was then used in a case study to demonstrate the potential benefit of the integrated simulation and analysis approach. This approach would further improve the engineering practice with cost savings, while also producing more accurate and consistent analysis results. Marzougui et al. (2004) developed a detailed suspension model and incorporated it into the previously developed FE model of a Chevrolet C2500 pickup truck (Zaouk et al. 1997). Pendulum tests were

conducted at the FHWA Federal Outdoor Impact Laboratory (FOIL) and the test data were compared with simulation results of deformations, displacements, and accelerations at various locations. Crash simulations were performed using the upgraded vehicle model and the results were compared with crash data from previously conducted full-scale tests.

To facilitate the use of FE simulations to evaluate roadside safety structures at higher test levels specified by NCHRP Report 350, Mohan et al. (2007) improved and validated a previously developed model of a 1996 Ford F800 single unit truck. This 18,000-lb (8,172-kg) truck was used as the standard TL-4 vehicle in NCHRP Report 350. Simulations were performed using the improved model and the results were compared with those from a full-scale crash test. The global kinematics and the acceleration time histories of the truck from simulations were found to correlate well with the test data. The research also suggested considering frictions between the tires and barrier and between the tires and ground so as to correlate well on the vehicle's yaw.

In a study by Marzougui et al. (2007), the FE model of a W-beam guardrail was developed and validated using full-scale crash test data. The model was shown to give an accurate representation of the real system based on comparison of the vehicle's roll and yaw angles. Using the validated model, they performed four simulations of a passenger truck impacting the W-beam guardrails with different rail heights. The simulation results showed that the effectiveness of the barrier to redirect a vehicle could be compromised when the rail height was lower than the recommended value.

Researchers from the roadside safety group at Worcester Polytechnic Institute utilized FE models in a number of roadside safety studies. Ray (1996a) analyzed the data from full-scale crash tests and developed a criterion using statistical parameters to assess

the repeatability of a full-scale crash test. The evaluated simulation results were also compared to crash test data. Ray (1996b) reviewed the history of using FEA in roadside safety research and presented the vehicle, occupant, and roadside hardware models that had been developed to date. Ray and Patzner (1997) developed a nonlinear FE model of a modified eccentric loader terminal (MELT) that was common for W-beam guardrails and used it in simulating a full-scale crash test involving a small passenger car. Based on a comparison of simulation results with crash test data, the FE model was recommended to be used in the evaluation of new design alternatives. In the work of Patzner et al. (1999), they examined the effects of post and soil strengths on the overall performance of the MELT terminal system using a nonlinear FE model. A matrix of twelve simulations of particular full-scale crash test scenarios was used to establish the combinations of post and soil strengths from which favorable situation(s) could be identified. This parametric study showed that certain combinations of soil and post strengths could increase the hazardous possibilities of wheel snagging, pocketing, or rail penetration, while other combinations produced more favorable results.

Plaxico et al. (2000) compared the impact performance of two strong-post W-beam guardrails, the G4(2W) and G4(1W). After validating the FE model for the G4(2W) guardrail with data from a full-scale crash test, the FE model of the G4(1W) guardrail was developed. The two guardrails were compared with respect to deflection, vehicle redirection, and occupant risk factors. The two systems were found to perform similarly in collisions and satisfied the requirements of the NCHRP Report 350 for the Test 3-11 conditions. Using LS-DYNA simulations and laboratory experiments, Plaxico et al. (2003) investigated the failure mechanism of the bolted connection of a W-beam rail to a

guardrail post, which could have a significant effect on the performance of a guardrail system. A computationally efficient and accurate FE model of the rail-to-post connection was developed for use in the performance evaluation of guardrail systems using LS-DYNA. Orengo et al. (2003) presented a method to model tire deflation in LS-DYNA simulations along with examples of the use of this improved model. The simulation results showed that deflated tires had significantly different behaviors from those of inflated tires as observed in real world crashes and in full-scale crash tests. A vehicles' kinematics were found to be strongly coupled to the behaviors of deflated tires. Therefore, modeling such behaviors is critical to roadside hardware simulations. In a separate study by Ray et al. (2004), LS-DYNA simulations were used to determine if an extruded aluminum bridge rail would pass the full-scale crash tests for TL-3 and TL-4 conditions of NCHRP Report 350. The simulation results, which were supported by a subsequent AASHTO load and resistance factor design (LRFD) analysis, indicated a high likelihood of passing the crash tests.

FE simulations have also been used by researchers at the Midwest Roadside Safety Facility (MwRSF). Reid (1996) utilized FEA to study the influence of material properties on automobile crash structures and attempted to develop crashworthiness guidelines for design engineers. In one of his later works, Reid (1998) demonstrated through the use of two simple examples, contact definition and damping, how potential modeling issues could easily be overlooked in FE impact simulations. He also suggested ways to check for modeling errors and how to make improvements. In a collaborative work to improve the FE model of a Chevrolet C2500 pickup truck (Reid and Marzougui 2002; Tiso et al. 2002), structural modeling methods were introduced for model improvement through

refining meshes, using more sophisticated material models, adding details to simplified components, and improving connections between components. Suspension modeling, which was critical to the correct vehicle dynamic responses, was also investigated in this collaborative work and a new model was successfully developed with significant improvements.

To educate roadside safety engineers and promote the use of simulations, Reid (2004) summarized ten years of the simulation efforts on the development of new roadside safety accessories performed at the MwRSF. In the work of Reid and Hiser (2004), they studied the friction effects between solid elements and for component connections, as well as their interactions in crash modeling and analysis. In their work on modeling bolted connections that allowed for slippage, Reid and Hiser (2005) investigated two modeling techniques that were based on discrete-spring clamping and stressed clamping using deformable elements. The simulation results for both models compared well with test data, with the stressed clamping model using deformable elements having better accuracy accompanied with a significantly increased computational cost. Hiser and Reid (2005) also investigated improved FE modeling methods for slip base structures, which could have a considerable potential for reducing the amount of crash resistance and thus occupant injury. They developed and evaluated two bolt preloading methods, with one using discrete spring elements and the other using pre-stressed solid elements. Similar to their findings in the work of modeling hook-bolts, they found that the method using solid elements was more accurate than that using discrete spring elements when the impact conditions became more severe. The results showed that the slip base model was acceptable in both end-on impact and length of need impact simulations.

In 2009, Reid et al. (2009) investigated the potential of increasing the suggested flare rates for strong-post W-beams to reduce guardrail installation lengths, which would result in decreased guardrail construction, maintenance costs, and impact frequency. Both computer simulations and full-scale crash tests were used in the evaluation of increased flare rates up to and including 5H:1V. Simulation results indicated that the conventional G4(1S) guardrail modified to incorporate a routed wood blockout could not successfully meet NCHRP Report 350 crash test criteria when installed at any flare rates steeper than the recommended 15H:1V in the *Roadside Design Guide*. Their study also showed that the MGS could meet NCHRP Report 350 impact criteria when installed at a 5H:1V flare rate, yet with greater impact severities observed from the tests than anticipated. The research also indicated that whenever roadside or median slopes are relatively flat (10H:1V or less), increasing the flare rate on guardrail installations became practical and had some major advantages including significantly reducing the guardrail lengths and associated costs. The study, however, did not give any indications of W-beam performance on steeper slopes.

FE simulations were also found in the work of other researchers in roadside safety research. Whitworth et al. (2004) evaluated the crashworthiness of a modified W-beam guardrail using detailed FE models of a guardrail and a Chevrolet C2500 pickup truck. The simulation results were compared and found to be in agreement with crash test data in terms of roll and yaw angles. Simulations were also performed to evaluate the effects of certain guardrail design parameters, such as rail mounting height and routed/non-routed blockouts, on the crashworthiness and safety performance of the system. In the work of Bligh et al. (2004), FEA was utilized to develop new roadside features to address

three roadside safety issues. An alternative design to the popular T6 tubular W-beam bridge rail was developed to address problems with vehicle instability observed in full-scale crash testing. A retrofit connection to Texas DOT's grid-slot portable concrete barrier was developed to limit dynamic barrier deflections to levels that were more practical for work zone deployments. Finally, crashworthy mow strip configurations were developed for use when vegetation controls around guard fence systems were desired to reduce the cost and risk associated with hand mowing.

Computer simulations were also used by international researchers on roadside safety research. Using LS-DYNA simulations, Atahan (2002) analyzed a strong-post W-beam guardrail system that failed in a previously conducted full-scale crash test. After identifying the cause of failure and incorporating necessary improvements, a new W-beam guardrail was developed and showed improved performance based on simulation results. Atahan (2003) also studied the performance of the G2 steel weak-post W-beam guardrail system installed at the slope-break point on non-leveled terrains using LS-DYNA simulations. The simulation results showed that there was a risk of increased vehicle instability when the roadside slope adjacent to the W-beam guardrail became steeper than 6H:1V. This work demonstrated the effectiveness of FE simulations for its reliability of replicating the actual dynamic interactions and mechanics of the crash. Atahan also pointed out that the use of a real soil model other than the simplified spring soil model could improve the accuracy of FE simulations but would significantly increase the computational costs.

Using LS-DYNA simulations, Fang et al. (2010) conducted a study to evaluate the performance of three types of barriers on sloped medians: a single-faced W-beam

guardrail, two designs of double-faced W-beam guardrails, and a low-tension cable barrier. The three types of barriers were evaluated under vehicular impacts at multiple speeds and impact angles. The simulation results suggested that the effectiveness of the W-beam guardrails and cable barriers could be reduced on sloped medians compared to their performance on flat terrain as specified in NCHRP Report 350. It was observed from all barrier types that the frequency and severity of vehicle rollover rose with increased impact angles. It was also observed that the performance of the barriers investigated in this project exceeded the TL-3 requirements of NCHRP Report 350, considering the large median slopes (4H:1V and 2.5H:1V) and having higher impact speeds than the standard impact conditions.

Dorcely and McKyes (2010) theoretically investigated the interactions between barrier posts and soil near the crown of a slope. The theoretical results matched smoothly to the case where the slope was far away from the post and predicted a gradual reduction of maximum horizontal soil resistance by up to 60% when a post was installed near the crown of a slope. By installing the post to a greater depth, the resistance of a post could be increased. The theoretical increase of depth by 36% almost doubled the maximum horizontal post resistance. It was found to be critical that a post be surrounded by heavily compacted soil, which can lead to a horizontal resistance four times that of lightly compacted soil. The surface roughness of the post, such as a concrete post, was also found to almost double the horizontal resistance versus that of a smooth surfaced post. These results would be further justified by conducting follow-up studies using FE simulations and crash tests.

Vehicular impact height is one of the important parameters in evaluating the performance of barrier systems. The vehicle's impact height can vary depending on the trajectory of the vehicle along the median and the lateral offset of the barrier. The performances of the modified G4(1S) W-beam guardrail, modified thrie-beam guardrail, Midwest Guardrail System, and modified weak post W-beam guardrail were analyzed by Ferdous et al. (2011) using LS-DYNA. Each model was validated based on the results obtained from existing crash tests. Using vehicle models from NCHRP Report 350, the override and under-ride limits for each guardrail model were identified. The performance limit of each barrier was determined by parametrically varying the vehicle impact height to determine at what point the override or rollover for the pickup truck and under-ride for the small passenger car would occur.

In 2012, Marzougui et al. (2012) investigated some barrier systems that passed the requirements of NCHRP Report 350, but failed to pass the MASH requirements, to determine if the barrier systems could be retrofitted with various modifications to improve the performance. The modifications were conducted on six G9 thrie-beam guardrails and three G4(1S) W-beam guardrails using FE simulations. The simulation results showed that with the proposed modifications, the guardrails that originally failed to pass the MASH requirements were able to retain the vehicle under MASH TL-3 conditions and reduce the propensity to vault over the guardrails.

Hampton et al. (2013) performed a similar simulation in an effort of evaluating the performance of strong-post W-beam guardrails with missing posts under impact conditions specified by NCHRP Report 350. The effects of missing posts on the guardrail's performance were quantitatively evaluated using FE models of crash tests

under impacts of a 4,409-lb (2,000-kg) pickup truck. Simulations where one, two, or three posts were removed from the guardrails were conducted with varying points of impact to evaluate the effects of missing posts. The FE simulation results demonstrated that guardrails with even one missing post could have a remarkably decreased performance under vehicular impacts due to wheel snagging. It was also observed that both the maximum deflection and maximum rail tension were greatly increased as more posts were removed from the guardrail. The overall conclusion of the study was that even if one post was missing, the guardrail performance could be significantly reduced and post replacement should be a high-priority repair for guardrail maintenance.

Ferdous et al. (2013) furthered the research from NCHRP Project 22-22 to include numerical simulations in performance evaluation of commonly used traffic barriers on roadside and median slopes. The modified G4(1S) W-beam guardrail, modified thrie-beam guardrail, Midwest guardrail system, and modified weak-post W-beam guardrail were selected for evaluation. The barriers were placed on both the foreslope and backslope when testing the truck model, while placing them near the bottom of the ditch for the small-car test. The modified G4(1S) system was found to have the lowest override limit due to its lower rail mounting height of 28 inches. This system was also prone to more vehicle post-snagging due to the narrower blockout than that of the Midwest guardrail system. For the truck, placing the W-beam farther up the slope towards the shoulder produced results that were expected to pass the safety evaluation criteria and an increase in the median slope would require the W-beam to be even farther up. Since NCHRP Report 350 was used as the safety standard in this study, the results are expected to change if MASH guidelines were adhered to.

Mongiardini and Reid (2013) investigated relevant phenomena in simulation models that would help create a more accurate representation of the kinematics and dynamics of an actual full-scale crash test. Modifications to the steering system, tire size, and bumper failure mechanism were analyzed. A properly working steering system was found to have an insignificant role because the vehicle was redirected by the barrier system, and the tires were forced to slide over the ground. Although the bumper usually plays a relatively minimal role in a full-scale crash test, the definition of a failure mechanism for the front bumper was found to be crucial for simulating the vehicle kinematics. Without this failure mechanism, the bumper would restrict the wheel from steering properly when the wheel contacted the barrier post. This caused the tire to roll over the second post during impact, thus limiting the proper redirection of the vehicle. Similarly, the correct modeling of tire size was essential for simulating the interaction between the wheel and posts.

Abu-Odeh et al. (2013) evaluated post placement positioning when the rail is over the slope breaking point. Even though the AASHTO *Roadside Design Guide* recommends that posts be installed two feet in front of a slope break, there are often restrictive environmental conditions, such as mountainous terrain, where this is not feasible. The simulation results indicated that a 31 inch W-beam guardrail system with 8 foot long posts, spaced 6.25 feet apart on centers met MASH TL-3 criteria. In these simulations, the guardrail system was placed one foot down from the slope break on a 2H:1V slope and the posts were placed off splice. Full-scale crash tests were used to confirm the simulation results.

FE simulations, particularly conducted with LS-DYNA, have been used increasingly more in roadside safety research. In addition to the abovementioned references, FHWA published several manuals on using LS-DYNA material models and evaluation of these models (Lewis 2004; Murray et al. 2005; Murray 2007; Reid et al. 2004). These references can also be useful in the crash modeling work using LS-DYNA.

CHAPTER 2: CONTACT THEORY AND METHODS

Contact analysis and handling are the most important and computationally expensive constituents for finite element (FE) solutions to contact problems. Contact refers to the touching of two separate objects or a single object touching itself. There are different contact methods that can be employed to FE solutions, but in this work the penalty method was used extensively and will be discussed in the following chapter.

2.1 Contact Analysis and Methods

The penalty method is used in both explicit and implicit FEA programs for the treatment of contacts. In a contact problem with two separate objects, there is a separation between the master and slave surface, where the slave surface mesh should be comparable to or finer than the master surface mesh. It should be noted that for single surface contacts the slave surface is typically defined as a list of part ID's with no master surface needing to be defined, due to contact being considered between all parts in the slave list, including self-contact of each part. Each of these surfaces is subdivided into segments that are bounded by nodes of the FE mesh, as shown in Figure 2.1. In the penalty method, imaginary normal interface springs are placed between two surfaces of the penetrating segments, shown in Figure 2.2, and the repulsive spring force is proportional to the penetration distance. The stiffness of the spring is called the contact stiffness, which depends on the contacting material and geometric properties that will be described below. The three current implementations of the penalty algorithm are the

standard penalty formulation, the soft constraint penalty formulation, and the segment-based penalty formulation.

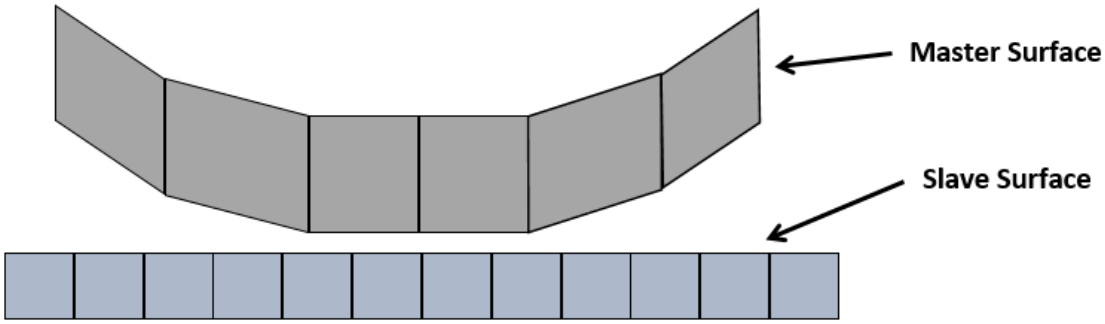

Figure 2.1: Master and slave surfaces.

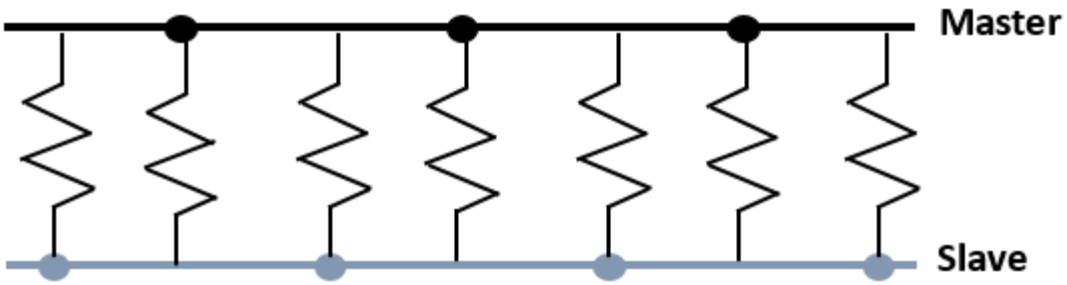

Figure 2.2: Imaginary normal interface springs.

The standard penalty formulation involves checking for penetrations of each slave node through the master surface at each time step. If there is no penetration, nothing is done and the simulation moves on to the next time step. If a slave node does penetrate, a repulsive force, which may be thought of as a spring force, is applied between the slave node and its contact point. The contact force is calculated to send the two objects out of intersection until the next time step and has a magnitude that is proportional to the amount of penetration. This force is assembled into a vector that is substituted into the global equation of motion given by

$$\boldsymbol{M}\ddot{\boldsymbol{d}}(t) + \boldsymbol{F}^{int}\big(\boldsymbol{d}(t)\big) + \boldsymbol{F}^{c}\big(\boldsymbol{d}(t)\big) = \boldsymbol{F}^{ext}(t) \tag{2.1}$$

where t is the time, $\boldsymbol{M}$ is the mass matrix, $\ddot{\boldsymbol{d}}(t)$ is the acceleration vector, $\boldsymbol{F}^{int}$ is the internal force vector, $\boldsymbol{d}(t)$ is the displacement vector, $\boldsymbol{F}^{c}$ is the contact force vector, and $\boldsymbol{F}^{ext}$ is the external force vector. The contact force is calculated by

$$F^{c} = -lk \tag{2.2}$$

where l is the penetration depth and k is the contact stiffness of the imaginary spring.

The varying penalty formulation methods focus on assigning different values to the contact stiffness. For the standard penalty formulation, shell elements have a contact stiffness defined by

$$k = \frac{SKA}{\max(shell\ diagonal\ lengths)} \tag{2.3}$$

where S is the stiffness scale factor, K is the material's bulk modulus, and A is the face area of the element. For solid elements, the contact stiffness is defined by

$$k = \frac{SKA^2}{\mathrm{V}} \tag{2.4}$$

where V is the volume of the element.

The standard penalty formulation approach is most stable when the contacting materials have similar values for the bulk modulus since the stiffness calculations include this value. When contacting materials have vastly different bulk modulus values (e.g. steel-foam) there is an excessive amount of penetration due to the undesired effect on the contact stiffness from the soft material. The soft constraint penalty formulation is used to eliminate these excessive penetrations by calculating an additional contact stiffness that is based on the stability of a local spring-mass system. This soft constraint contact stiffness is defined by

$$k = .5 \cdot SOFSCL \cdot m^* \cdot (\frac{1}{\Delta t}) \tag{2.5}$$

where $SOFSCL$ is a softness scale factor, m^* is a function of the mass of the slave and master nodes, and Δt is the size of the time step. This additional stiffness is compared to the values calculated from the standard penalty formulation, and in general, the maximum stiffness is used for the contact force.

The segment-based penalty formulation applies a slave segment-master segment approach instead of the standard slave node-master segment. This approach is useful in situations where there are non-nodal penetrations, such as cases with edge-to-edge or surface-to-surface contacts. The segment-bases contact stiffness is defined by

$$k = .5 \cdot SLSFAC \cdot \begin{Bmatrix} SFS \\ or \\ SFM \end{Bmatrix} \cdot \left(\frac{m_1 m_2}{m_1 + m_2}\right) \cdot (\frac{1}{\Delta t})^2 \tag{2.6}$$

where $SLSFAC$ is the sliding scale factor, SFS is the slave segment penalty stiffness factor, SFM is the master segment penalty stiffness, and m_1 and m_2 are the respective masses of the slave and master segments. These segment masses are equal to the element mass for a shell and half the element mass for a solid. This formulation distributes contact forces more realistically over each node for the segment in contact (Hallquist 2006).

2.2 Contact Handling in LS-DYNA

One of the simplest contact algorithms used in LS-DYNA is the tied-nodes-to-surface contact, which is used for tying two surfaces together with different meshes and is shown in Figure 2.3. The slave nodes are constrained to the master surface for all the translational degrees of freedom, meaning the slave part will have the same translational displacements as the master surface. When defining the slave nodes and master surface, the master should be more coarsely meshed for tying similar materials together or the

stiffer material for dissimilar materials. It should be noted that this contact does not work well for tying together a deformable body with a rigid body and that nodes used in one tied interface cannot be used in another tied interface.

Figure 2.3: Tied-nodes-to-surface contact.

Another more complicated and computationally costly contact algorithm used in LS-DYNA is the automatic-surface-to-surface contact. The automatic modifier means that at each time step the assignment of the slave and master nodes and segments is made automatically. This is a two-way contact treatment that checks for penetration between the slave nodes and master surface, as well as between the master nodes and slave surface, as shown in Figure 2.4. This approach allows the selection of master and slave surfaces to be arbitrary, which can be beneficial when the orientations of contacting parts are not known at the onset. This contact is ideal for surfaces sliding against each other where most of the elements are initially in contact.

Figure 2.4: Automatic-surface-to-surface contact.

The automatic-surface-to-surface contact has the disadvantage that it is unable to handle self-interactions of parts. Since this is a common occurrence is crash simulations, another approach for contact treatment involves defining all parts in one slave set and eliminating the need for master set. The automatic-single-surface contact applies this approach and is among the most widely used contact types in LS_DYNA when there are a large number of potentially contacting parts. This contact checks for penetrations between any two surfaces of all parts defined in the slave set, including self-contact for each part that is shown in Figure 2.5. The automatic-single-surface contact implements a segment-based penalty formulation because segments instead of nodes are checked for penetrations through other segments.

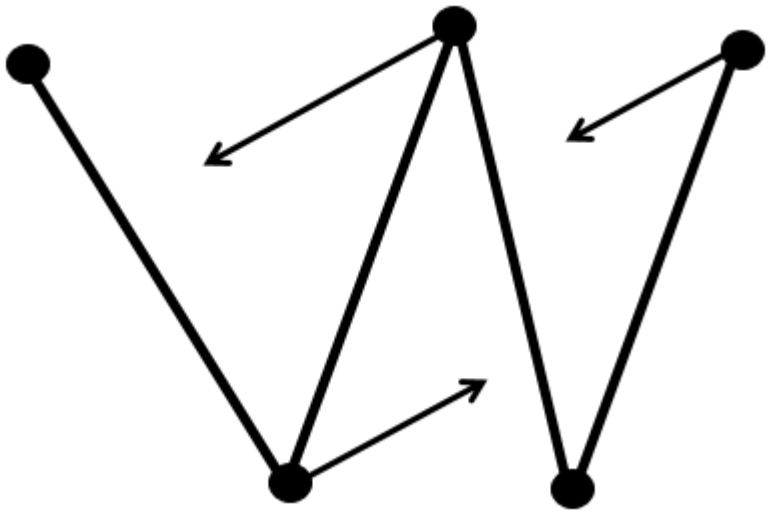

Figure 2.5: Self-contact checking for automatic-single-surface contact.

A variant of the automatic-single-surface contact that can also handle self-interactions of parts and only needs a slave set defined is the automatic-general-interior contact. This contact algorithm uses three contact segments for each slave node instead of the two segments used in the automatic-single-surface contact, as well as having a

frequency of bucket-sorting ten times larger. This bucket sorting refers to the number of time steps between each bucket sort, which is the method in with a contact searches to identify potential master contact segments for any given slave node. The automatic-general-interior contact has the capability of detecting beam-to-beam, beam-to-shell edge, shell edge-to-edge contacts, as well as contacts between internal edges of shell elements, as shown in Figure 2.6. The additional option of SOFT=1 is activated to effectively treat contact of dissimilar materials. This is the most comprehensive contact treatment with significantly more computational expense than the other contact types mentioned. The automatic-general-interior contact has been found to have reliable numerical stability for contacts involving large deformations.

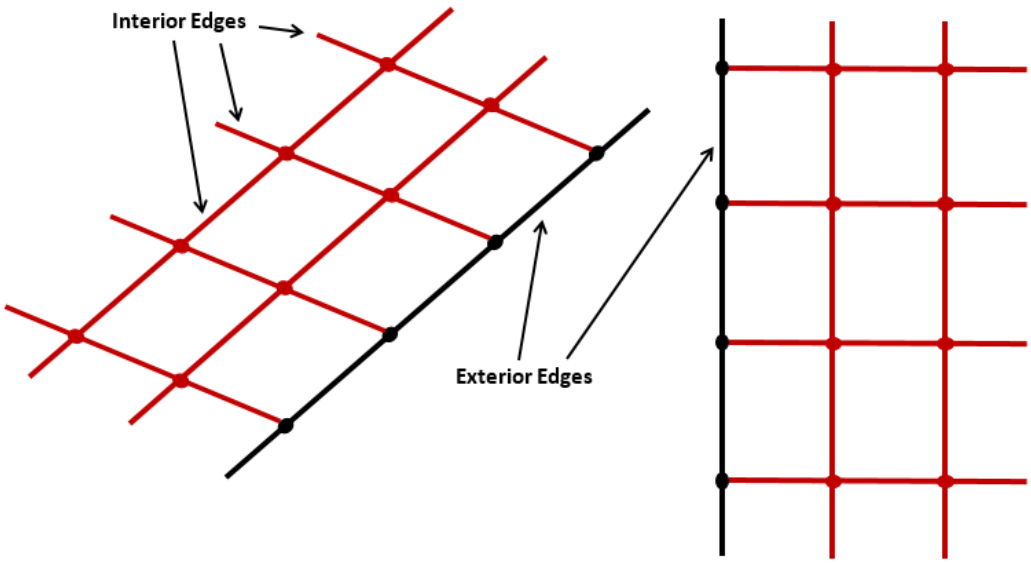

Figure 2.6: Shell edge-to-edge contact for automatic-general-interior.

CHAPTER 3: FINITE ELEMENT MODELING

The objective of this research was to evaluate the performance of single- and double-faced W-beam guardrails under MASH TL-3 conditions. Both single- and double-faced guardrails were tested at two rail heights, 29 and 31 inches. For the double-faced guardrail at each of the two rail heights, an alternative design in which the backside rail (i.e., the rail facing the ditch) was dropped to a lower height was also evaluated. Both the single- and double-faced guardrails were evaluated on a 2.5H:1V sloped median, as shown in Figure 3.1.

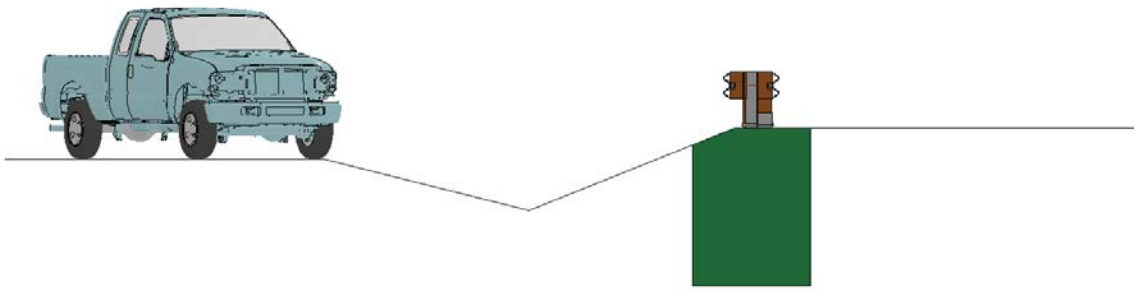

Figure 3.1: 2.5H:1V sloped median.

The simulation work, summarized in Table 3.1, included two vehicle models, a 1996 Dodge Neon and a 2006 Ford F250, and the six guardrail models. The FE models of the passenger car, pickup truck, and a single-faced G4(1S) strong-post W-beam guardrail were obtained from the NCAC and modified to correct modeling issues and to meet the NCDOT design specifications. Crash simulations were performed for all six guardrails

under MASH TL-3 conditions. MASH TL-3 conditions include a passenger car between 2,365 and 2,475 lbs. (1,075 and 1,125 kg) or a pickup truck between 4,890 and 5,110 lbs. (2,220 and 2,320 kg). The test conditions are a vehicle speed of 62 mph (100km/h) and an impact angle of 25 degrees.

Table 3.1: Categories of simulation work.

Case No.	Guardrail Type	Impacting Side	Vehicle	MASH Impact Conditions	Impact Angle	Impact Speed
1	29-inch Single-faced	Front-side	Neon	TL-3	25°	62.1 mph (100 km/h)
			F250			
	31-inch Single-faced		Neon			
			F250			
2	29-inch Double-faced	Front-side	Neon			
			F250			
	31-inch Double-faced		Neon			
			F250			
3	29-inch Double-faced	Backside	Neon			
			F250			
	31-inch Double-faced		Neon			
			F250			
4	29-inch Double-faced (lowered back side rail)	Front-side	Neon			
			F250			
	31-inch Double-faced (lowered back side rail)		Neon			
			F250			
5	29-inch Double-faced (lowered back side rail)	Backside	Neon			
			F250			
	31-inch Double-faced (lowered back side rail)		Neon			
			F250			

3.1 FE Models of Testing Vehicles

The vehicle models used were a 1996 Dodge Neon passenger car and a 2006 Ford F250 pickup truck, as shown in Figure 3.2. The 1996 Dodge Neon had a curb weight of 2,414 lbs. (1,095 kg), overall length of 171.8 in (4.36 m), overall width of 67.5 in (1.71 m), overall height of 52.8 in (1.34 m), and ground clearance of 5.7 in (145 mm). The 2006 Ford F250 had a curb weight of 5,690 lbs. (2,581 kg), overall length of 226.4 in

(5.75 m), overall width of 79.9 in (2.03 m), overall height of 76.5 in (1.94 m), and ground clearance of 8.3 in (211 mm). The Dodge Neon is within the acceptable range of mass for MASH TL-3, while the Ford F250 is slightly higher.

a. 1996 Dodge Neon b. 2006 Ford F250

Figure 3.2: FE models of the two vehicles used in crash simulations.

The FE model of the 2006 Ford F250 contains a total of 746 parts that were discretized into 737,986 nodes and 736,096 elements (25,905 solid, 2,305 beam, 707,656 shell, and 230 other elements). Eleven different constitutive models were used including the piecewise linear plasticity model defined for most steel components, the linear and nonlinear elastic spring model for the suspension springs, the viscous damping model for the shock absorbers, the low-density foam model for the radiator core, the spot-weld model for sheet metal connections, the viscos-elastic model for rubber cushions, and the null material model defined for contact purposes. Hourglass control was used on various components that could potentially experience large deformations. The FE model of the F250 was originally developed at NCAC and validated using frontal-impact tests that

were conducted on flat terrain according to the Federal Motor Vehicle Safety Standards (FMVSS).

The FE model of the 1996 Dodge Neon contains a total of 339 parts that were discretized into 283,683 nodes and 270,953 elements (2,852 solid, 92 beam, 267,775 shell, and 234 other elements). Ten different constitutive models were used including the piecewise linear plasticity model defined for most steel components, the elastic model for the tires and a few other components, the viscous damping model for the shock absorbers, the low-density foam model for the radiator core, the spot-weld model for sheet metal connections, the Blatz-Ko rubber model for nearly incompressible rubber cushions, the rigid model for most mounting hardware, and the null material model defined for contact purposes. Hourglass control was used on various components that could potentially experience large deformations. The FE model of the Dodge Neon was originally developed at NCAC and validated with the NHTSA's Frontal New Car Assessment Program (NCAP) tests.

3.2 FE Models of the W-Beam Guardrails

The single-faced G4(1S) W-beam guardrail was originally developed at NCAC. It contained six different constitutive models including the piecewise linear plasticity model defined for most steel components, the elastic model for the wood blockouts and terminal posts, the soil and foam model used for the soils around posts, the rigid model for the bolts and road surface, the nonlinear elastic spring model used for the bolt-tensioning spring (used on the long-bolts connecting the W-beam rails and wood blockouts to the posts), and the null material model used for contact purposes. The guardrail models, including the soil foundations, were obtained from previous NCDOT research projects

(Fang et al. 2010; Fang et al., 2013). These models use the same material model and properties as the original NCAC model. The first modification that needed to be made involved moving the rail splices from the posts to the mid-span of two adjacent posts for the 31-in model. Figure 3.3 illustrates the differences between the splice locations for the 29- and 31-in guardrail models used in this thesis.

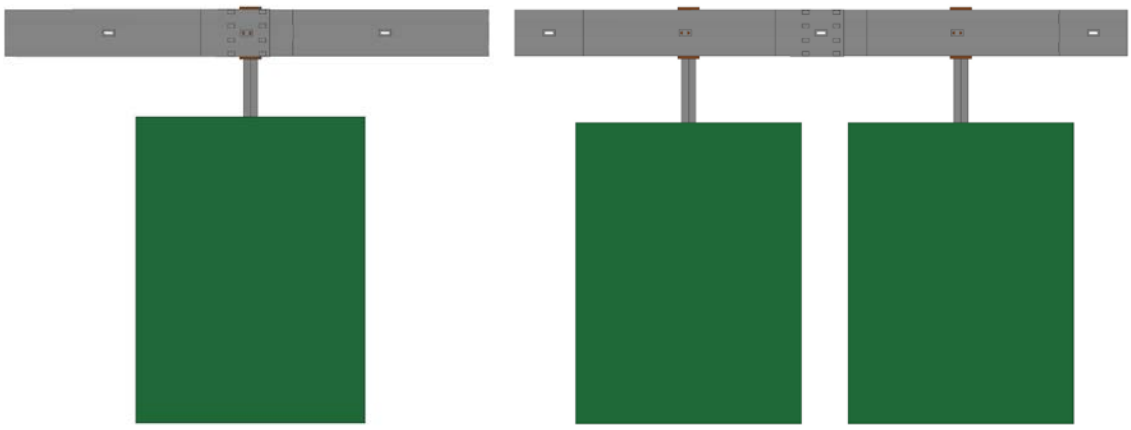

a. Splice location on the 29-in guardrail b. Splice location on the 31-in guardrail

Figure 3.3: The FE models for different splice locations.

The first design of the double-faced guardrail was created by duplicating the W-beam and wood blockouts from the single-faced guardrail and attaching them to the opposite side of the post. For the second design of the double-faced guardrail, the backside rail was lowered by 2.1 in (53.3 mm) so that the top of the backside rail was either 29- or 31-in when measured from grade. Figure 3.4 illustrates the two double-faced guardrail designs, both of which are used for this thesis.

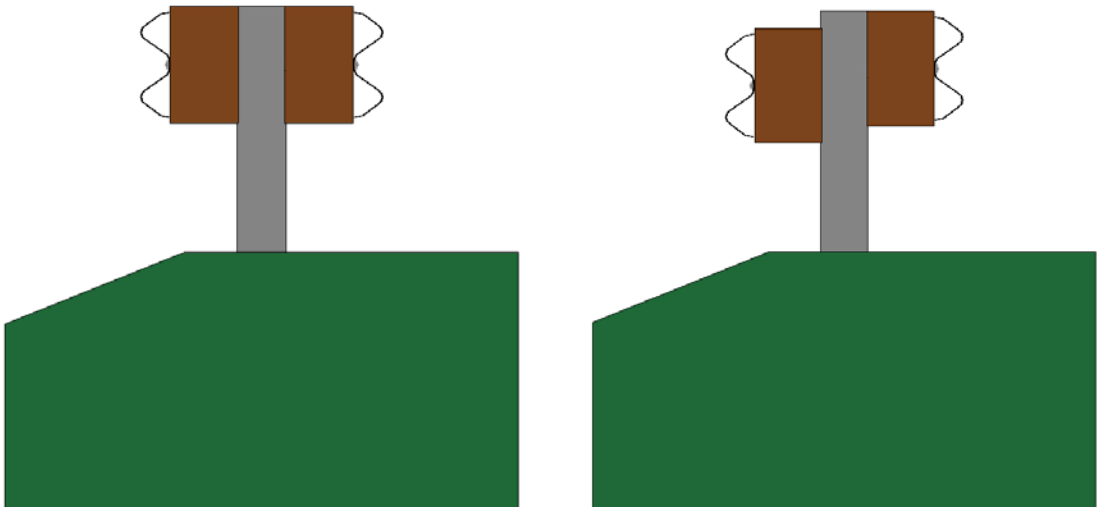

a. Original double-faced design b. Lowered backside design

Figure 3.4: The FE models for double-faced guardrails.

Once the segments of the single- and double-faced guardrails were modified and/or created, they were duplicated to create the entire 400-ft (122-m) section of guardrails. This duplication of the guardrail section was done with an in-house script developed to replicate not only the parts, nodes, elements, and material properties, but also the contact definitions defined between each pair of parts. The program was also capable of merging the ends of adjacent segments with proper numbering and contact definitions. With this program, the guardrail model was generated by duplicating the length-of-need section and connecting to two terminal sections that were obtained from the original guardrail model and modified for the double-faced guardrails. Figures 3.5 and 3.6 illustrate the full FE models a single-faced and a double-faced guardrail, respectively, placed on the 2.5H:1V slope of a six-lane 46-foot median divided freeway.

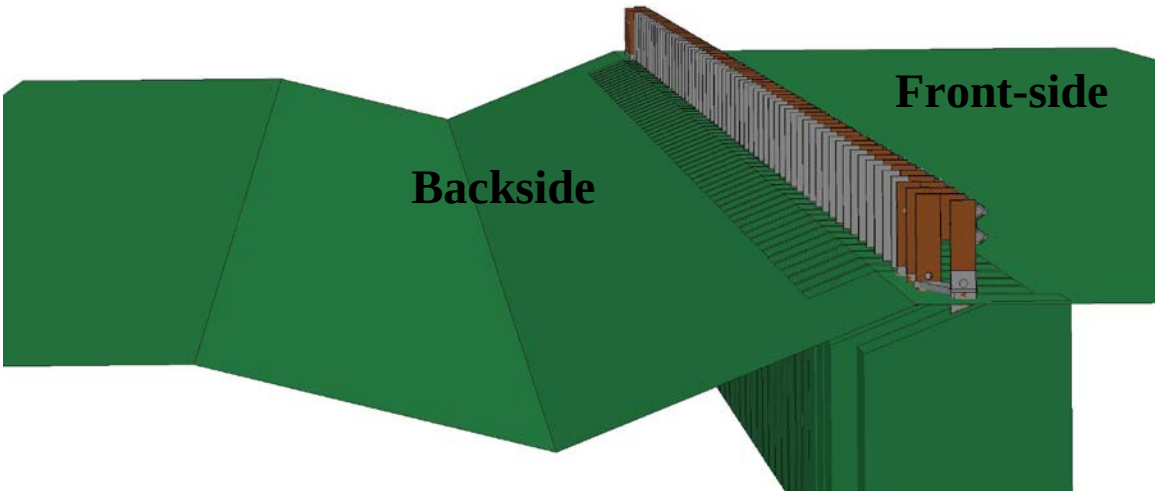

Figure 3.5: The full FE model for single-faced guardrail.

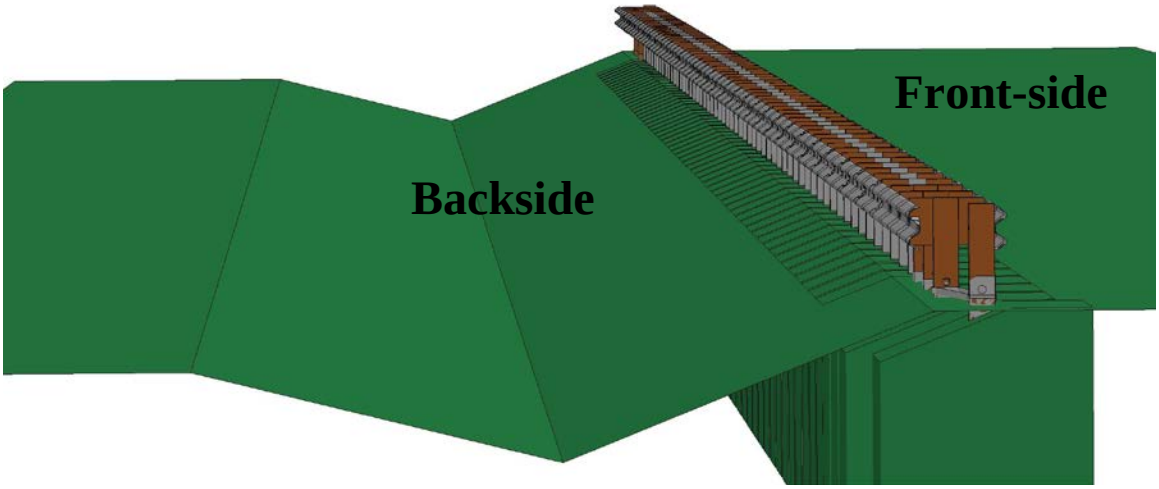

Figure 3.6: The full FE model for double-faced guardrail.

3.3 Simulation Setup

The six guardrail models were combined with the two vehicle models to create twenty individual crash simulations that can be categorized into five major cases:

Case 1: Two front-side impact simulations for each of the 29- and 31-in single-faced guardrails, conducted under MASH TL-3 conditions using both vehicle models, as shown in Figure 3.7.

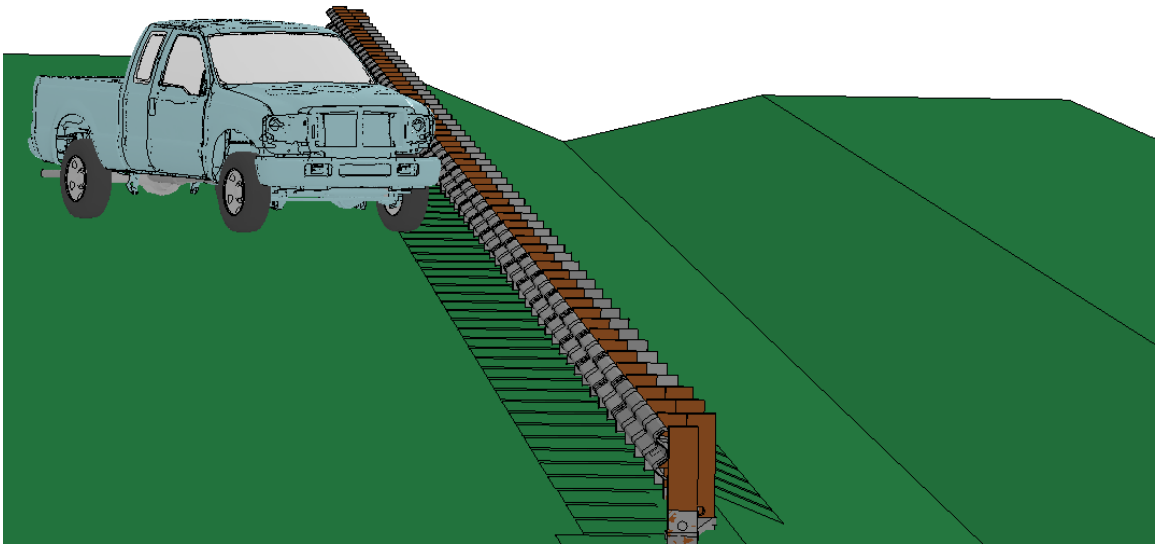

Figure 3.7: FE model for single-faced front-side impact.

Case 2: Two front-side impact simulations for each of the 29- and 31-in double-faced guardrails, conducted under MASH TL-3 conditions using both vehicle models.

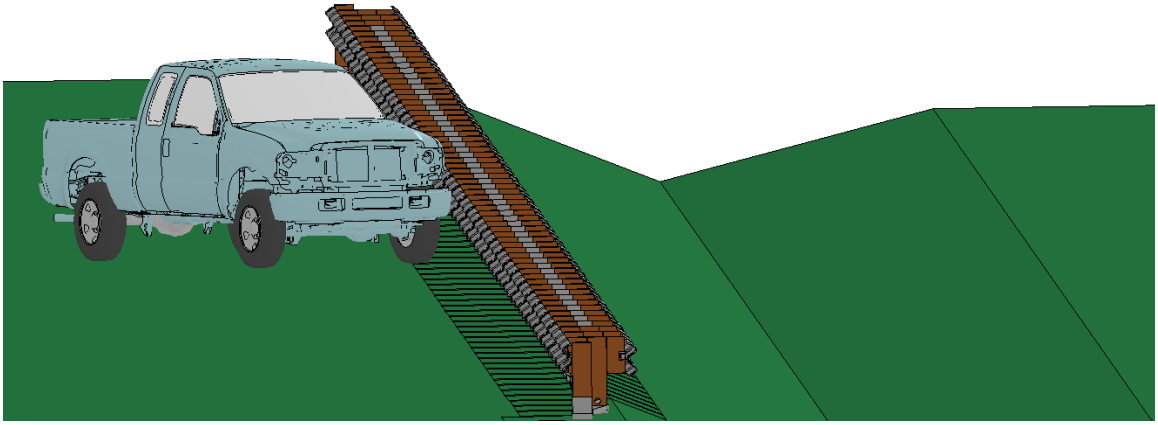

Figure 3.8: FE model for double-faced front-side impact.

Case 3: Two backside impact simulations for each of the 29- and 31-in double-faced guardrails, conducted under MASH TL-3 conditions using both vehicle models

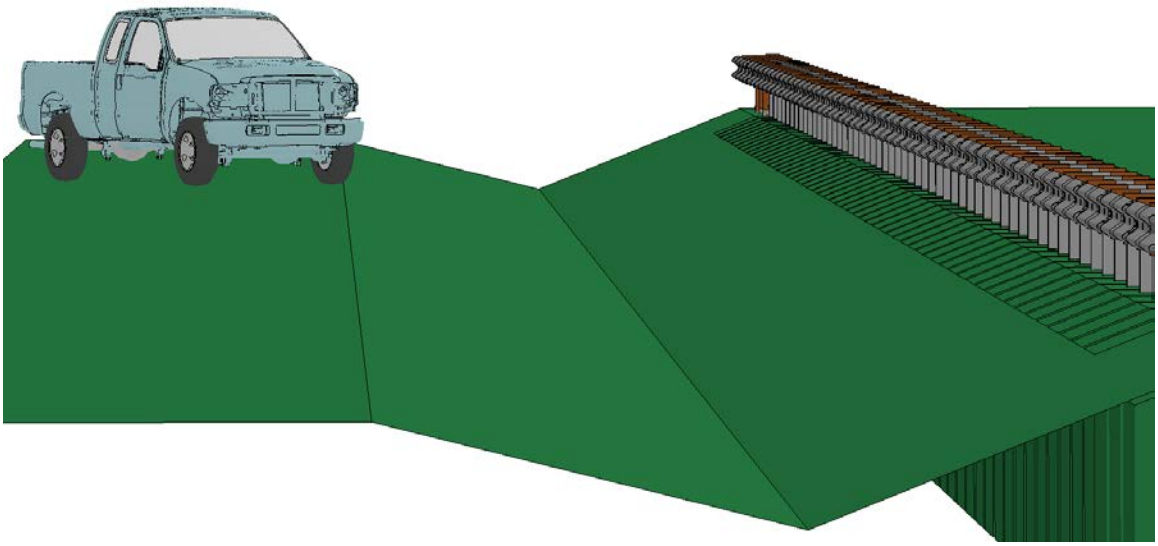

Figure 3.9: FE model for double-faced backside impact.

Case 4: Two front-side impact simulations for each of the 29- and 31-in double-faced guardrails with a lowered backside rail, conducted under MASH TL-3 conditions using both vehicle models.

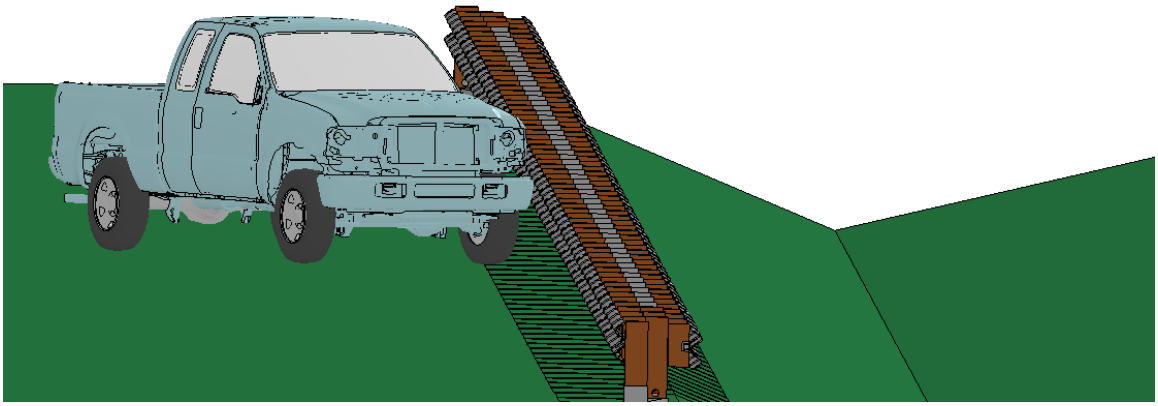

Figure 3.10: FE model for double-faced, lowered backside rail, front-side impact.

Case 5: Two backside impact simulations for each of the 29- and 31-in double-faced guardrails with a lowered backside rail, conducted under MASH TL-3 conditions using both vehicle models.

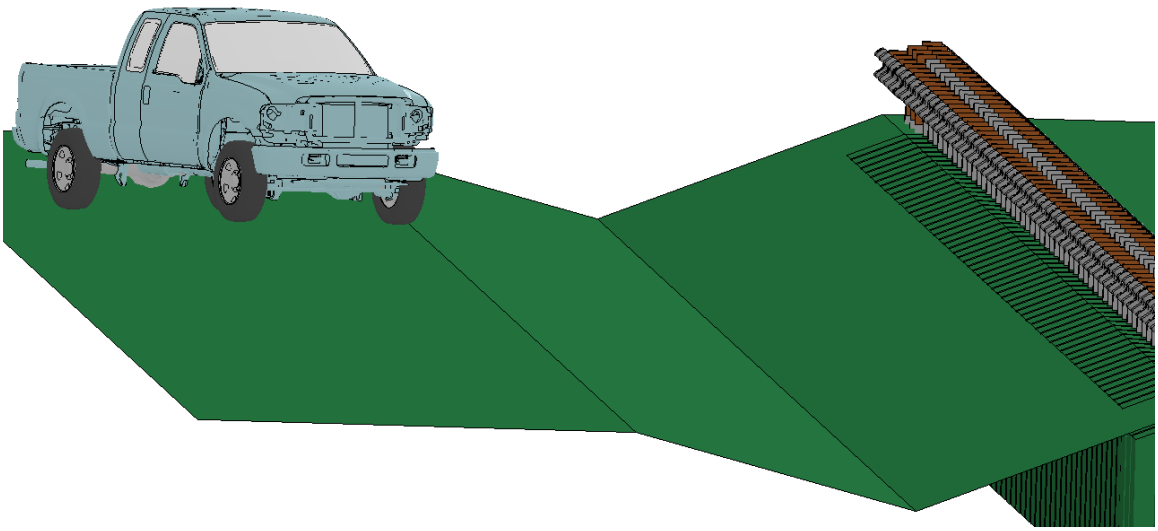

Figure 3.11: FE model for double-faced, lowered backside rail, backside impact.

CHAPTER 4: PERFORMANCE EVALUATION OF W-BEAM GUARDRAILS

In this chapter, the FE simulation results of the five cases listed in Table 3.1 are presented and analyzed to determine the performance of different guardrail designs. The single-faced guardrails at placement heights of 29- and 31-inches were tested using both the Dodge Neon and Ford F250 impacting from the front-side at 62.1 mph (100 km/h) and a 25° impact angle. The double-faced guardrails with placement heights of 29- and 31-inches, both with and without a lowered backside rail, were evaluated under impacts of both vehicles from front-side and backside, with the same impact conditions as those for the single-faced guardrail. It should be noted that these deterministic simulation results can be used to interpret the performance trends of W-beam guardrails, but should not be used to draw definitive conclusions about their performance for a specific crash event.

In order to assess the vehicular responses after impacting the guardrail, pertinent data were gathered from simulation results and analyzed. The data collected included the vehicles' displacements along the *x*-, *y*-, and *z*-axis, the speeds along the *x*- and *y*-axis, and the yaw, pitch, and roll angles. The yaw is the rotation around the vertical axis, the pitch is the rotation around the side-to-side axis, and the roll is the rotation around the front-to-back axis, as shown in Figure 4.1. The MASH exit box criterion was used to assess the post-impact trajectory of the vehicle for MASH evaluation criterion N. Figure 4.2 illustrates the definition of the exit box, which begins at the last point of contact of

the vehicle's wheel track with the initial traffic face of the barrier, as well as showing the exit angle. Table 4.1 gives the exit box dimensions for the Dodge Neon and Ford F250. For a simulation to be considered safe under the exit box criterion, all four wheel tracks must remain inside the exit box within the distance B. High vehicular exit angle or spin-out of the vehicle, resulting from excessive pocketing or snagging of the vehicle, are not desirable and are also mentioned. It should be noted that although the exit box criterion is a useful tool for determining the post-impact vehicular trajectories, it is not sufficient to determine if the vehicle has been safely redirected. The maximum deflection of the barrier and the time that it occurred are also noted. In addition to the exit box criterion, the MASH evaluation criterion F, which specifies a maximum of 75° roll and pitch angles, was also used in the evaluation.

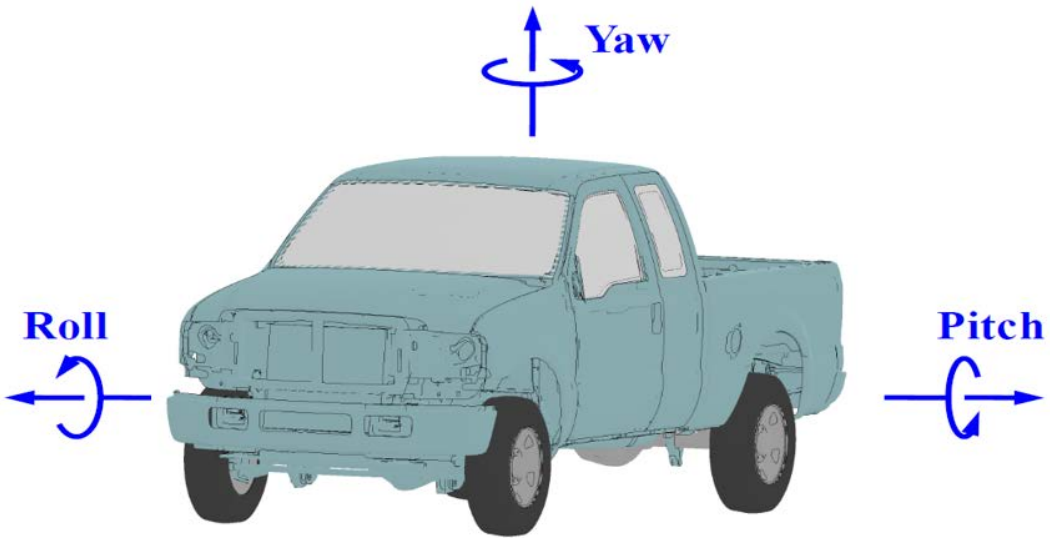

Figure 4.1: Definition of yaw, pitch, and roll angles.

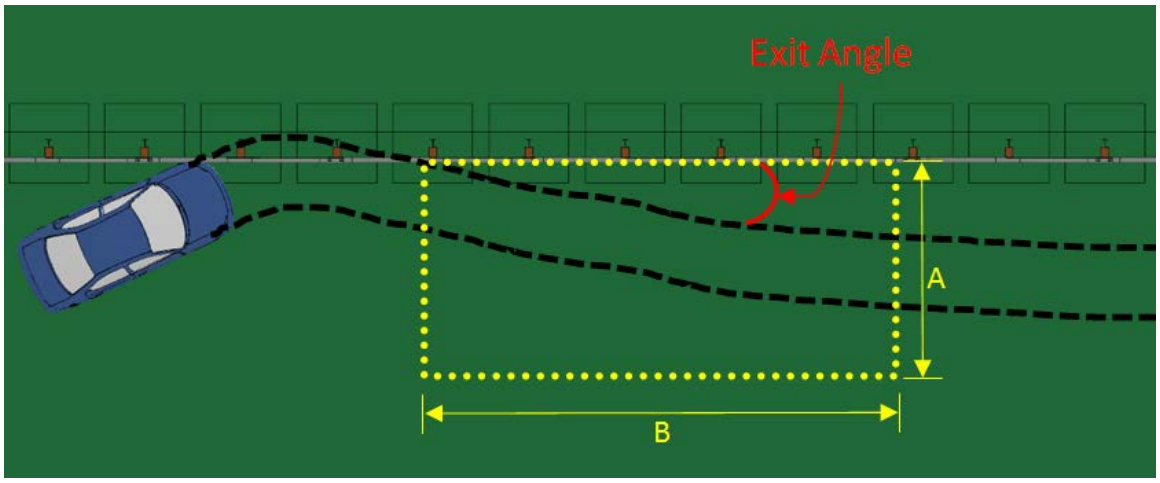

Figure 4.2: Exit Box criterion in MASH.

Table 4.1: Exit box dimensions for test vehicles.

Vehicle	**A**	**B**
1996 Dodge Neon	15.1 ft (4.6 m)	32.8 ft (10.0 m)
2006 Ford F250	16.9 ft (5.15 m)	32.8 ft (10.0 m)

4.1 Single-faced Guardrails

The analysis of the single-faced 29- and 31-inch strong-post W-beam guardrails were performed through four simulations of Case 1, for vehicular impacts of both the 1996 Dodge Neon and the 2006 Ford F250 under MASH TL-3 conditions. Table 4.2 shows the simulation conditions and a summary of the guardrail performance in terms of vehicular responses.

Table 4.2: Simulation results for single-faced guardrails.

Impacting Side	Guardrail Height	Test Vehicle	Test Results
Front	29 inches	Dodge Neon	Vehicle not redirected safely by guardrail (spin-out and outside exit box)
		Ford F250	Vehicle not redirected safely by guardrail (spin-out and outside exit box)
	31 inches	Dodge Neon	Vehicle not redirected safely by guardrail (spin-out and outside exit box)
		Ford F250	Vehicle not redirected safely by guardrail (spin-out and outside exit box)

Figure 4.3 shows the displacement path of the Dodge Neon impacting the 29-inch single-faced W-beam guardrail from the front-side. The guardrail is shown in its original shape, and the exit box is denoted by the yellow rectangle. The yaw, pitch, and roll angles of the Dodge Neon are shown in Figure 4.4. The Dodge Neon had a continuously increasing yaw angle, indicating that the vehicle continuously spun and consequently went outside the exit box. The roll and pitch angles were less than twenty degrees in either positive or negative direction and thus passed the MASH evaluation criterion F.

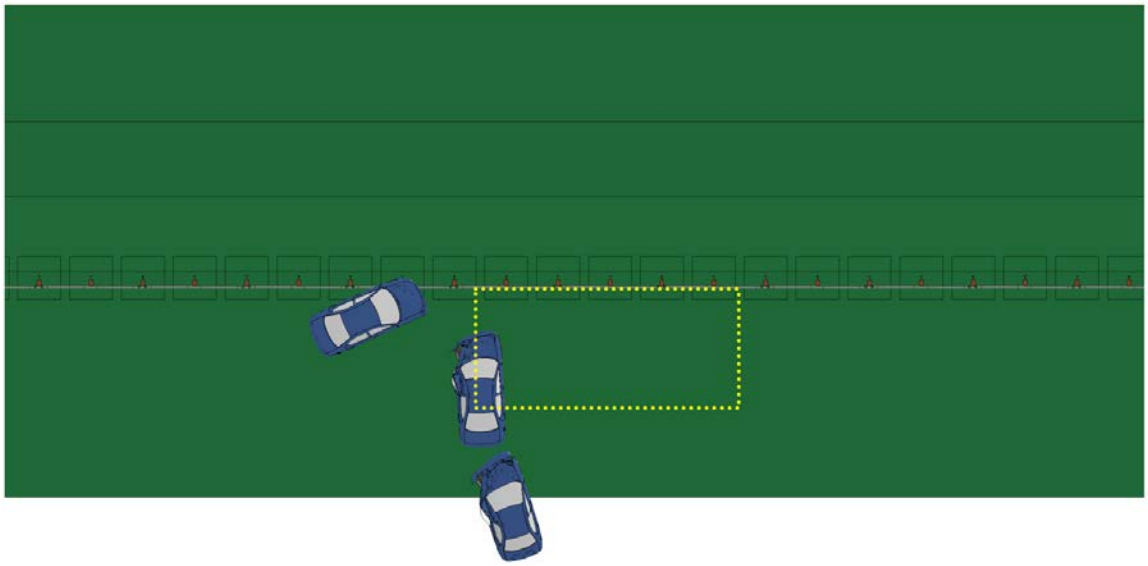

Figure 4.3: Displacement path and exit box for Neon impacting 29-inch single-faced guardrail.

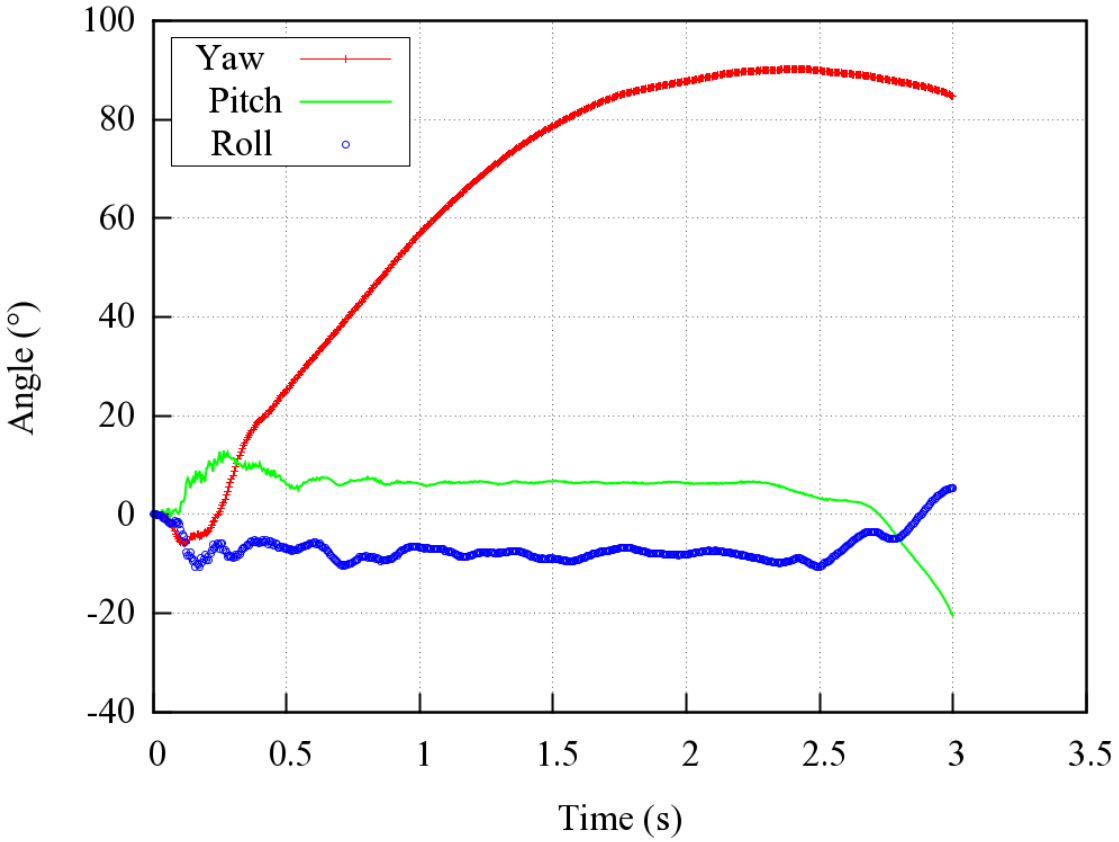

Figure 4.4: Yaw, pitch, and roll angles for Neon impacting 29-inch single-faced guardrail.

Figure 4.5 shows views of vehicle-barrier interaction at the time when the maximum deflection of the guardrail occurred. It can be seen that the damaged guardrail sections are small and localized, which serves as an indication of a relatively low impact severity. The time histories of transverse displacements and speeds measured at the center of gravity (CG) point of the vehicle are shown in Figure 4.6. The transverse speed remained at 3 m/s towards the travel lane with spinning (i.e., loss of control of the vehicle). As seen in Figure 4.3, the vehicle has entered the travel lane, so the chance of getting involved in a secondary collision is relatively high.

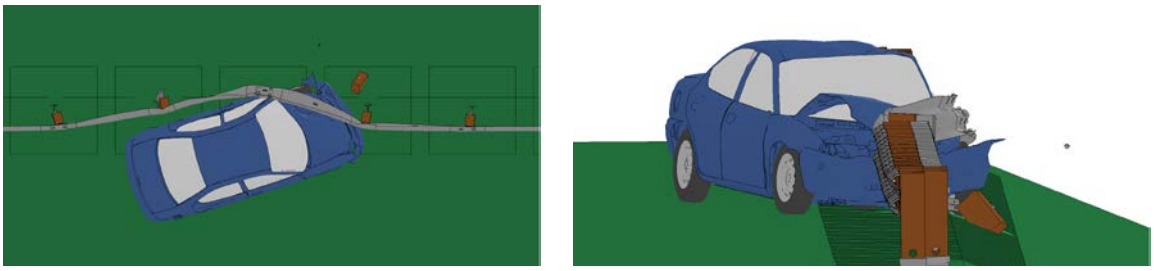

Top view Front view

Figure 4.5: Maximum deflection of W-beam for Neon impacting 29-inch single-faced guardrail.

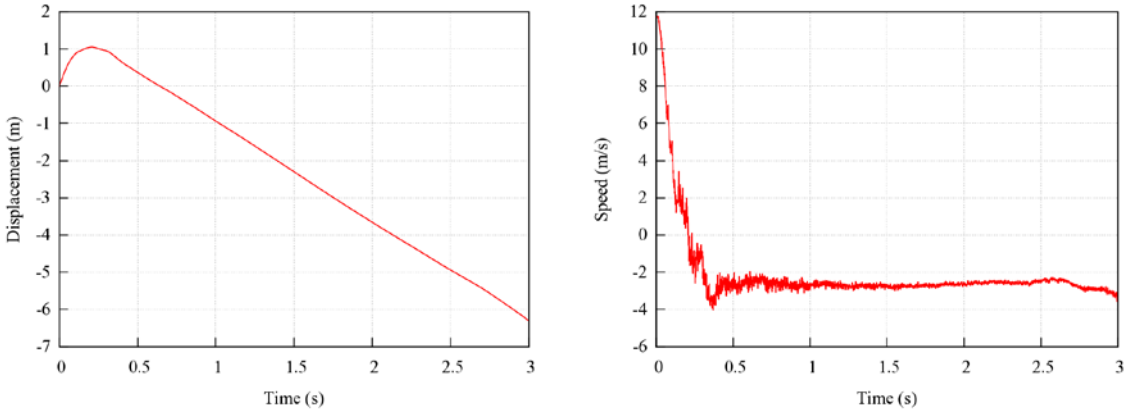

Transverse displacements Transverse speeds

Figure 4.6: Transverse displacements and speeds for Neon impacting 29-inch single-faced guardrail.

Figure 4.7 shows the displacement path of the Ford F250 impacting the front-side of the 29-inch single-faced W-beam guardrail. The Ford F250 was initially redirected parallel to the guardrail, but started to spin counterclockwise due to snagging on a guardrail post. This can be seen from the yaw angle shown in Figure 4.8 that starts to increase at 0.6 seconds. Due to the continuous spin, the vehicle went outside the exit box. The pitch and roll angles of the Ford F250 are also shown in Figure 4.8. The roll and pitch angles were less than twenty degrees in either positive or negative direction and thus passed the MASH evaluation criterion F.

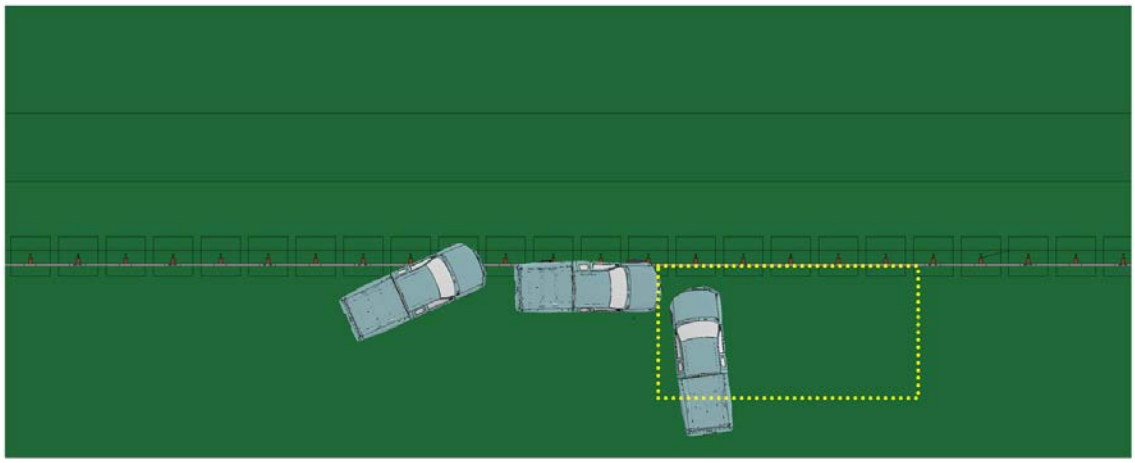

Figure 4.7: Displacement path and exit box for F250 impacting 29-inch single-faced guardrail.

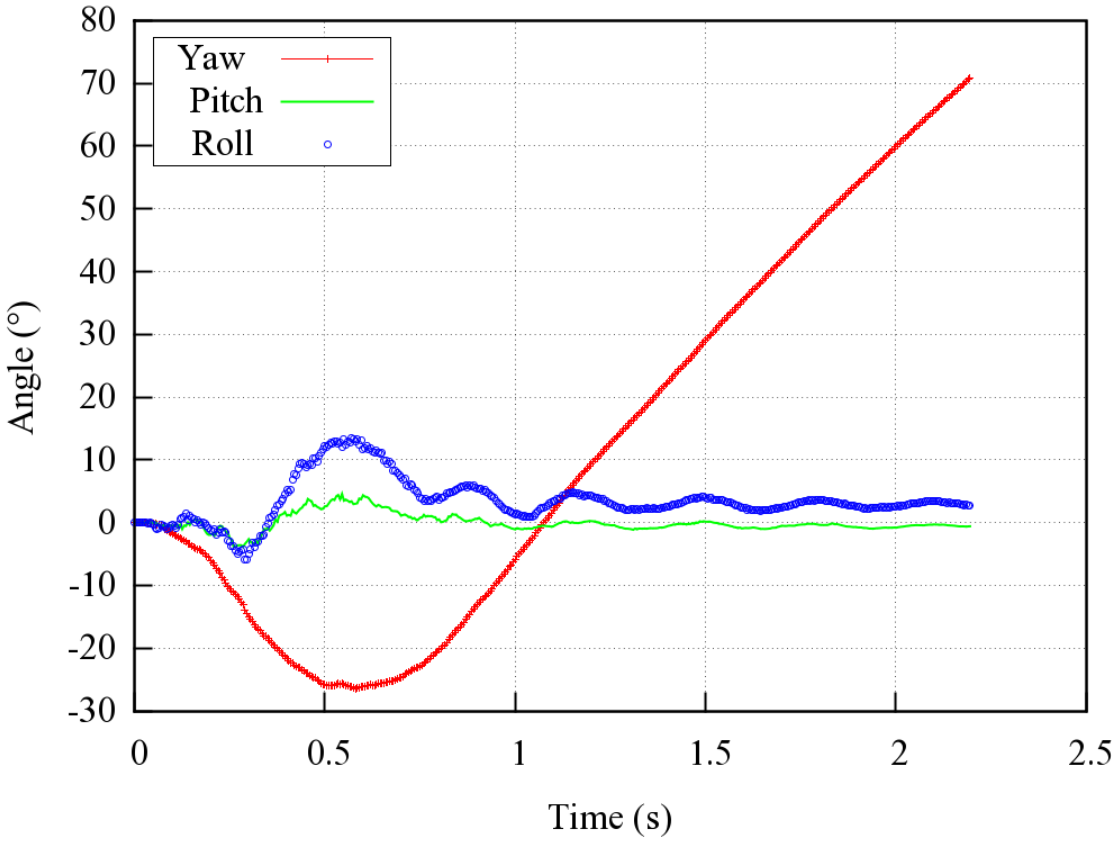

Figure 4.8: Yaw, pitch, and roll angles for F250 impacting 29-inch single-faced guardrail.

Figure 4.9 shows views of vehicle-barrier interaction at the time when the maximum deflection of the guardrail occurred. It can be seen that the damaged guardrail sections are small and localized, which serves as an indication of a relatively low impact severity. The time histories of transverse displacements and speeds measured at the CG point of the vehicle are shown in Figure 4.10. The transverse speed remained at 2 m/s towards the travel lane with spinning (i.e., loss of control of the vehicle). As seen in Figure 4.7, the vehicle has entered the travel lane, so the chance of getting involved in a secondary collision is relatively high.

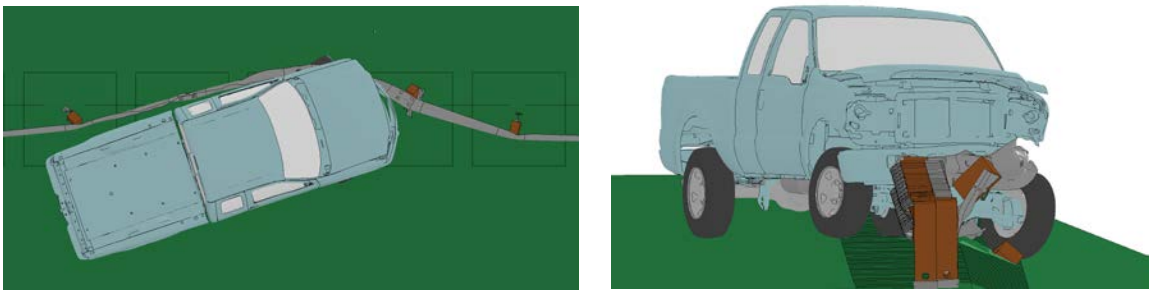

Top view Front view

Figure 4.9: Maximum deflection of W-beam for F250 impacting 29-inch single-faced guardrail.

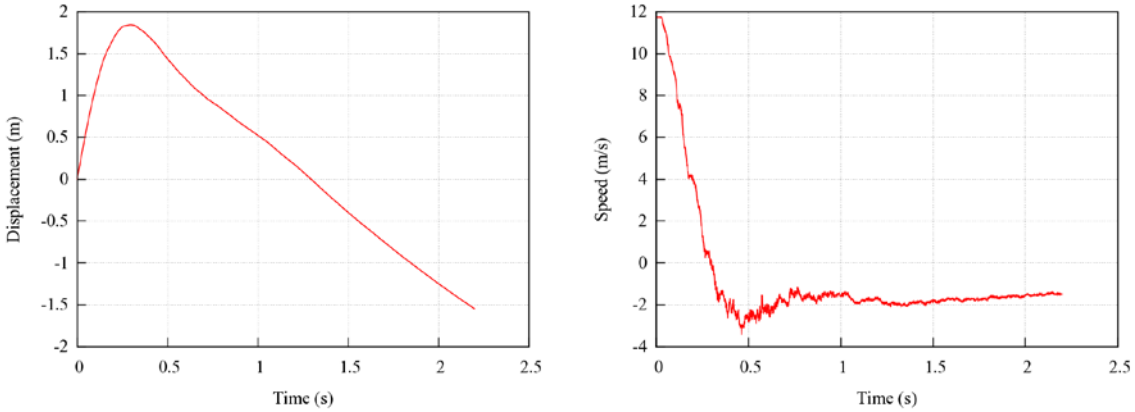

Transverse displacements Transverse speeds

Figure 4.10: Transverse displacements and speeds for F250 impacting 29-inch single-faced guardrail.

Figure 4.11 shows the displacement path of the Dodge Neon in the front-side impact on the 31-inch single-faced W-beam guardrail. The yaw, pitch, and roll angles of the Dodge Neon are shown in Figure 4.12. Similar to the case of the Dodge Neon impacting the 29-inch single-faced guardrail, the vehicle spun counterclockwise after striking and snagging on a post. The vehicle continuously spun, as seen from the continuously increasing yaw angle, and consequently went outside the exit box. The roll and pitch angles were less than twenty degrees in either positive or negative direction and thus passed the MASH evaluation criterion F.

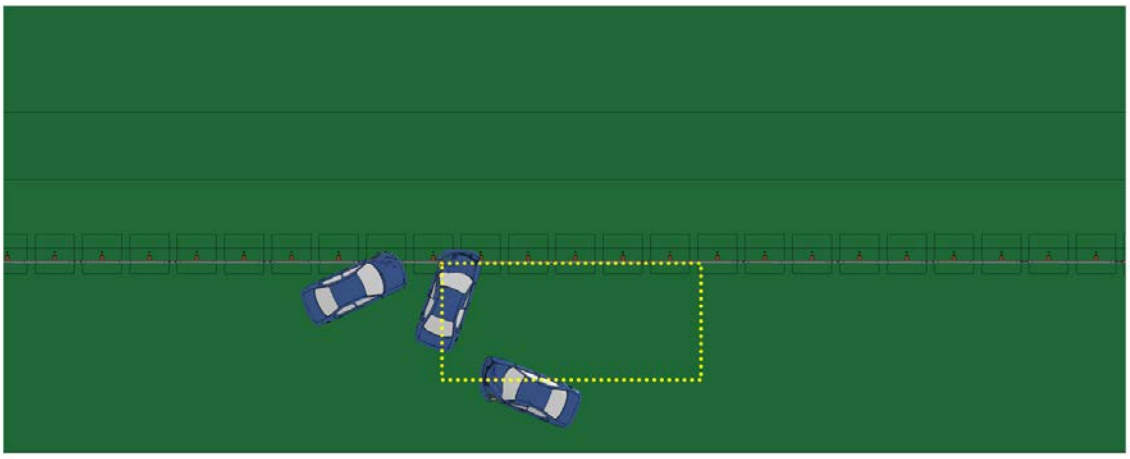

Figure 4.11: Displacement path and exit box for Neon impacting 31-inch single-faced guardrail.

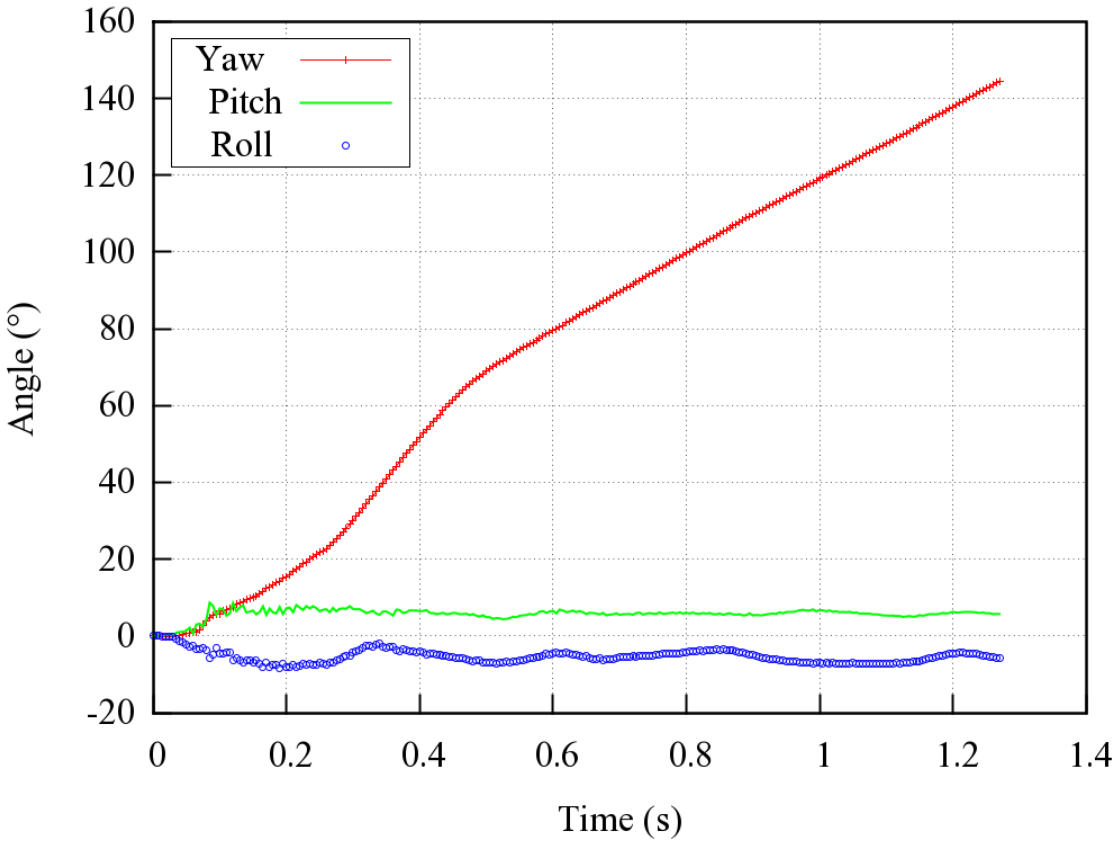

Figure 4.12: Yaw, pitch, and roll angles for Neon impacting 31-inch single-faced guardrail.

Figure 4.13 shows views of vehicle-barrier interaction at the time when the maximum deflection of the guardrail occurred. It can be seen that the damaged guardrail

sections are small and localized, similar to the case of the 29-inch single-faced guardrail under the impact of the Dodge Neon. The time histories of transverse displacements and speeds measured at the CG point of the vehicle are shown in Figure 4.14. The maximum transverse displacement of the vehicle was approximately 20% more than that seen with the 29-inch single-faced guardrail due to the vehicle under-riding the 31-inch guardrail. The transverse speed remained at 5 m/s towards the travel lane with spinning (i.e., loss of control of the vehicle), which is 2 m/s higher than seen with the 29-inch single-faced guardrail. As seen in Figure 4.11, the vehicle has entered the travel lane, so the chance of getting involved in a secondary collision is relatively high.

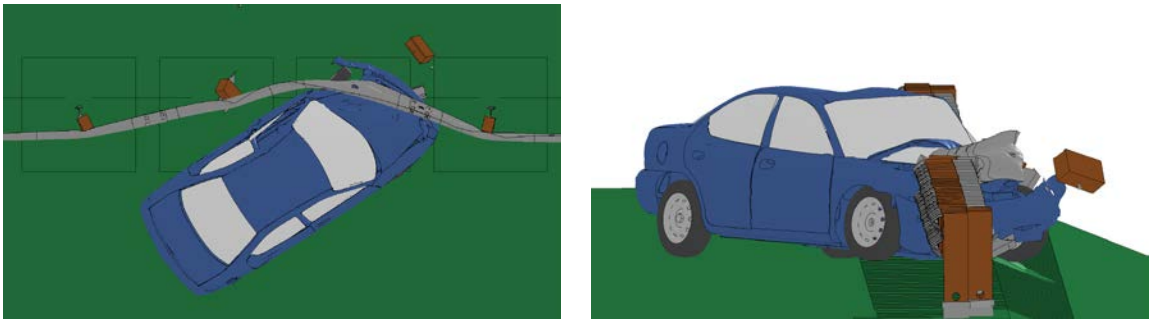

Top view Front view

Figure 4.13: Maximum deflection of W-beam for Neon impacting 31-inch single-faced guardrail.

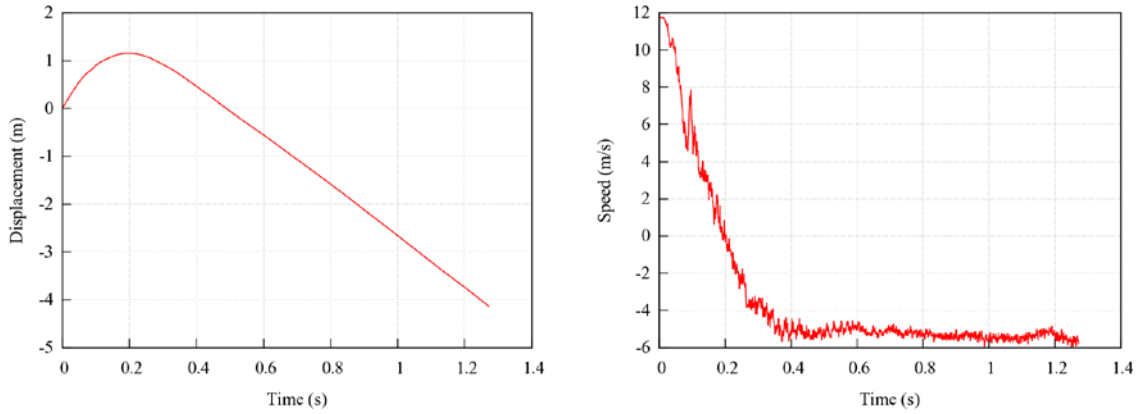

Transverse displacements Transverse speeds

Figure 4.14: Transverse displacements and speeds for Neon impacting 31-inch single-faced guardrail.

Figure 4.15 shows the displacement path of the Ford F250 impacting the 31-inch single-faced guardrail from the front-side. The yaw, pitch, and roll angles of the Ford F250 are shown in Figure 4.16. The post-impact response of the Ford F250 in this case was similar to the case of Ford F250 impacting the 29-inch guardrail in which the vehicle spun counterclockwise due to snagging and consequently went outside the exit box. The roll and pitch angles were less than twenty degrees in either positive or negative direction and thus passed the MASH evaluation criterion F.

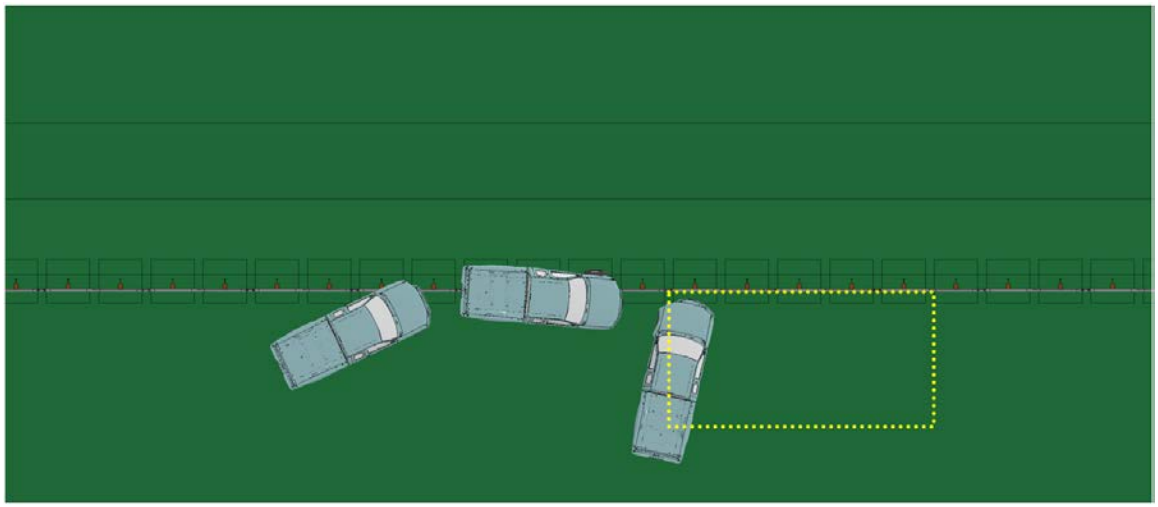

Figure 4.15: Displacement path and exit box for F250 impacting 31-inch single-faced guardrail.

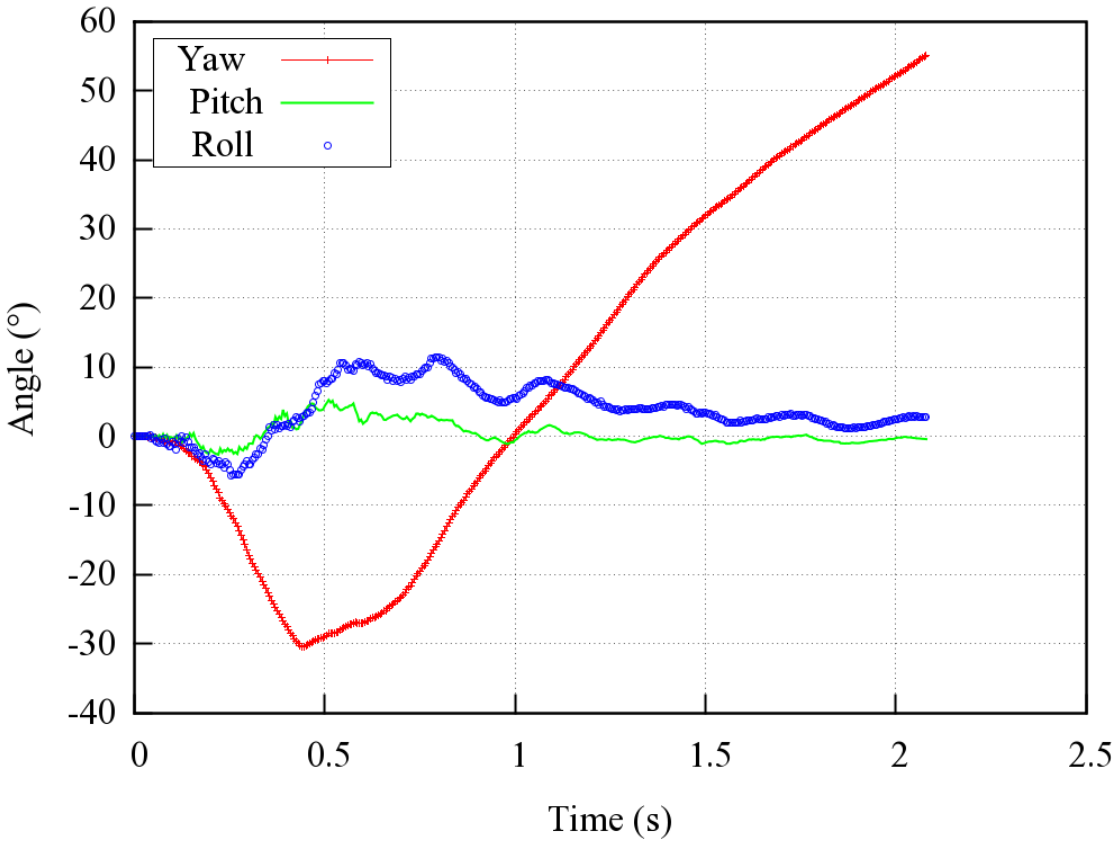

Figure 4.16: Yaw, pitch, and roll angles for F250 impacting 31-inch single-faced guardrail.

Figure 4.17 shows views of vehicle-barrier interaction at the time when the maximum deflection of the guardrail occurred. It can be seen that the damaged guardrail

sections are small and localized, similar to that of the 29-inch guardrail. The time histories of transverse displacements and speeds measured at the CG point of the vehicle are shown in Figure 4.18. The Ford F250 had a similar transverse displacement as seen with the 29-inch single-faced guardrail even with the increased barrier height. The transverse speed remained at 1 m/s towards the travel lane with spinning (i.e., loss of control of the vehicle), which was 1 m/s lower than that seen with the 29-inch single-faced guardrail. As seen in Figure 4.15, the vehicle has entered the travel lane, so the chance of getting involved in a secondary collision is relatively high.

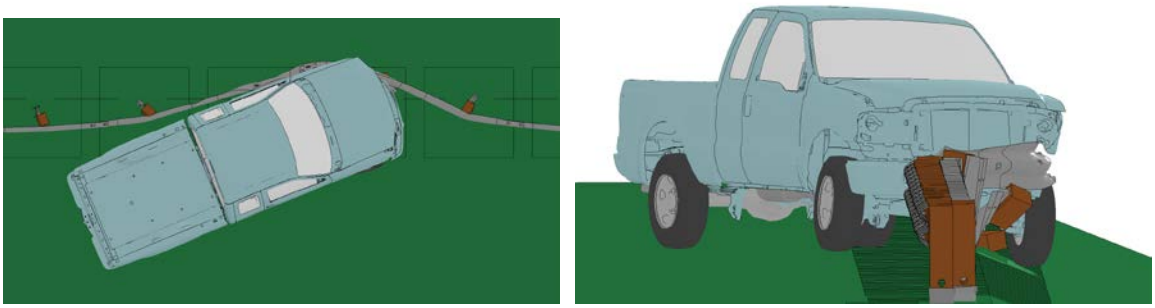

Top view Front view

Figure 4.17: Maximum deflection of W-beam for F250 impacting 31-inch single-faced guardrail.

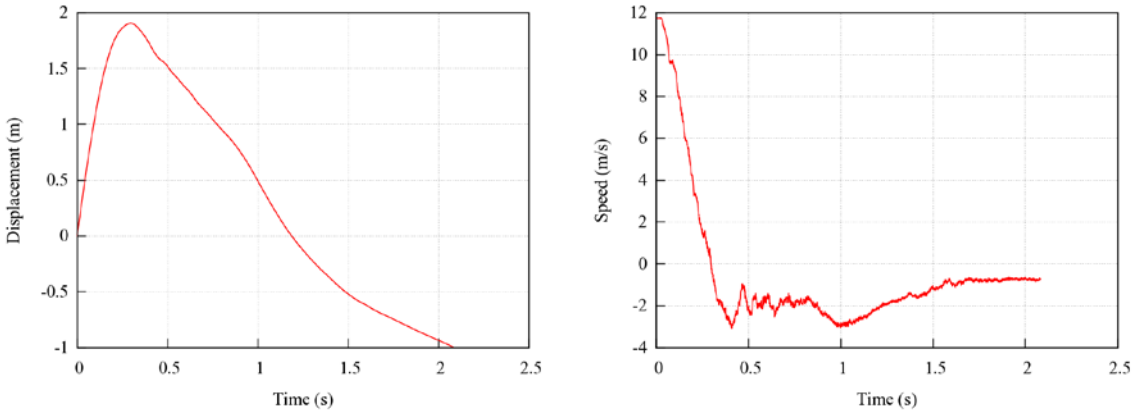

Transverse displacements Transverse speeds

Figure 4.18: Transverse displacements and speeds for F250 impacting 31-inch single-faced guardrail.

4.2 Double-faced Guardrails

The analysis of the double-faced 29- and 31-inch strong-post W-beam guardrail was performed through eight simulations of Cases 2 and 3, including both front-side and backside vehicular impacts by the 1996 Dodge Neon and the 2006 Ford F250 at MASH TL-3 conditions. Table 4.3 shows the simulation conditions and a summary of the guardrail performance in terms of post-impact vehicular responses.

Table 4.3: Simulation results for double-faced guardrails.

Impacting Side	**Guardrail Height**	**Test Vehicle**	**Test Results**
Front	29 inches	Dodge Neon	Vehicle not redirected safely by guardrail (spin-out and outside exit box)
		Ford F250	Vehicle redirected safely by guardrail (tire snagged on guardrail)
	31 inches	Dodge Neon	Vehicle not redirected safely by guardrail (spin-out and outside exit box)
		Ford F250	Vehicle not redirected safely by guardrail (outside exit box)
Back	29 inches	Dodge Neon	Vehicle not redirected safely by guardrail (roll angle greater than 75°)
		Ford F250	Vehicle not redirected safely by guardrail (spin-out and outside exit box)
	31 inches	Dodge Neon	Vehicle redirected safely by guardrail
		Ford F250	Vehicle not redirected safely by guardrail (spin-out and outside exit box)

4.2.1 Front-side Impacts on the Double-faced Guardrail

Figure 4.19 shows the displacement path of the Dodge Neon impacting the front-side of the 29-inch double-faced W-beam guardrail shown in its original shape along with the exit box denoted by the yellow rectangle. The yaw, pitch, and roll angles of the Dodge Neon are shown in Figure 4.20. The roll and pitch angles were less than twenty degrees in either positive or negative direction and thus passed the MASH evaluation criterion F. However, the vehicle had a continuously increasing yaw angle after 0.13 seconds, indicating a continuous spinning of the vehicle. Similar to its responses impacting the single-faced guardrails, the Dodge Neon snagged on the post, continuously spun counterclockwise, and consequently went outside the exit box.

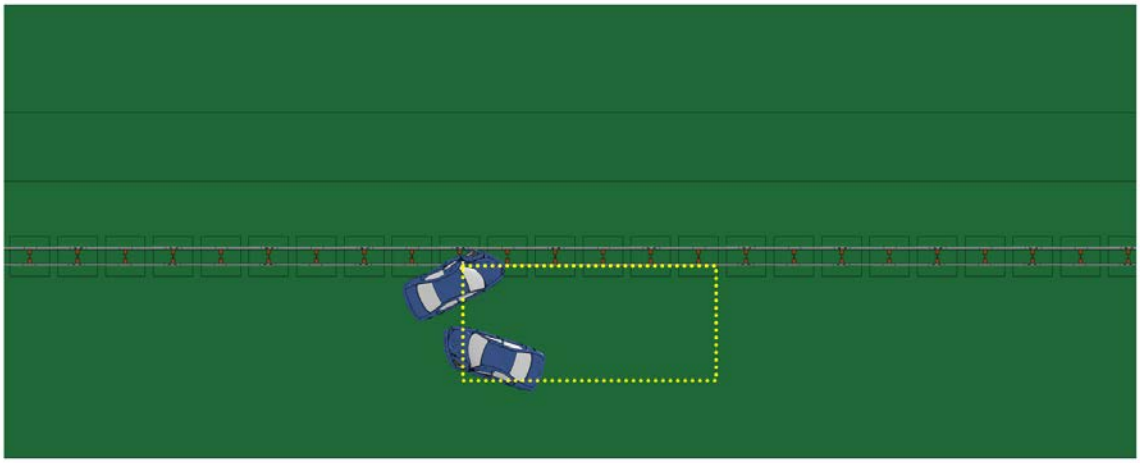

Figure 4.19: Displacement path and exit box for Neon impacting front-side of 29-inch double-faced guardrail.

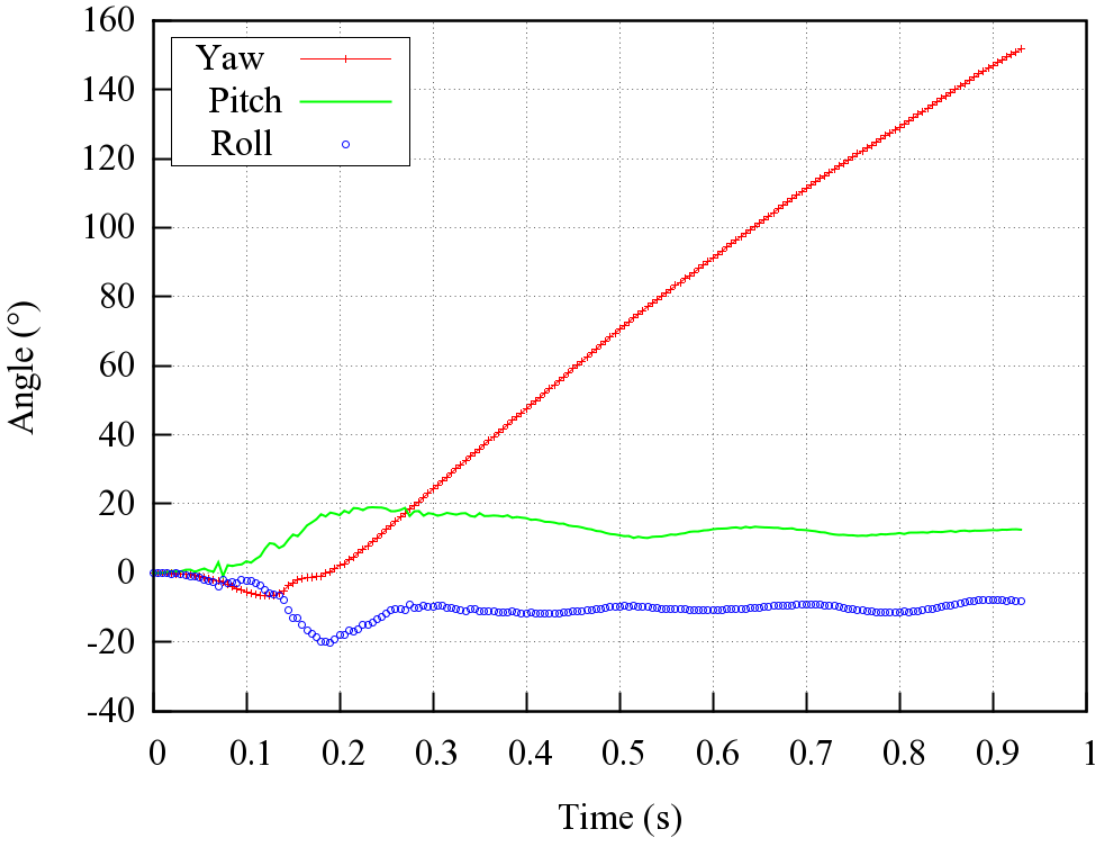

Figure 4.20: Yaw, pitch, and roll angles for Neon impacting front-side of 29-inch double-faced guardrail.

Figure 4.21 shows views of vehicle-barrier interaction at the time when the maximum deflection of the guardrail occurred. It can be seen that the damaged guardrail sections are small and localized, which serves as an indication of a relatively low impact severity. The time histories of transverse displacements and speeds measured at the CG point of the vehicle are shown in Figure 4.22. The transverse speed remained at 5 m/s towards the travel lane with spinning (i.e., loss of control of the vehicle). As seen in Figure 4.19, the vehicle has entered the travel lane, so the chance of getting involved in a secondary collision is relatively high.

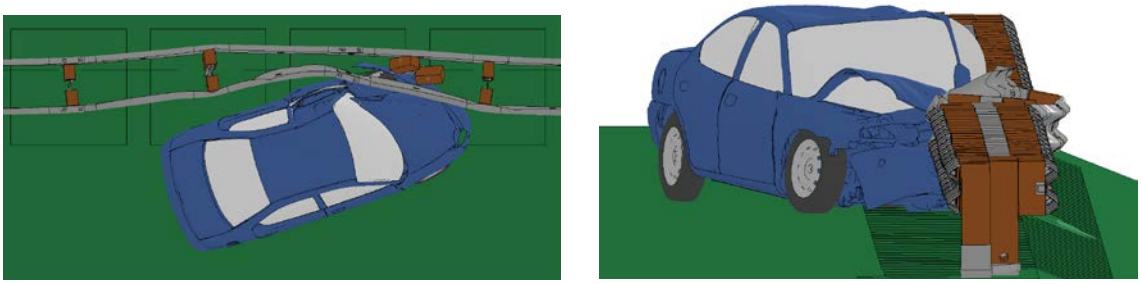

Top view Front view

Figure 4.21: Maximum deflection of W-beam for Neon impacting front-side of 29-inch double-faced guardrail.

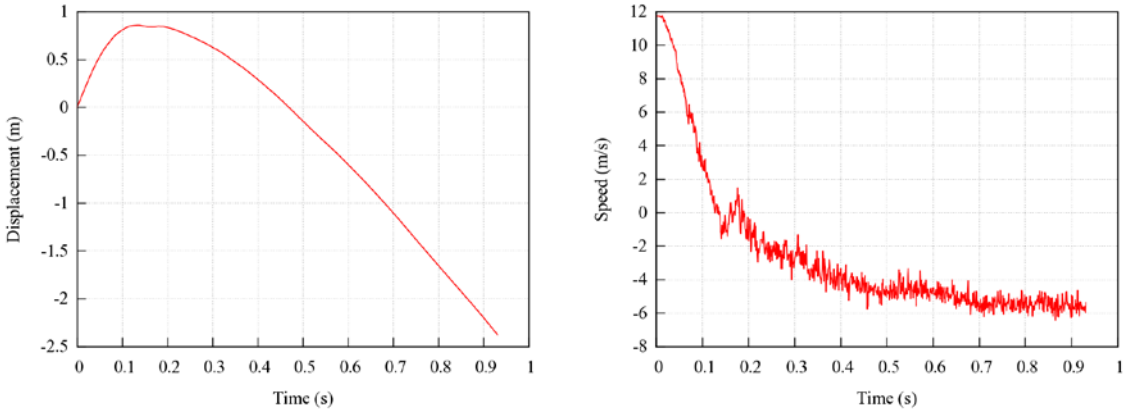

Transverse displacements Transverse speeds

Figure 4.22: Transverse displacements and speeds for Neon impacting front-side of 29-inch double-faced guardrail.

Figure 4.23 shows the displacement path of the Ford F250 impacting the front-side of the 29-inch double-faced guardrail. There is no exit box and resulting exit angle due to the tire being snagged by the W-beam and consequently the vehicle never leaving contact with the guardrail. The yaw, pitch, and roll angles of the Ford F250 are shown in Figure 4.24. The roll and pitch angles were less than ten degrees in either positive or negative direction and thus passed the MASH evaluation criterion F.

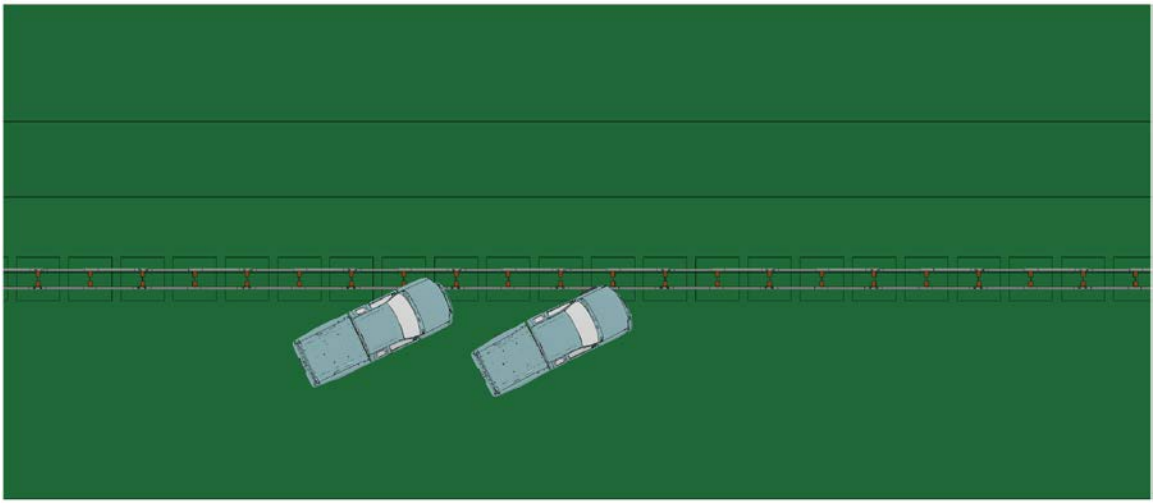

Figure 4.23: Displacement path for F250 impacting front-side of 29-inch double-faced guardrail.

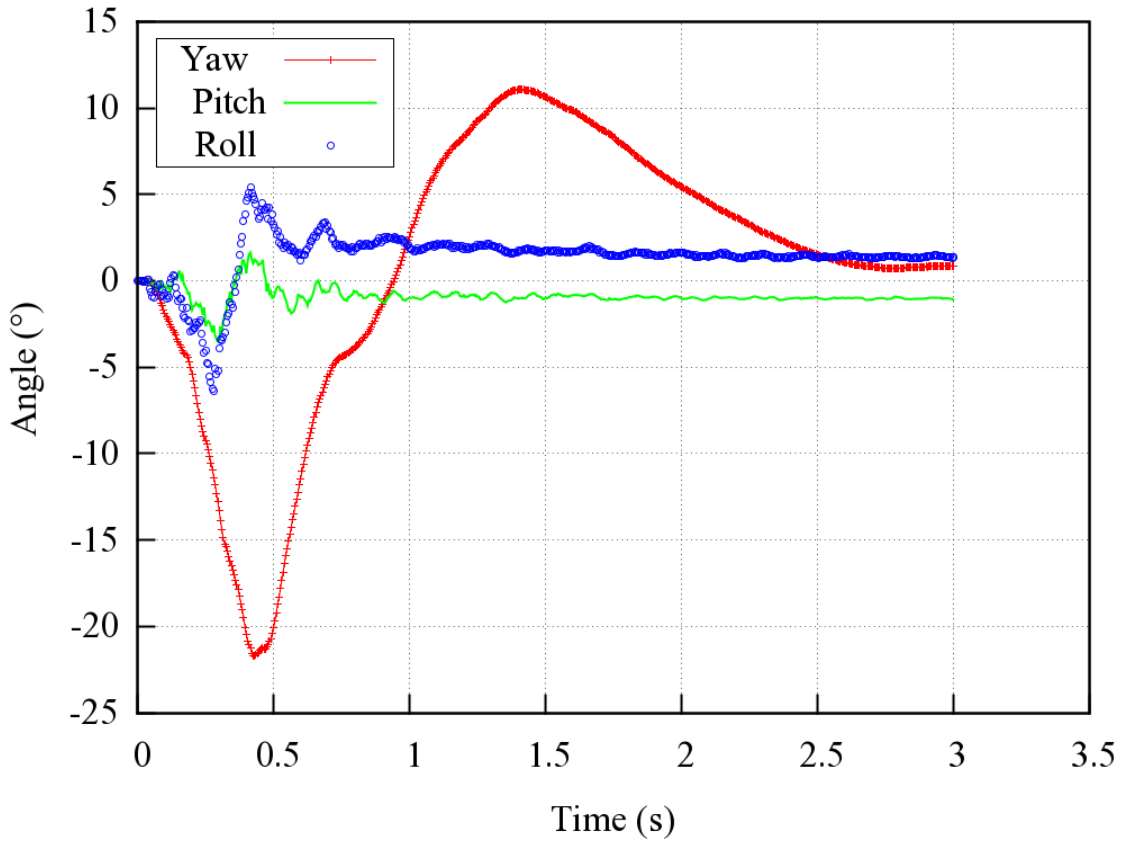

Figure 4.24: Yaw, pitch, and roll angles for F250 impacting front-side of 29-inch double-faced guardrail.

Figure 4.25 shows views of vehicle-barrier interaction at the time when the maximum deflection of the guardrail occurred. It can be seen that the damaged guardrail

sections are small and localized. The time histories of transverse displacements and speeds measured at the CG point of the vehicle are shown in Figure 4.26. The transverse speed was approximately zero, indicating no further displacement would occur towards either the travel lane or the guardrail. Even though the MASH exit box criterion was not met, the probability of having a secondary collision is small because of the vehicle being snagged by the guardrail.

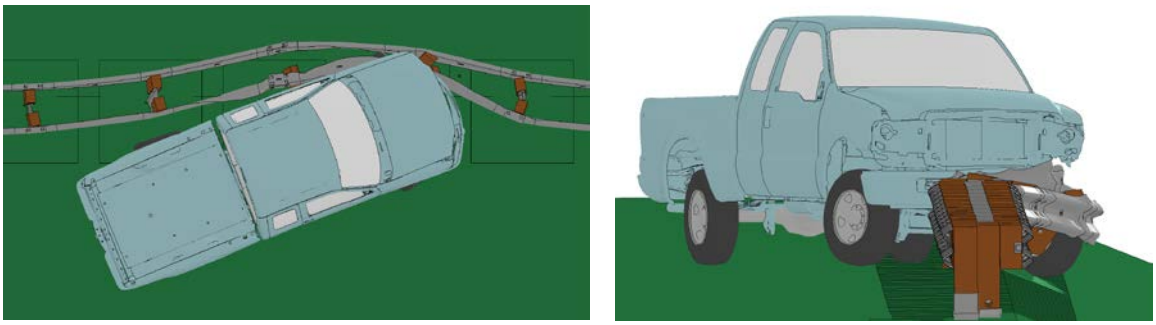

Top view Front view

Figure 4.25: Maximum deflection of W-beam for F250 impacting front-side of 29-inch double-faced guardrail.

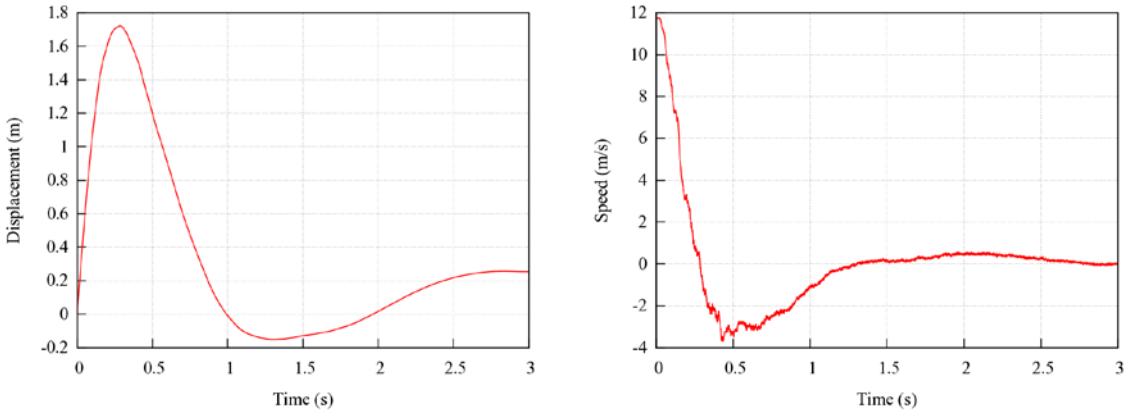

Transverse displacements Transverse speeds

Figure 4.26: Transverse displacements and speeds for F250 impacting front-side of 29-inch double-faced guardrail.

Figure 4.27 shows the displacement path of the Dodge Neon impacting the front-side of the 31-inch double-faced W-beam guardrail. The yaw, pitch, and roll angles of the Dodge Neon are shown in Figure 4.28. The roll and pitch angles were less than twenty degrees in either positive or negative direction and thus passed the MASH evaluation criterion F. However, as indicated by the continuously increasing yaw angle, the Dodge Neon had a continuous, counterclockwise spinning after impacting the guardrail and consequently went outside the exit box.

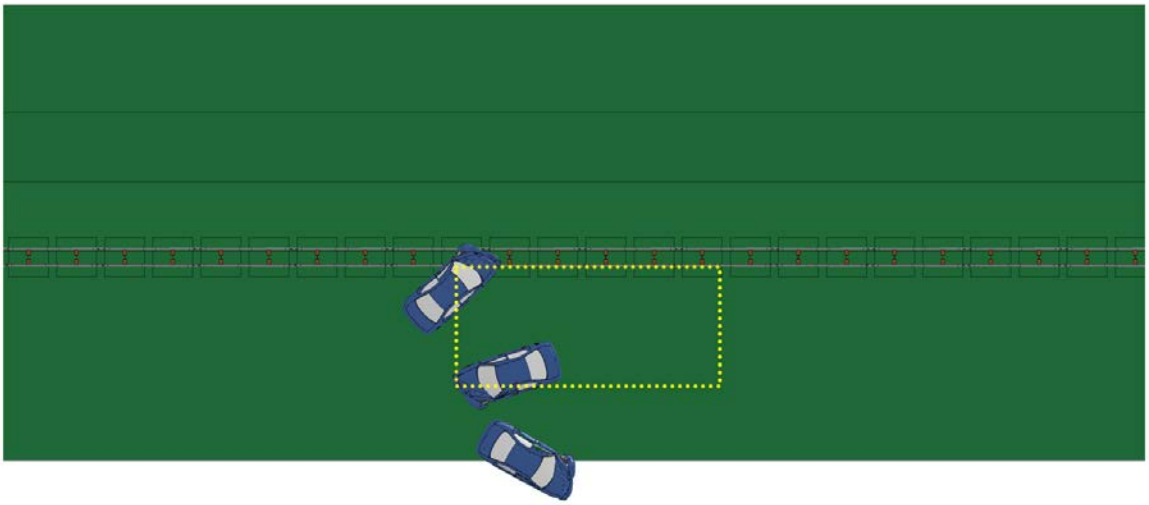

Figure 4.27: Displacement path and exit box for Neon impacting front-side of 31-inch double-faced guardrail.

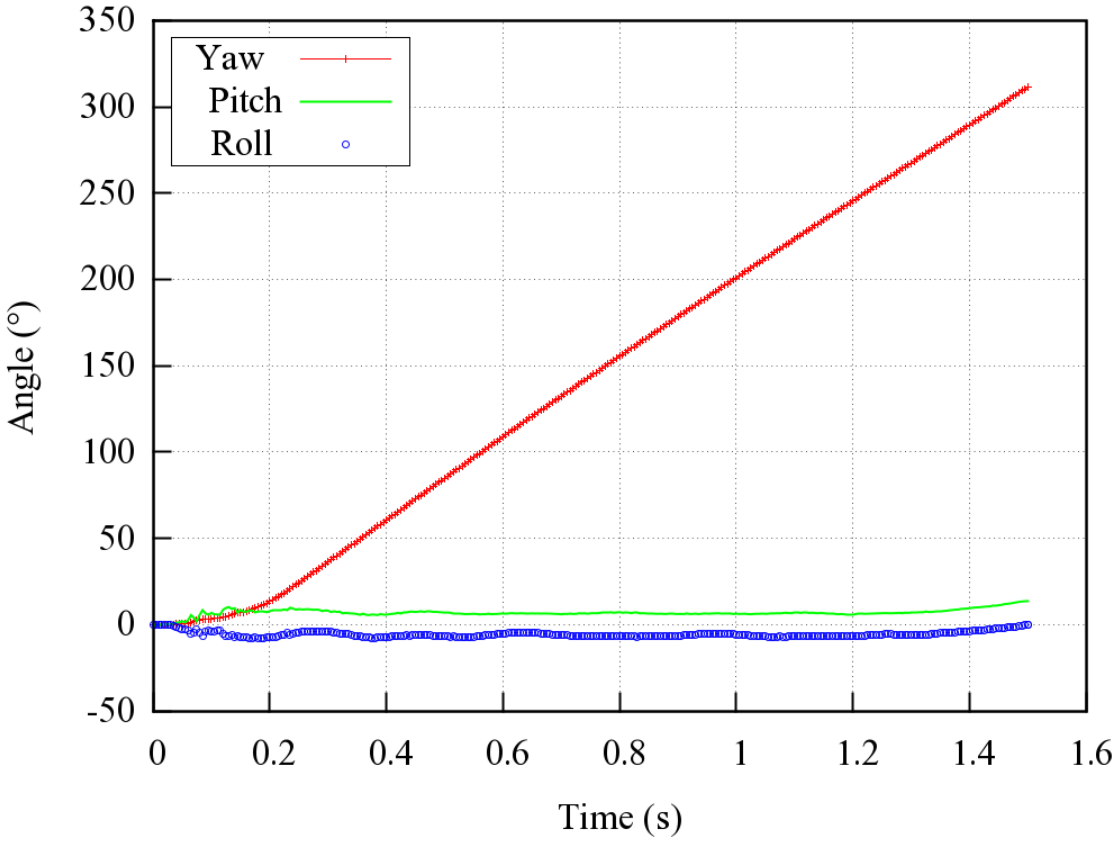

Figure 4.28: Yaw, pitch, and roll angles for Neon impacting front-side of 31-inch double-faced guardrail.

Figure 4.29 shows views of vehicle-barrier interaction at the time when the maximum deflection of the guardrail occurred, showing relatively small and localized damaged guardrail sections. The time histories of transverse displacements and speeds measured at the CG point of the vehicle are shown in Figure 4.30. The maximum transverse displacement of the Dodge Neon was larger than that seen with the 29-inch double-faced guardrail due to the vehicle under-riding the guardrail a farther distance with the increased barrier height. The transverse speed remained at 7 m/s towards the travel lane with spinning (i.e., loss of control of the vehicle), which was 2 m/s higher than that with the 29-inch double-faced guardrail. As seen in Figure 4.27, the vehicle has

entered the travel lane, so the chance of getting involved in a secondary collision is relatively high.

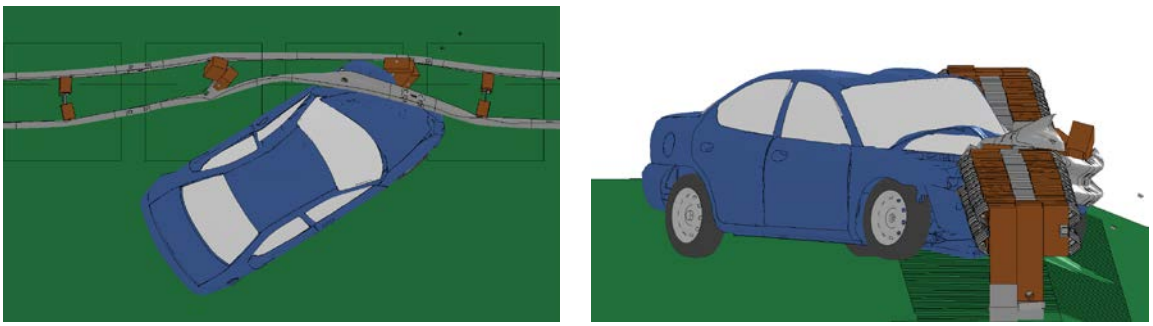

Top view Front view

Figure 4.29: Maximum deflection of W-beam for Neon impacting front-side of 31-inch double-faced guardrail.

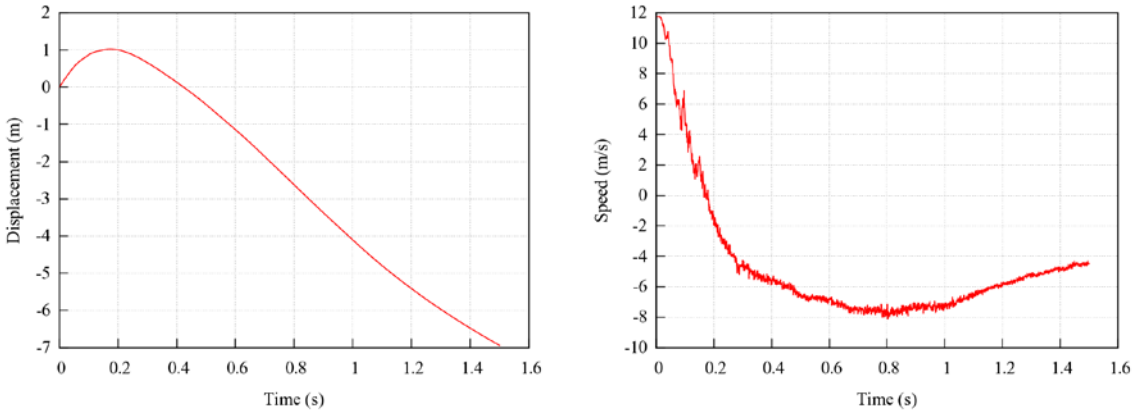

Transverse displacements Transverse speeds

Figure 4.30: Transverse displacements and speeds for Neon impacting front-side of 31-inch double-faced guardrail.

Figure 4.31 shows the displacement path of the Ford F250 impacting the front-side of the 31-inch double-faced W-beam guardrail and the yaw, pitch, and roll angles of the Ford F250 are shown in Figure 4.32. The exit angle of the Ford F250 was determined to be 5°, which was calculated using the impact angle (i.e., 25°) and the yaw angle at exit (i.e., 30°). The roll and pitch angles were less than ten degrees in either positive or

negative direction and thus passed the MASH evaluation criterion F. Unlike the 29-inch double-faced guardrail where the vehicle was snagged by the guardrail, the 31-inch double-faced guardrail was able to redirect the Ford F250 to be parallel to the guardrail. However, due to the existence of a counterclockwise rotation, the vehicle eventually went out of the exit box.

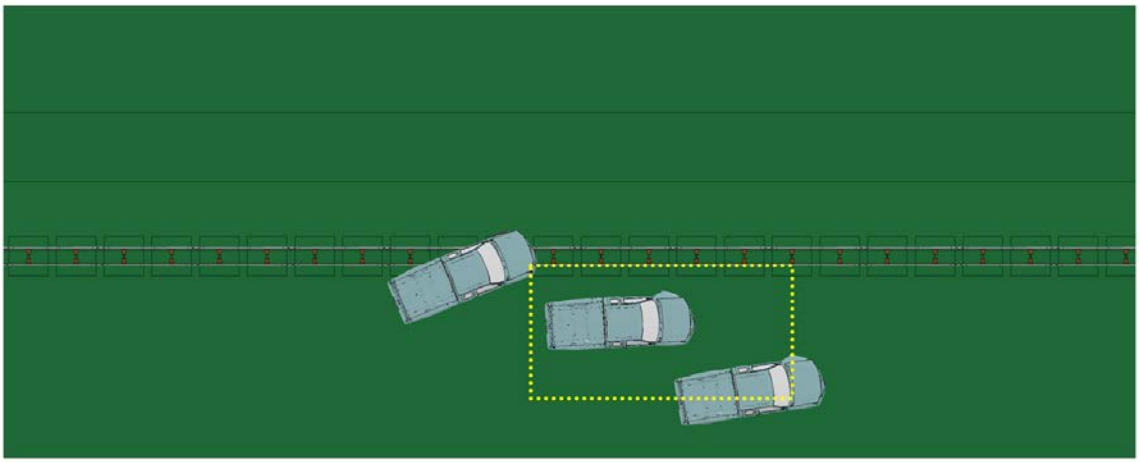

Figure 4.31: Displacement path for F250 impacting front-side of 31-inch double-faced guardrail.

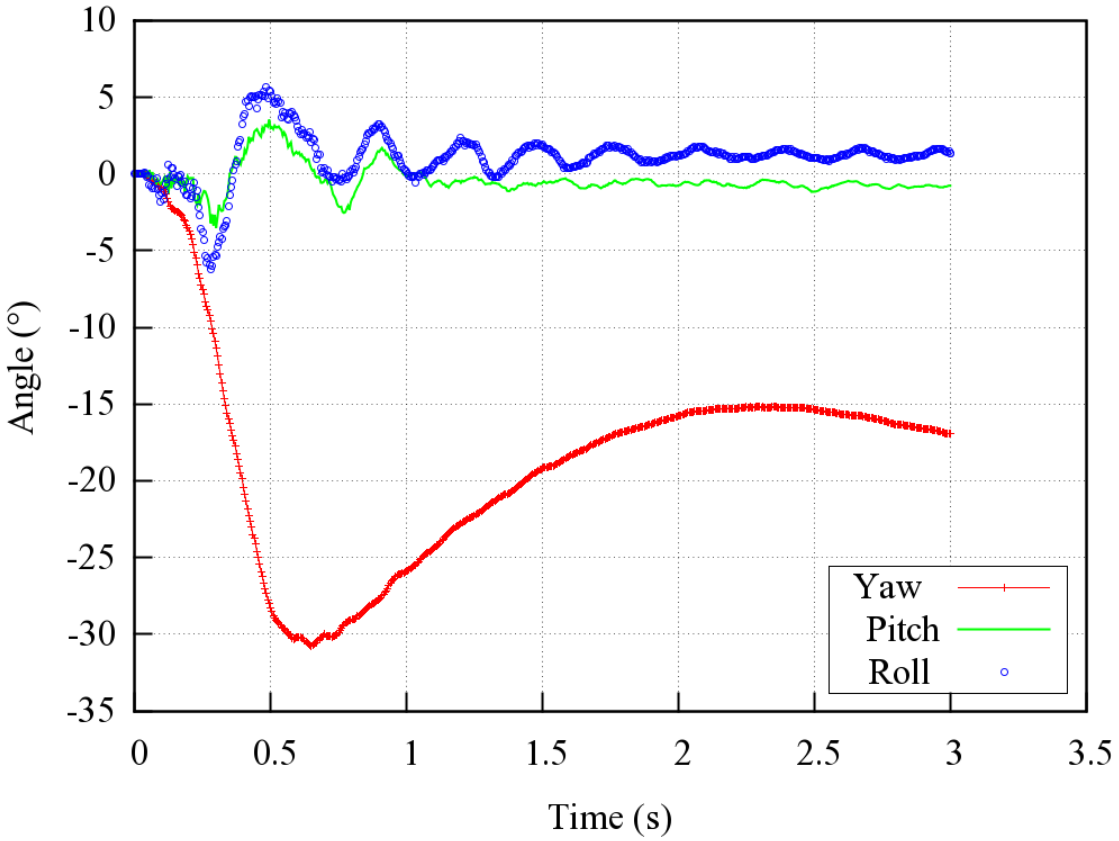

Figure 4.32: Yaw, pitch, and roll angles for F250 impacting front-side of 31-inch double-faced guardrail.

Figure 4.33 shows views of vehicle-barrier interaction at the time when the maximum deflection of the guardrail occurred. It can be seen that the damaged guardrail sections are small and localized as seen in the previous cases. The time histories of transverse displacements and speeds measured at the CG point of the vehicle are shown in Figure 4.34. The Ford F250 had a similar transverse displacement as seen with the 29-inch double-faced guardrail even with the increased barrier height. The transverse speed remained at 1 m/s towards the travel lane with spinning (i.e., loss of control of the vehicle). As seen in Figure 4.31, the vehicle has entered the travel lane, so the chance of getting involved in a secondary collision is relatively high.

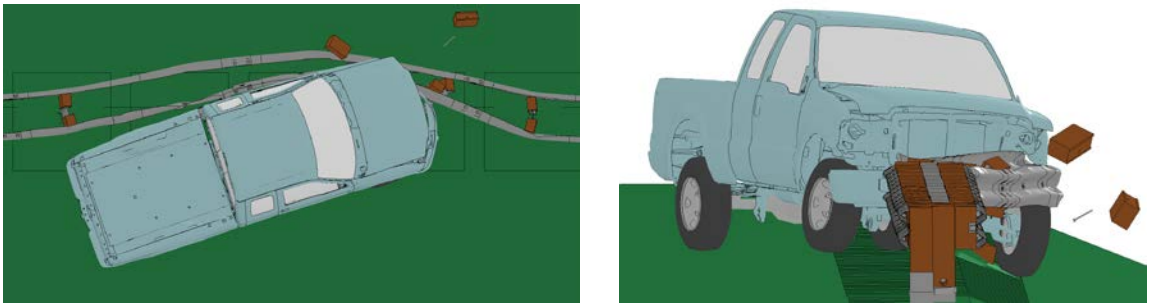

Top view Front view

Figure 4.33: Maximum deflection of W-beam for F250 impacting front-side of 31-inch double-faced guardrail.

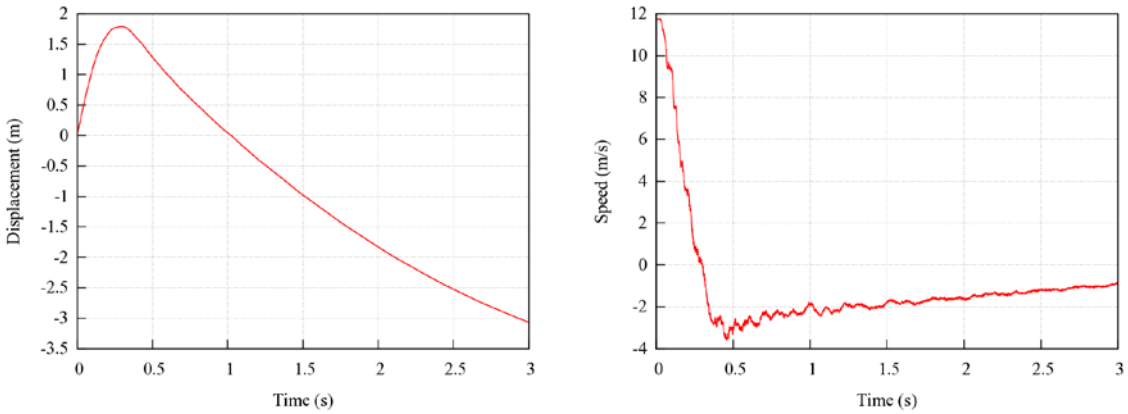

Transverse displacements Transverse speeds

Figure 4.34: Transverse displacements and speeds for F250 impacting front-side of 31-inch double-faced guardrail.

4.2.2 Backside Impacts on the Double-faced Guardrail

Figure 4.35 shows the displacement path of the Dodge Neon impacting the 29-inch double-faced guardrail from the backside. Given the large distance from the guardrail to the travel lane where the vehicle ran off, the exit box (denoted by the yellow rectangle) for a backside impact was only used as a convenient indicator of the vehicle's relative post-impact positions. The yaw, pitch, and roll angles of the Dodge Neon are shown in Figure 4.36. Although the exit angle of the Dodge Neon was determined to be

only 5°, the roll angle was greater than 75°, indicating a rollover of the vehicle and thus failed the MASH evaluation criterion F.

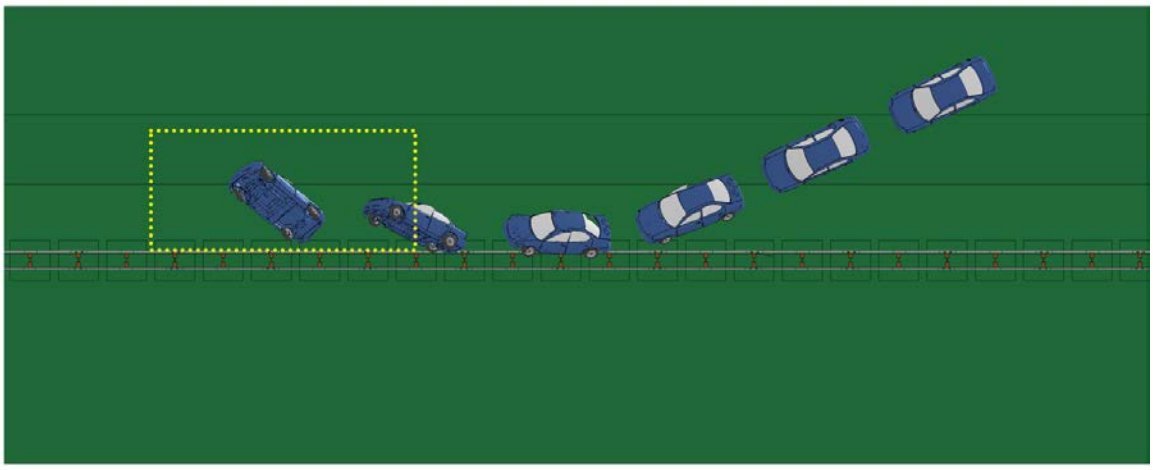

Figure 4.35: Displacement path and exit box for Neon impacting backside of 29-inch double-faced guardrail.

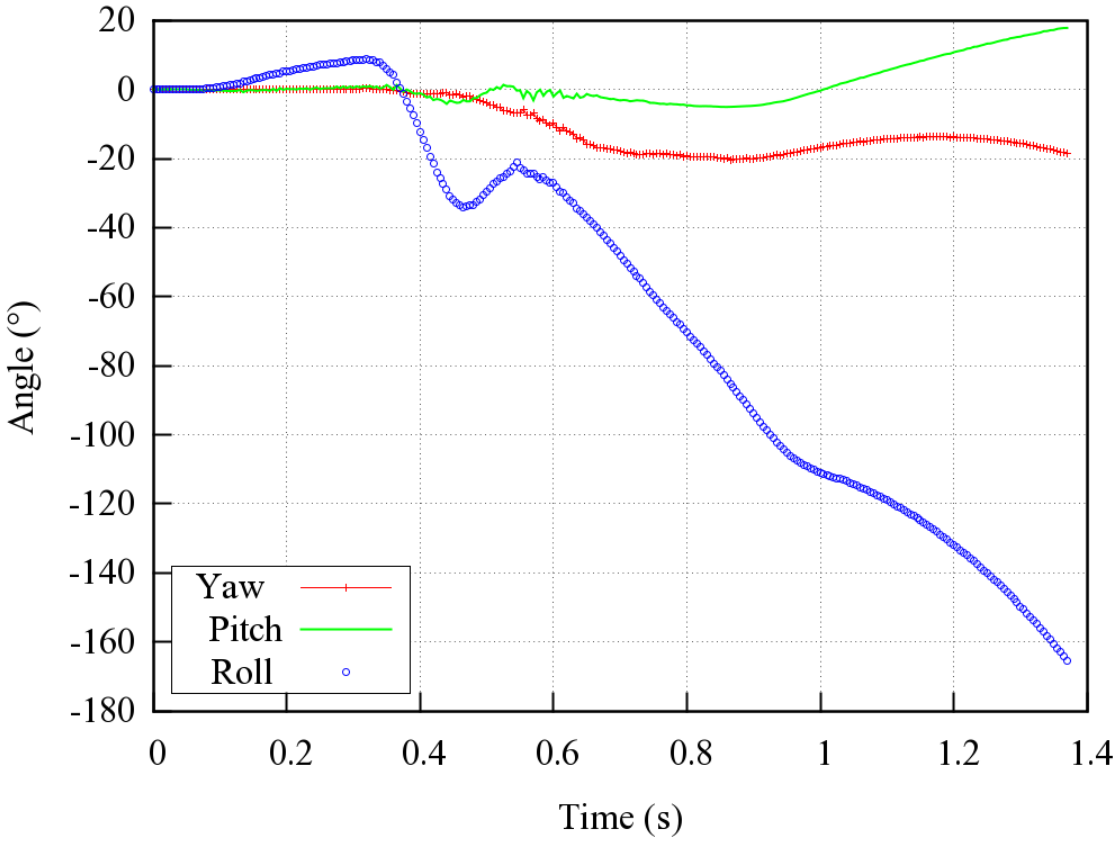

Figure 4.36: Yaw, pitch, and roll angles for Neon impacting backside of 29-inch double-faced guardrail.

Figure 4.37 shows views of vehicle-barrier interaction at the time when the maximum deflection of the guardrail occurred. It can be seen that the damaged guardrail sections are small and localized, which serves as an indication of a relatively low impact severity. The time histories of transverse displacements and speeds measured at the CG point of the vehicle are shown in Figure 4.38. The transverse speed remained at 3 m/s towards the median with rolling (i.e., loss of control of the vehicle). As seen in Figure 4.35, the vehicle rolled over towards the center of the median and would result in significant risk of occupant injury/fatality.

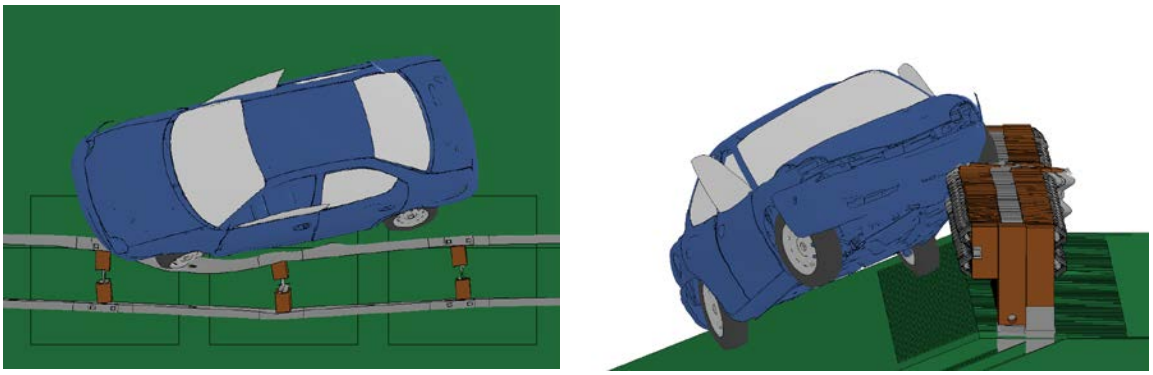

Top view Front view

Figure 4.37: Maximum deflection of W-beam for Neon impacting backside of 29-inch double-faced guardrail.

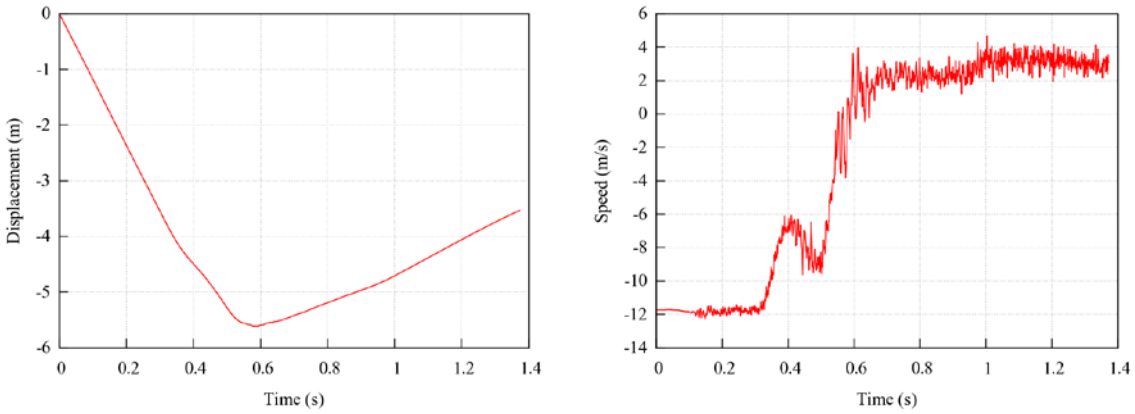

Transverse displacements Transverse speeds

Figure 4.38: Transverse displacements and speeds for Neon impacting backside of 29-inch double-faced guardrail.

Figure 4.39 shows the displacement path of the Ford F250 impacting the backside of the 29-inch double-faced guardrail. Although the vehicle was contained within the sloped median, the vehicle experienced significant rotation due to snagging on the post. The yaw, pitch, and roll angles of the Ford F250 are shown in Figure 4.40. The roll and pitch angles were less than thirty degrees in either positive or negative direction and thus passed the MASH evaluation criterion F. However, the vehicle continuously spun, as seen from the continuously increasing yaw angle, and consequently went outside the exit box.

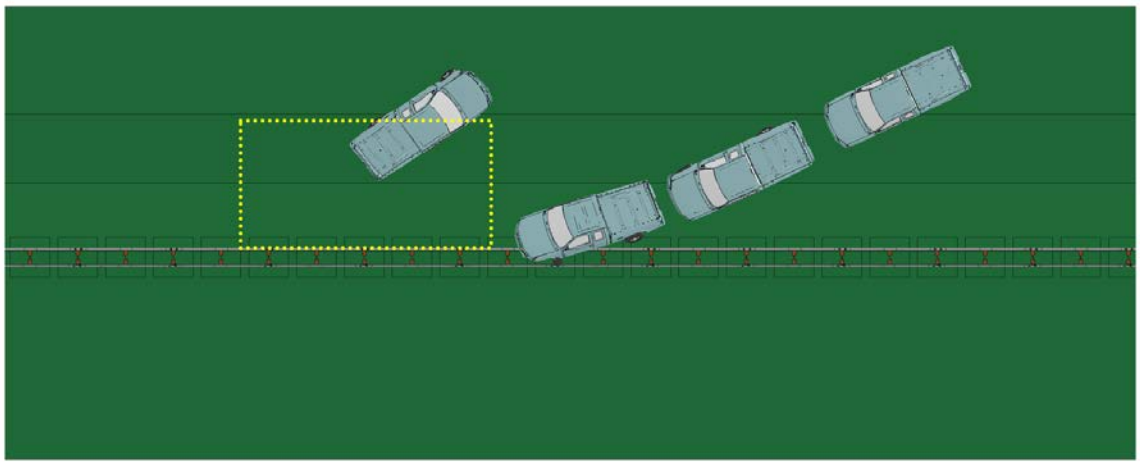

Figure 4.39: Displacement path for F250 impacting backside of 29-inch double-faced guardrail.

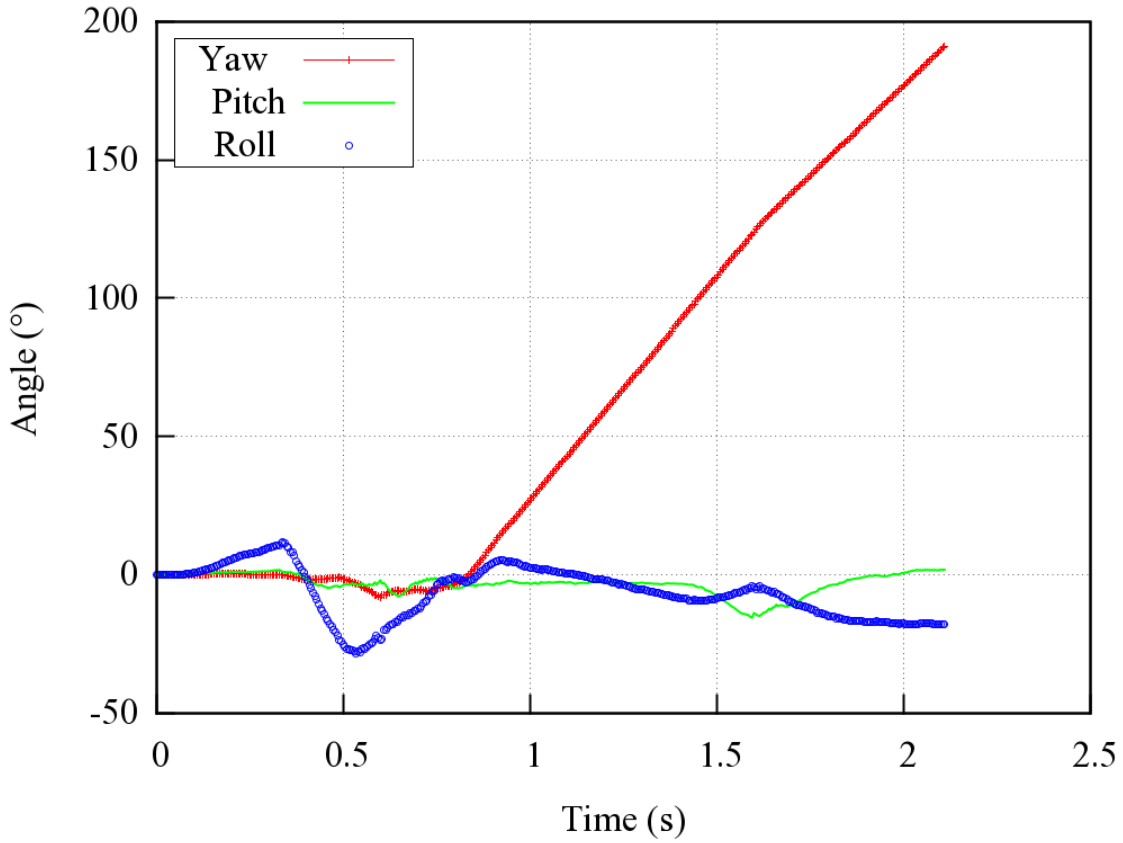

Figure 4.40: Yaw, pitch, and roll angles for F250 impacting backside of 29-inch double-faced guardrail.

Figure 4.41 shows views of vehicle-barrier interaction at the time when the maximum deflection of the guardrail occurred. It can be seen that the damaged guardrail

sections are small and localized, which serves as an indication of a relatively low impact severity. The time histories of transverse displacements and speeds measured at the CG point of the vehicle are shown in Figure 4.42. The transverse speed started at 5 m/s towards the median and then became 2 m/s towards the travel lane after impacting the median, all with spinning (i.e., loss of control of the vehicle). As seen in Figure 4.39, the vehicle has entered the travel lane, so the chance of getting involved in a secondary collision is relatively high.

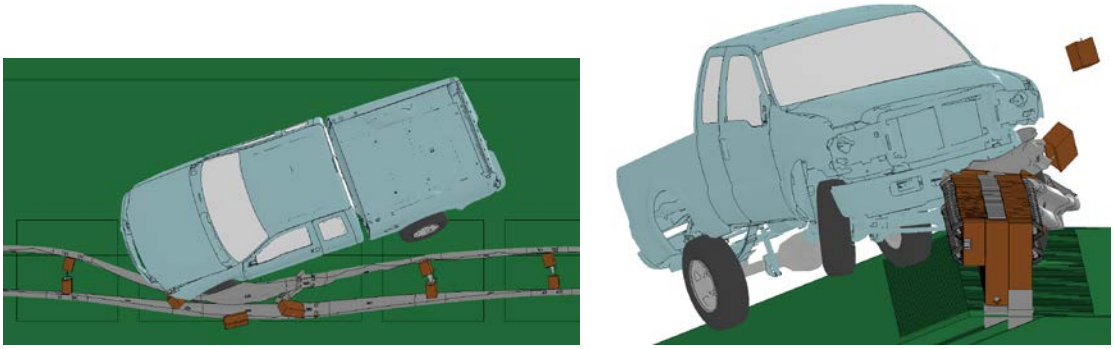

Top view Front view

Figure 4.41: Maximum deflection of W-beam for F250 impacting backside of 29-inch double-faced guardrail.

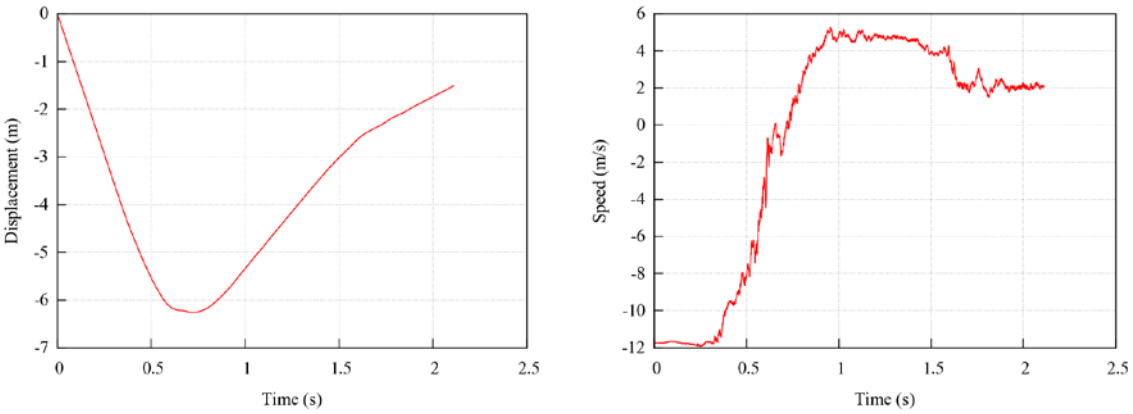

Transverse displacements Transverse speeds

Figure 4.42: Transverse displacements and speeds for F250 impacting backside of 29-inch double-faced guardrail.

Figure 4.43 shows the displacement path of the Dodge Neon impacting the backside of the 31-inch double-faced guardrail. It can be seen that the Dodge Neon was safely redirected and the exit box criterion was satisfied. The yaw, pitch, and roll angles of the Dodge Neon are shown in Figure 4.44. The exit angle of the Dodge Neon was determined to be 10° using the impact angle (i.e., 25°) and the yaw angle at exit (i.e., 35°). The roll and pitch angles were less than forty degrees in either positive or negative direction and thus passed the MASH evaluation criterion F.

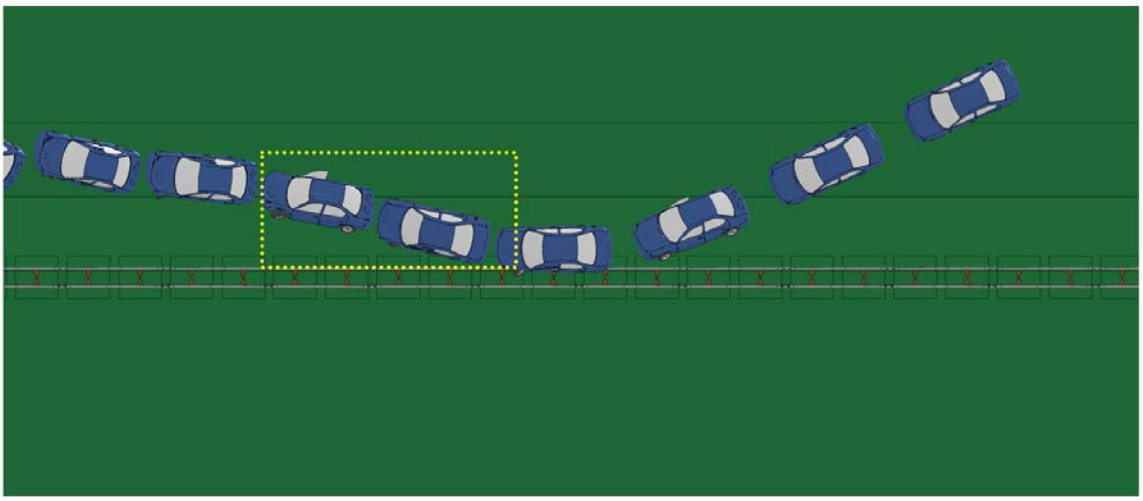

Figure 4.43: Displacement path and exit box for Neon impacting backside of 31-inch double-faced guardrail.

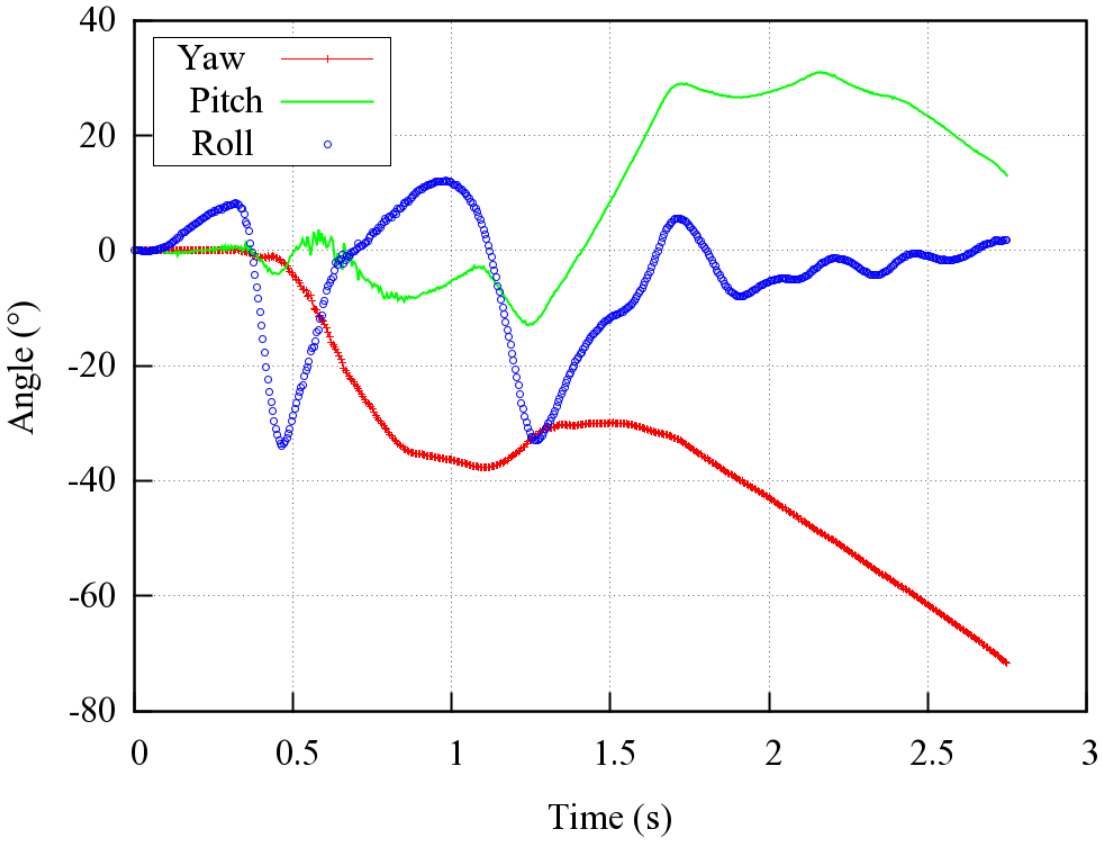

Figure 4.44: Yaw, pitch, and roll angles for Neon impacting backside of 31-inch double-faced guardrail.

Figure 4.45 shows views of vehicle-barrier interaction at the time when the maximum deflection of the guardrail occurred. It can be seen that the damaged guardrail sections are very small compared to that in the front-side impact by the same vehicle. The time histories of transverse displacements and speeds measured at the CG point of the vehicle are shown in Figure 4.46. The transverse speed started at 3 m/s towards the median, which is similar to the 29-inch double-faced guardrail, and then became 1 m/s towards the travel lane after impacting the median.

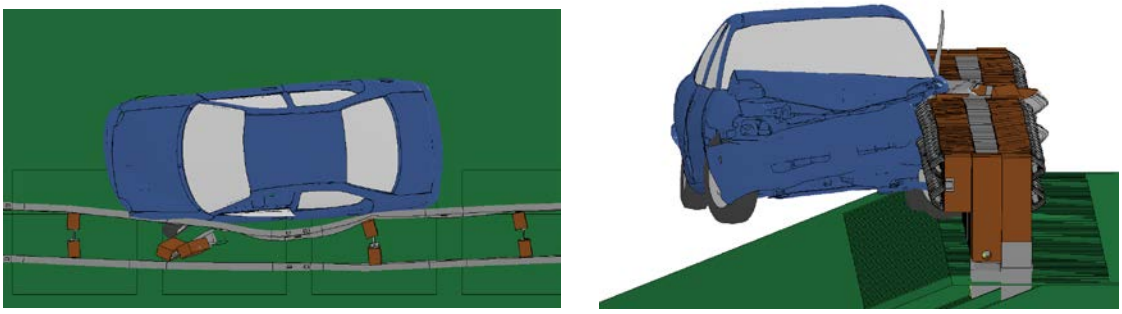

Top view Front view

Figure 4.45: Maximum deflection of W-beam for Neon impacting backside of 31-inch double-faced guardrail.

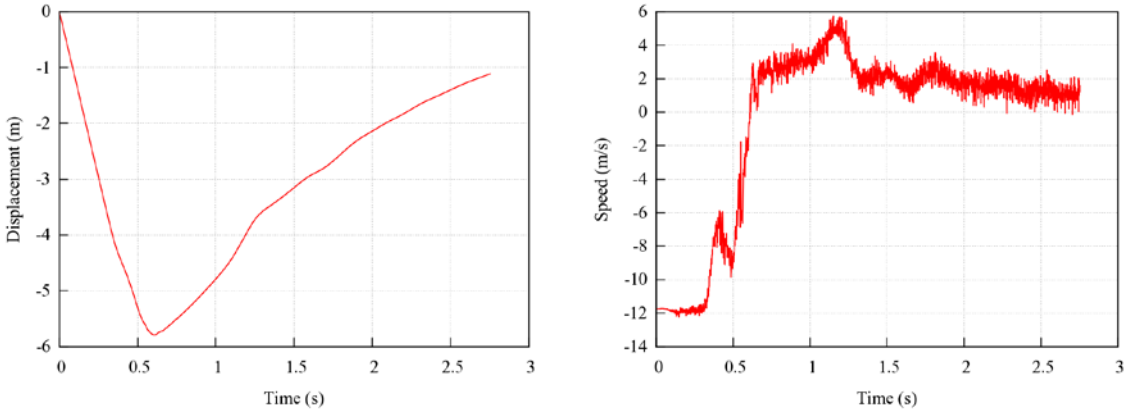

Transverse displacements Transverse speeds

Figure 4.46: Transverse displacements and speeds for Neon impacting backside of 31-inch double-faced guardrail.

Figure 4.47 shows the displacement path of the Ford F250 impacting the backside of the 31-inch double-faced guardrail. Similar to the backside impact on the 29-inch guardrail, the Ford F250 snagged on a guardrail post and spun counterclockwise, though the rotational angle was smaller than that with the 29-inch guardrail. The yaw, pitch, and roll angles of the Ford F250 are shown in Figure 4.48. The roll and pitch angles were less than thirty degrees in either positive or negative direction and thus passed the MASH evaluation criterion F. The continuously increasing yaw angle indicated a continuous

spinning of the vehicle, as seen in Figure 4.47, and consequently going outside the exit box.

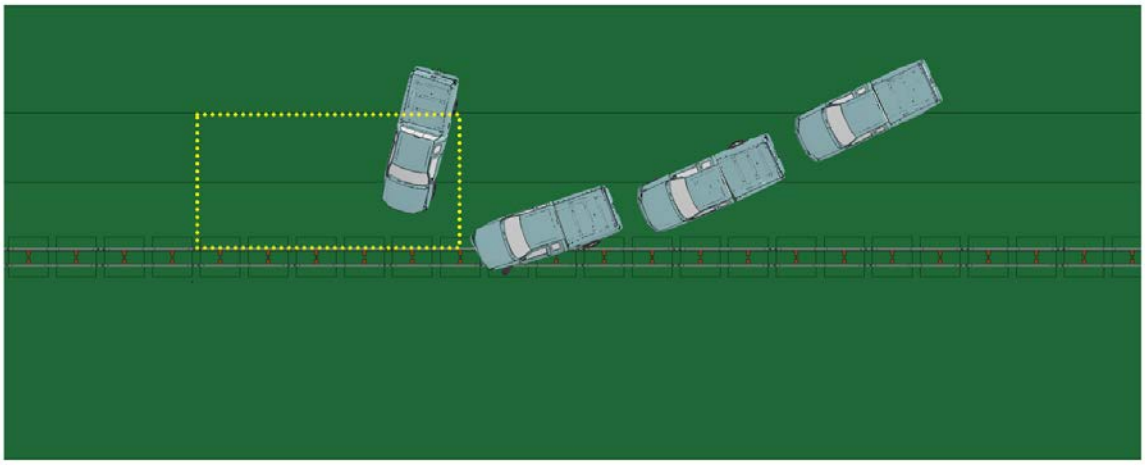

Figure 4.47: Displacement path for F250 impacting backside of 31-inch double-faced guardrail.

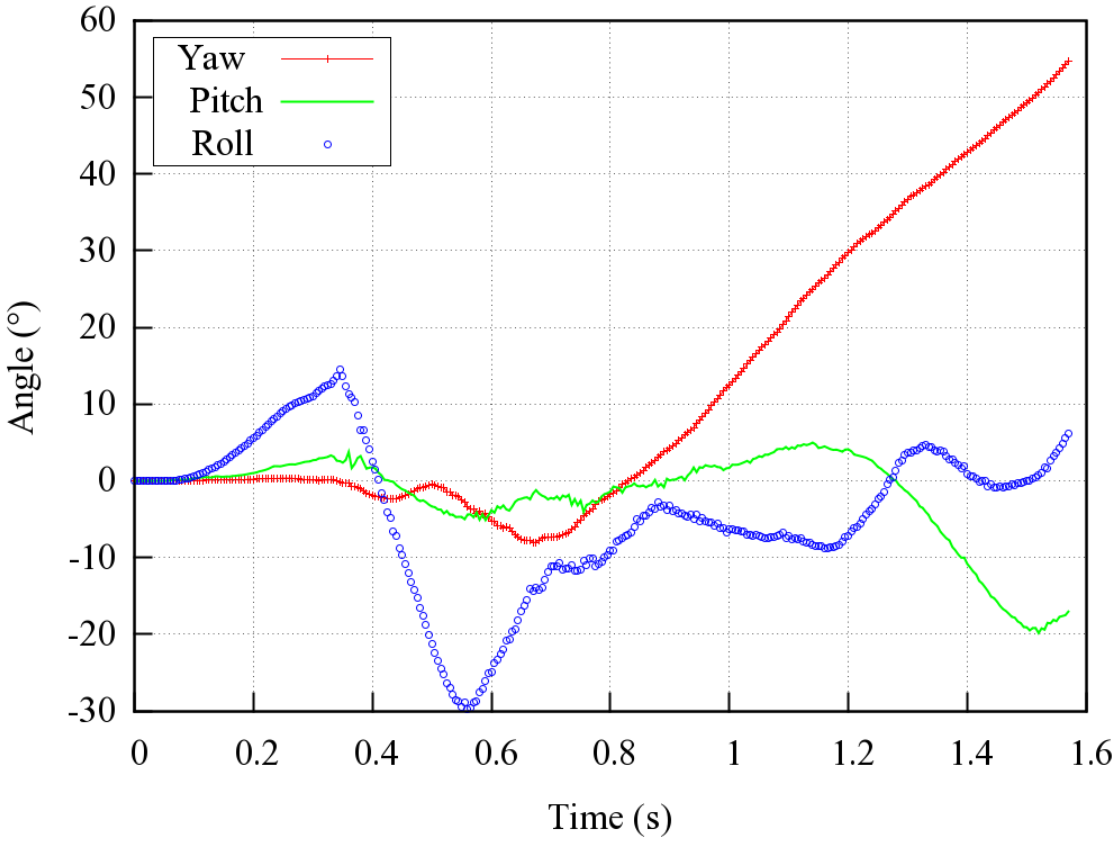

Figure 4.48: Yaw, pitch, and roll angles for F250 impacting backside of 31-inch double-faced guardrail.

Figure 4.49 shows views of vehicle-barrier interaction at the time when the maximum deflection of the guardrail occurred. It can be seen that the damaged guardrail sections are small and localized, which serves as an indication of a relatively low impact severity. The time histories of transverse displacements and speeds measured at the CG point of the vehicle are shown in Figure 4.50. The Ford F250 had a larger transverse displacement than that with the 29-inch double-faced guardrail. The transverse speed started at 5 m/s towards the median, which was similar to the 29-inch double-faced guardrail, and then became 4 m/s towards the travel lane after impacting the median. As seen in Figure 4.47, the vehicle has entered the travel lane, so the chance of getting involved in a secondary collision is relatively high. The simulation results for both 29-

and 31-inch double-faced guardrail were very similar in terms of post-impact vehicular responses.

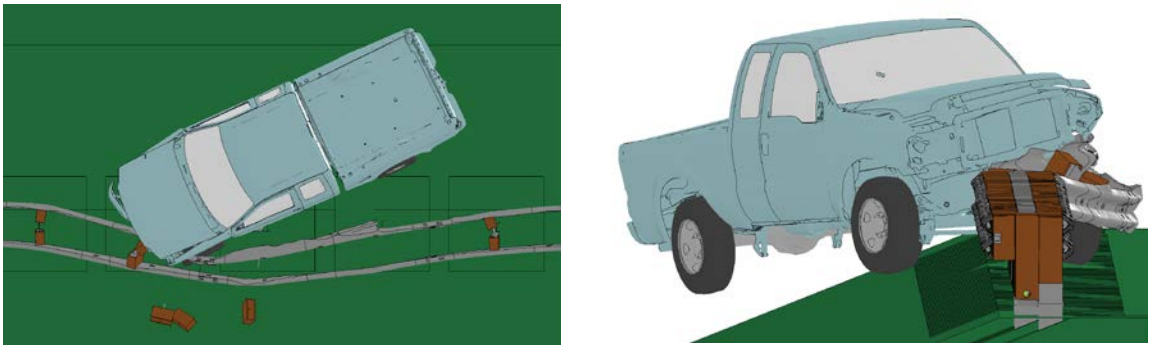

Top view Front view

Figure 4.49: Maximum deflection of W-beam for F250 impacting backside of 31-inch double-faced guardrail.

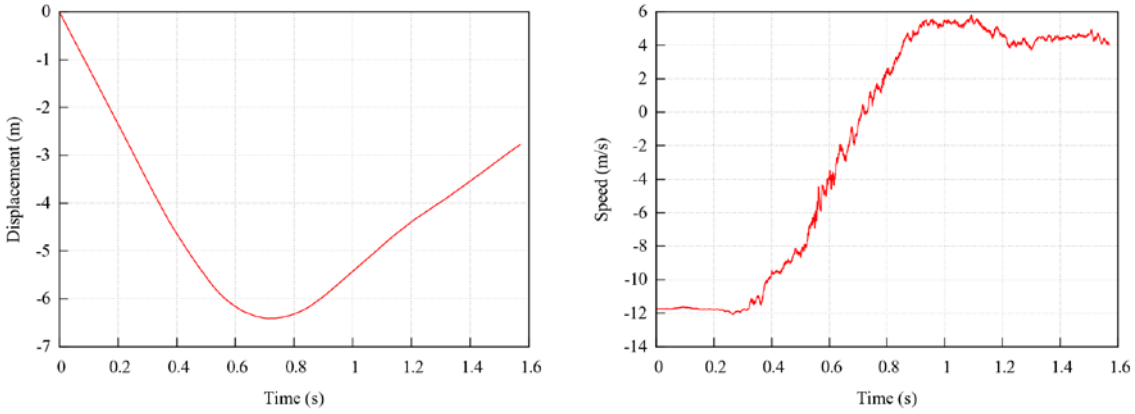

Transverse displacements Transverse speeds

Figure 4.50: Transverse displacements and speeds for F250 impacting backside of 31-inch double-faced guardrail.

4.3 Double-faced Guardrails with Lowered Backside Rails

The analysis of the double-faced 29- and 31-inch G4(1S) strong-post W-beam guardrail with lowered backside rails was performed through eight simulations of Cases 4 and 5, for front-side and backside vehicular impacts of both the 1996 Dodge Neon and

the 2006 Ford F250 under MASH TL-3 conditions. Table 4.4 shows the simulation conditions and a summary of the guardrail performance in terms of vehicular responses.

Table 4.4: Simulation results for double-faced guardrails with lowered backside rails.

Impacting Side	Guardrail Height	Test Vehicle	Test Results
Front	29 inches	Dodge Neon	Vehicle not redirected safely by guardrail (spin-out and outside exit box)
		Ford F250	Vehicle not redirected safely by guardrail (spin-out and outside exit box)
	31 inches	Dodge Neon	Vehicle not redirected safely by guardrail (spin-out and outside exit box)
		Ford F250	Vehicle not redirected safely by guardrail (spin-out and outside exit box)
Back	29 inches	Dodge Neon	Vehicle not redirected safely by guardrail (overrode barrier)
		Ford F250	Vehicle not redirected safely by guardrail (overrode barrier)
	31 inches	Dodge Neon	Vehicle not redirected safely by guardrail (roll angle greater than 75°)
		Ford F250	Vehicle not redirected safely by guardrail (spin-out and outside exit box)

4.3.1 Front-side Impacts on the Double-faced Guardrail with Lowered Backside Rails

Figure 4.51 shows the displacement path of the Dodge Neon impacting the front-side of the 29-inch double-faced W-beam guardrail with the lowered backside rail shown in its original shape along with the exit box denoted by the yellow rectangle. The yaw, pitch, and roll angles of the Dodge Neon are shown in Figure 4.52. The roll and pitch angles were less than twenty degrees in either positive or negative direction and thus

passed the MASH evaluation criterion F. However, the vehicle had a continuously increasing yaw angle after 0.2 seconds, indicating a continuous spinning of the vehicle. Similar to its responses impacting the single- and double-faced guardrails, the Dodge Neon snagged on the post, continuously spun counterclockwise, and consequently went outside the exit box.

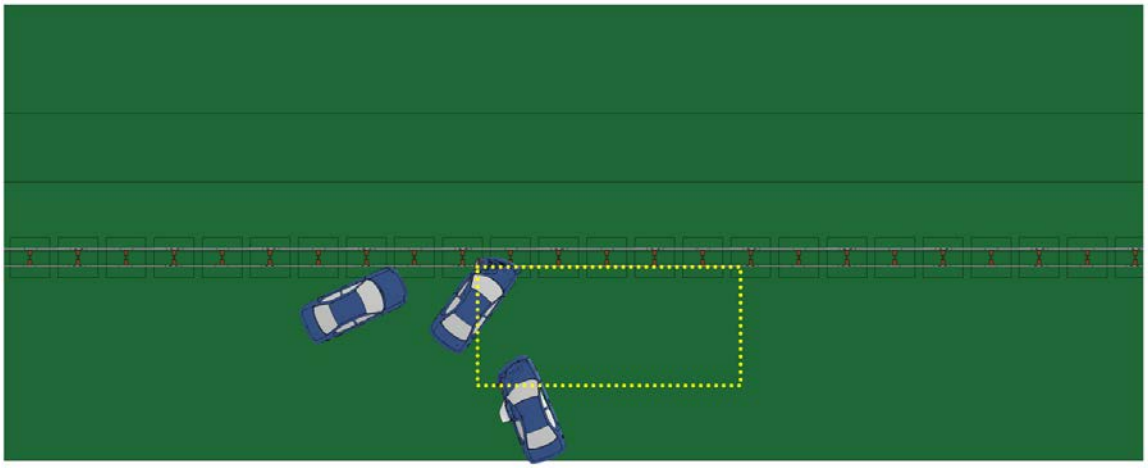

Figure 4.51: Displacement path and exit box for Neon impacting front-side of 29-inch double-faced guardrail with lowered backside rail.

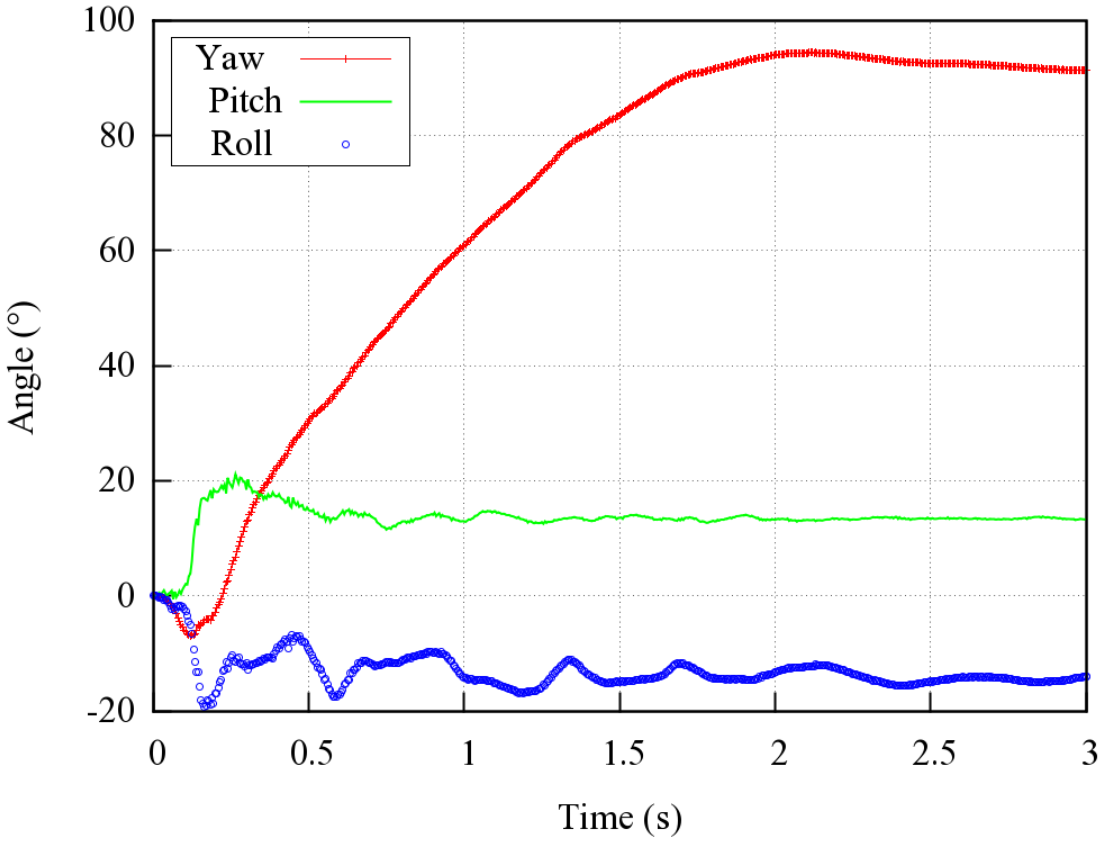

Figure 4.52: Yaw, pitch, and roll angles for Neon impacting front-side of 29-inch double-faced guardrail with lowered backside rail.

Figure 4.53 shows views of vehicle-barrier interaction at the time when the maximum deflection of the guardrail occurred. It can be seen that the damaged guardrail sections are small and localized, which serves as an indication of a relatively low impact severity. The time histories of transverse displacements and speeds measured at the CG point of the vehicle are shown in Figure 4.54. The transverse speed remained at 2 m/s towards the travel lane with spinning (i.e., loss of control of the vehicle). As seen in Figure 4.51, the vehicle has entered the travel lane, so the chance of getting involved in a secondary collision is relatively high.

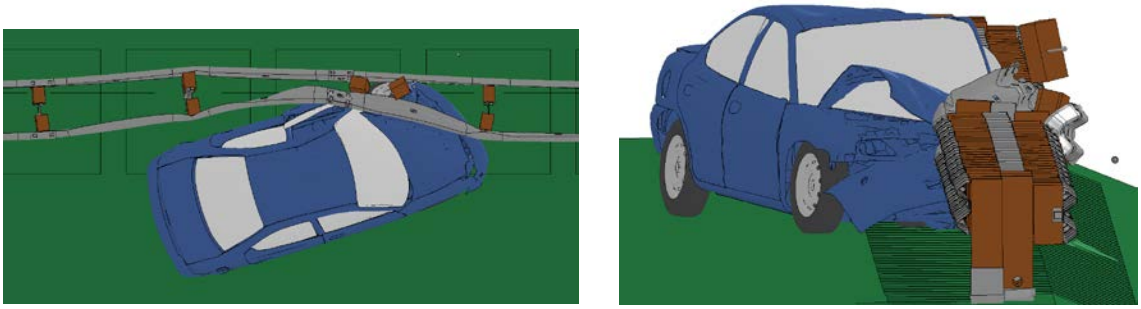

Top view Front view

Figure 4.53: Maximum deflection of W-beam for Neon impacting front-side of 29-inch double-faced guardrail with lowered backside rail.

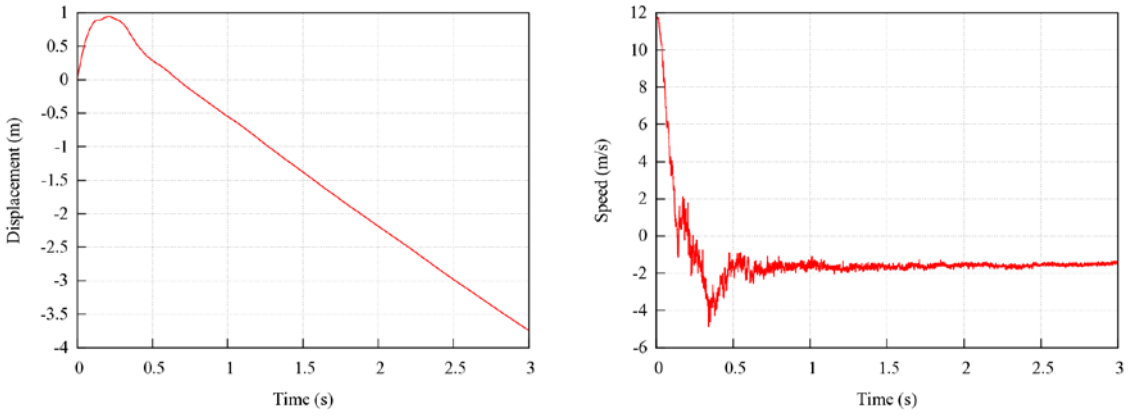

Transverse displacements Transverse speeds

Figure 4.54: Transverse displacements and speeds for Neon impacting front-side of 29-inch double-faced guardrail with lowered backside rail.

Figure 4.55 shows the displacement path of the Ford F250 impacting the front-side of the 29-inch double-faced W-beam guardrail with the lowered backside rail. The Ford F250 was initially redirected towards the parallel direction of the guardrail, but started to spin counterclockwise due to snagging on a guardrail post. This can be seen from the yaw angle shown in Figure 4.56 that starts to increase at 0.3 seconds. Due to the continuous spin, the vehicle went outside the exit box. The pitch and roll angles of the Ford F250 are also shown in Figure 4.56. The roll and pitch angles were less than ten

degrees in either positive or negative direction and thus passed the MASH evaluation criterion F.

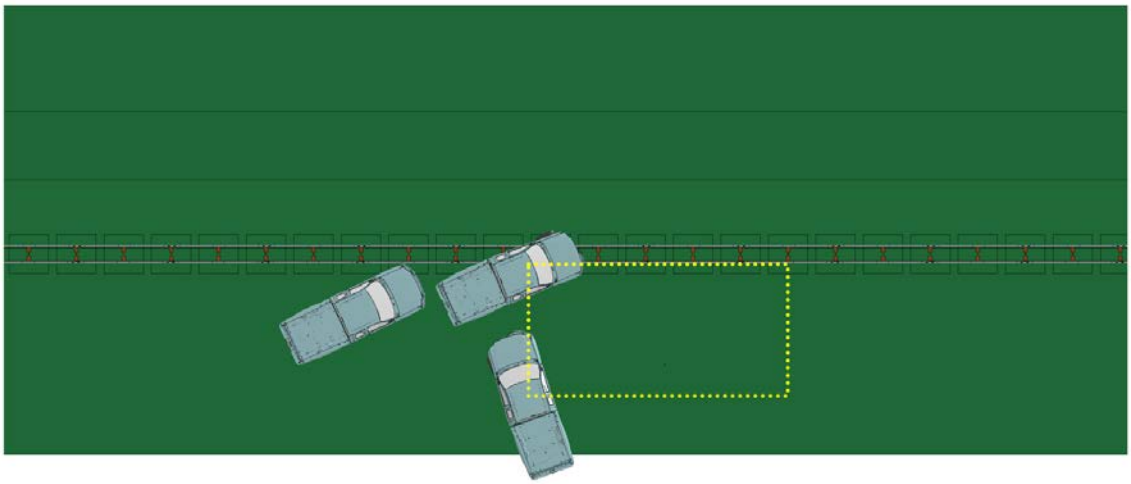

Figure 4.55: Displacement path for F250 impacting front-side of 29-inch double-faced guardrail with lowered backside rail.

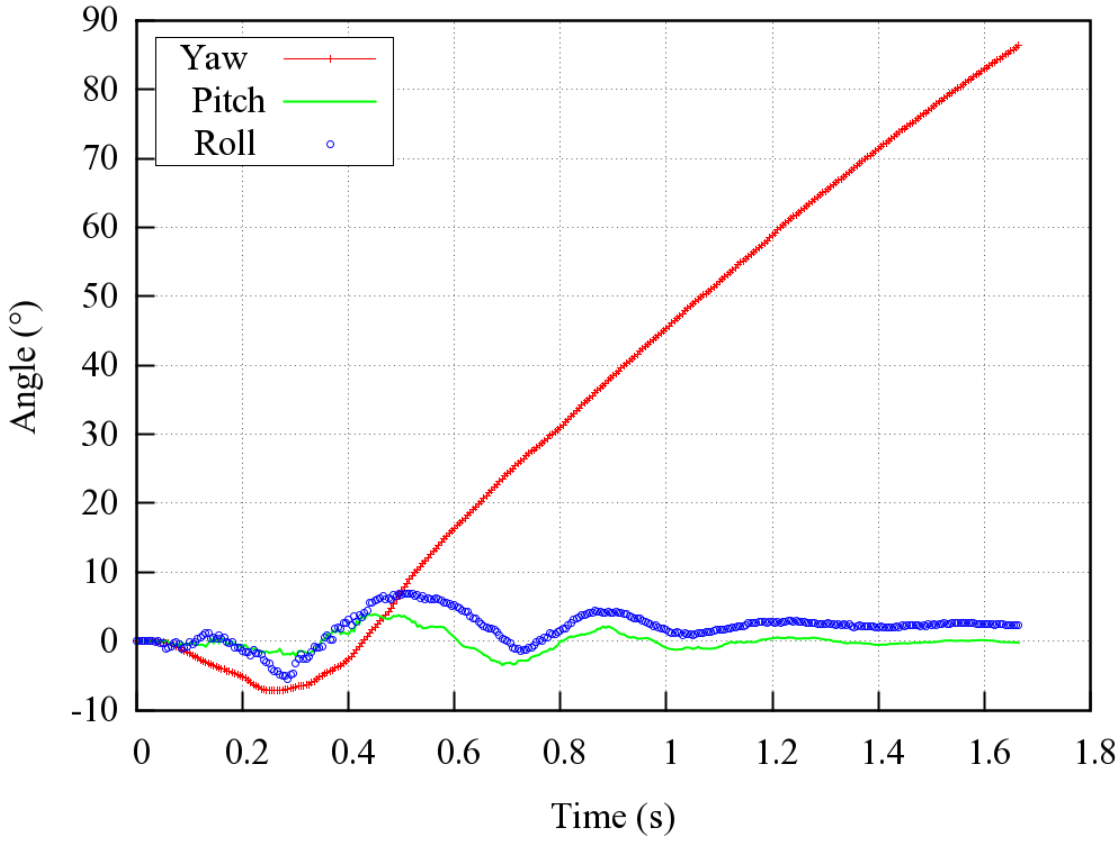

Figure 4.56: Yaw, pitch, and roll angles for F250 impacting front-side of 29-inch double-faced guardrail with lowered backside rail.

Figure 4.57 shows views of vehicle-barrier interaction at the time when the maximum deflection of the guardrail occurred. It can be seen that the damaged guardrail sections are small and localized, which serves as an indication of a relatively low impact severity. The time histories of transverse displacements and speeds measured at the CG point of the vehicle are shown in Figure 4.58. The transverse speed remained at 4 m/s towards the travel lane with spinning (i.e., loss of control of the vehicle). As seen in Figure 4.55, the vehicle has entered the travel lane, so the chance of getting involved in a secondary collision is relatively high.

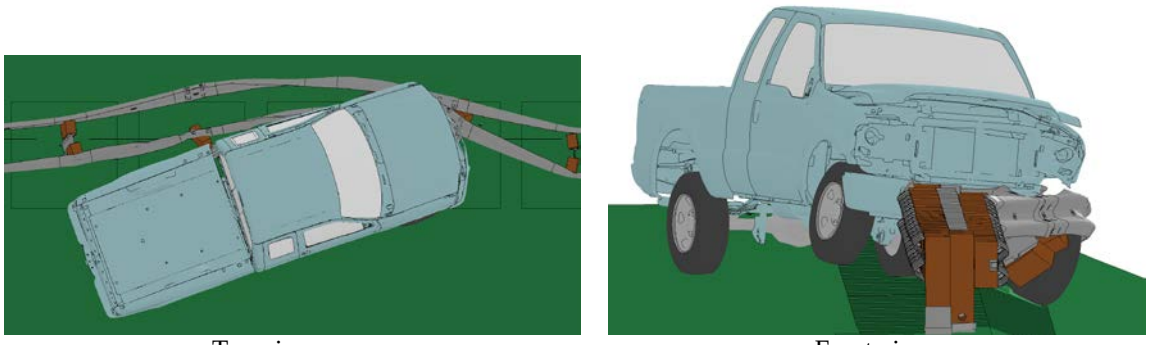

Top view Front view

Figure 4.57: Maximum deflection of W-beam for F250 impacting front-side of 29-inch double-faced guardrail with lowered backside rail.

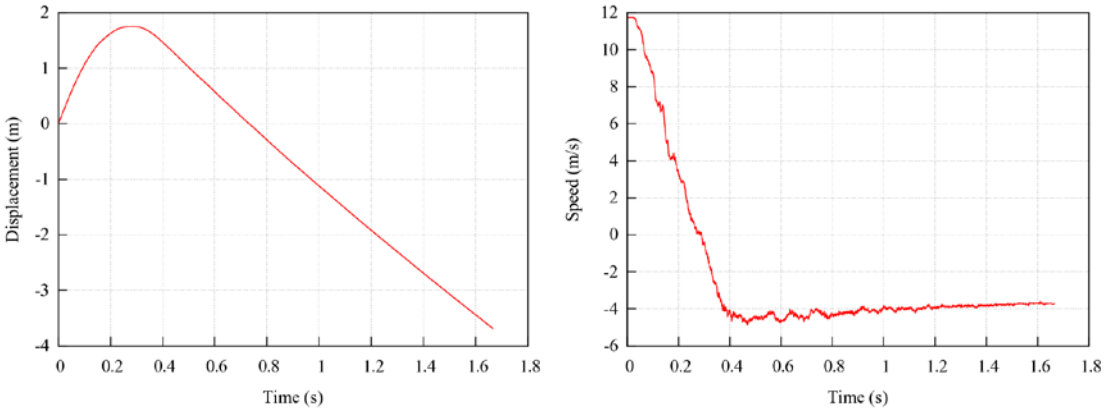

Transverse displacements Transverse speeds

Figure 4.58: Transverse displacements and speeds for F250 impacting front-side of 29-inch double-faced guardrail with lowered backside rail.

Figure 4.59 shows the displacement path of the Dodge Neon impacting the front-side of the 31-inch double-faced W-beam guardrail with the lowered backside rail. The yaw, pitch, and roll angles of the Dodge Neon are shown in Figure 4.60. The roll and pitch angles were less than thirty degrees in either positive or negative direction and thus passed the MASH evaluation criterion F. However, as indicated by the continuously increasing yaw angle, the Dodge Neon had a continuous, counterclockwise spinning after impacting the guardrail and consequently went outside the exit box.

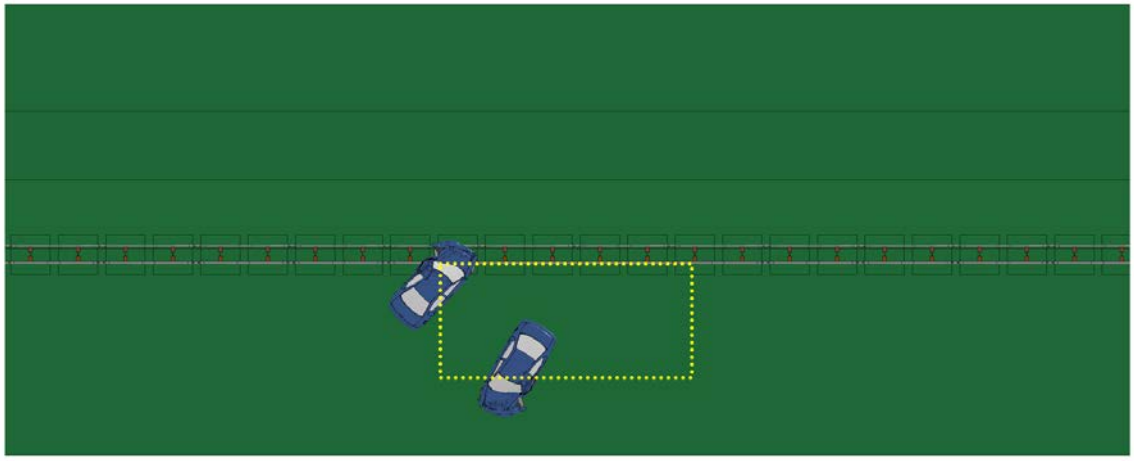

Figure 4.59: Displacement path and exit box for Neon impacting front-side of 31-inch double-faced guardrail with lowered backside rail.

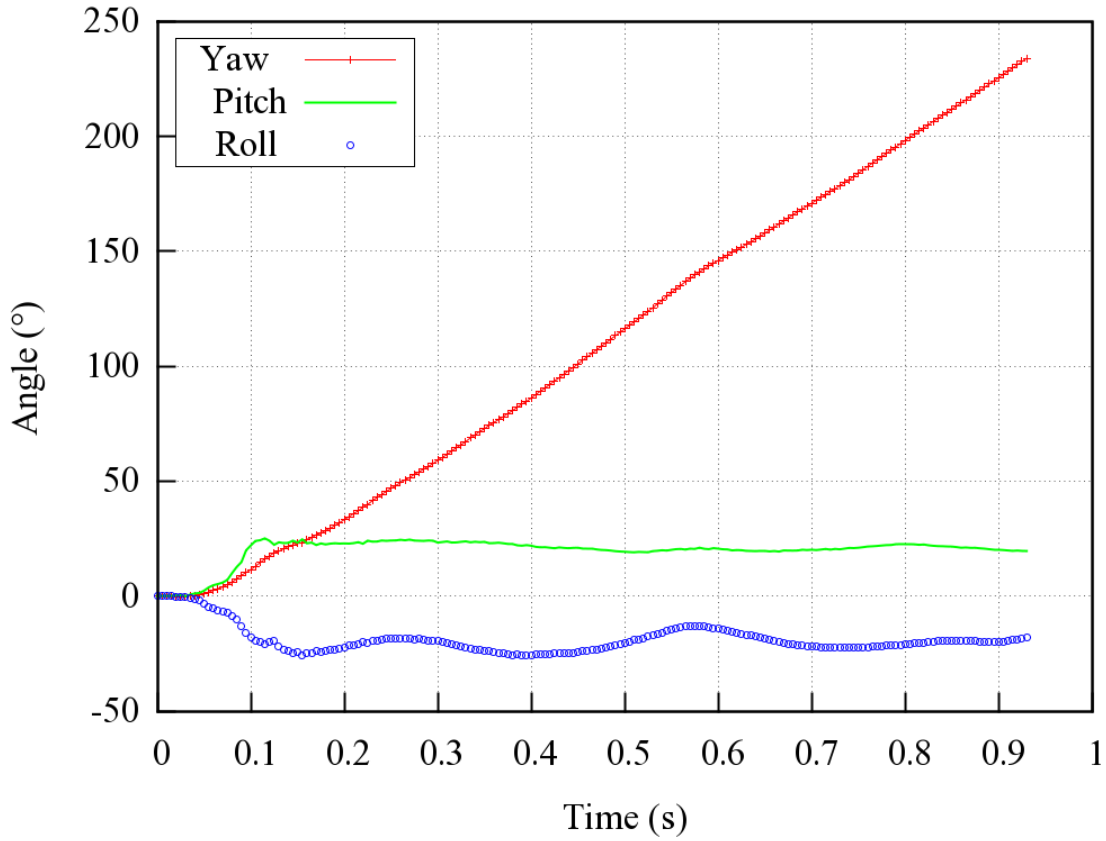

Figure 4.60: Yaw, pitch, and roll angles for Neon impacting front-side of 31-inch double-faced guardrail with lowered backside rail.

Figure 4.61 shows views of vehicle-barrier interaction at the time when the maximum deflection of the guardrail occurred, showing relatively small and localized damaged guardrail sections. The time histories of transverse displacements and speeds measured at the CG point of the vehicle are shown in Figure 4.62. The maximum transverse displacement of the Dodge Neon was larger than that seen with the 29-inch double-faced guardrail due to the vehicle under-riding the guardrail a farther distance with the increased barrier height. The transverse speed remained near 7 m/s towards the travel lane with spinning (i.e., loss of control of the vehicle), which was 5 m/s more than that with the 29-inch double-faced guardrail with the lowered backside rail. As seen in Figure 4.59, the vehicle has entered the travel lane, so the chance of getting involved in a secondary collision is relatively high.

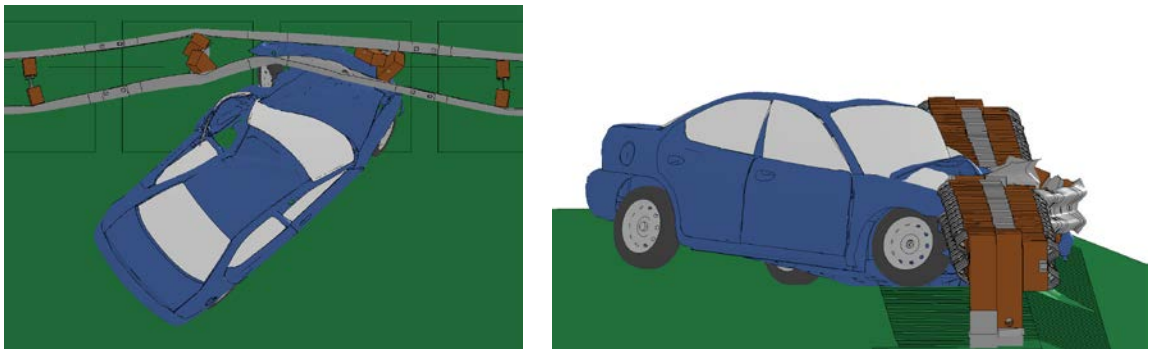

Top view Front view

Figure 4.61: Maximum deflection of W-beam for Neon impacting front-side of 31-inch double-faced guardrail with lowered backside rail.

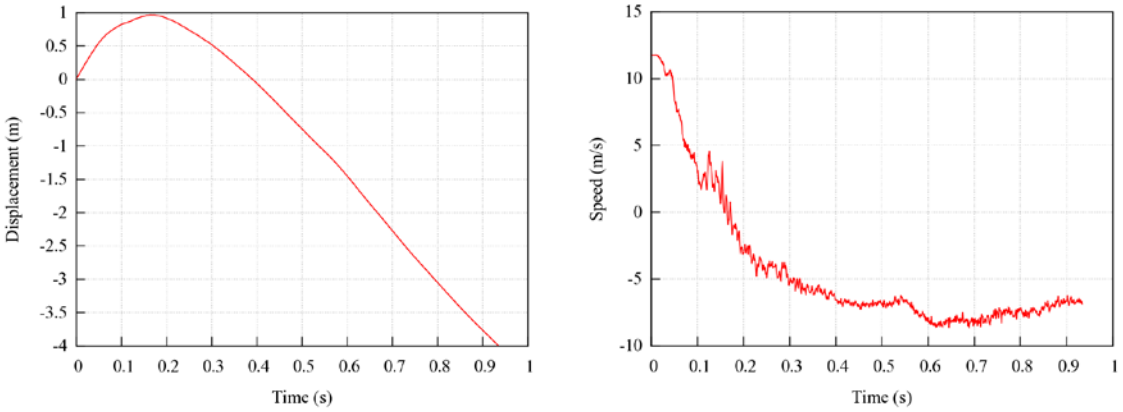

Transverse displacements Transverse speeds

Figure 4.62: Transverse displacements and speeds for Neon impacting front-side of 31-inch double-faced guardrail with lowered backside rail.

Figure 4.63 shows the displacement path of the Ford F250 impacting the front-side of the 31-inch double-faced W-beam guardrail with the lowered backside rail. The Ford F250 was initially redirected towards the parallel direction of the guardrail, but started to spin counterclockwise due to snagging on a guardrail post. This can be seen from the yaw angle shown in Figure 4.64 that starts to increase at 0.45 seconds. Due to the continuous spin, the vehicle went outside the exit box. The pitch and roll angles of the Ford F250 are also shown in Figure 4.64. The roll and pitch angles were less than ten degrees in either positive or negative direction and thus passed the MASH evaluation criterion F.

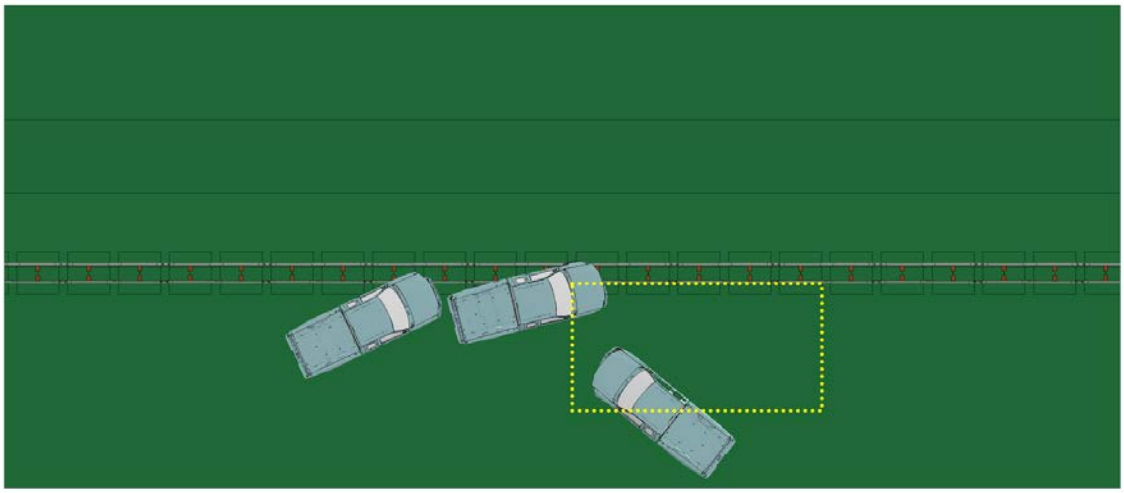

Figure 4.63: Displacement path for F250 impacting front-side of 31-inch double-faced guardrail with lowered backside rail.

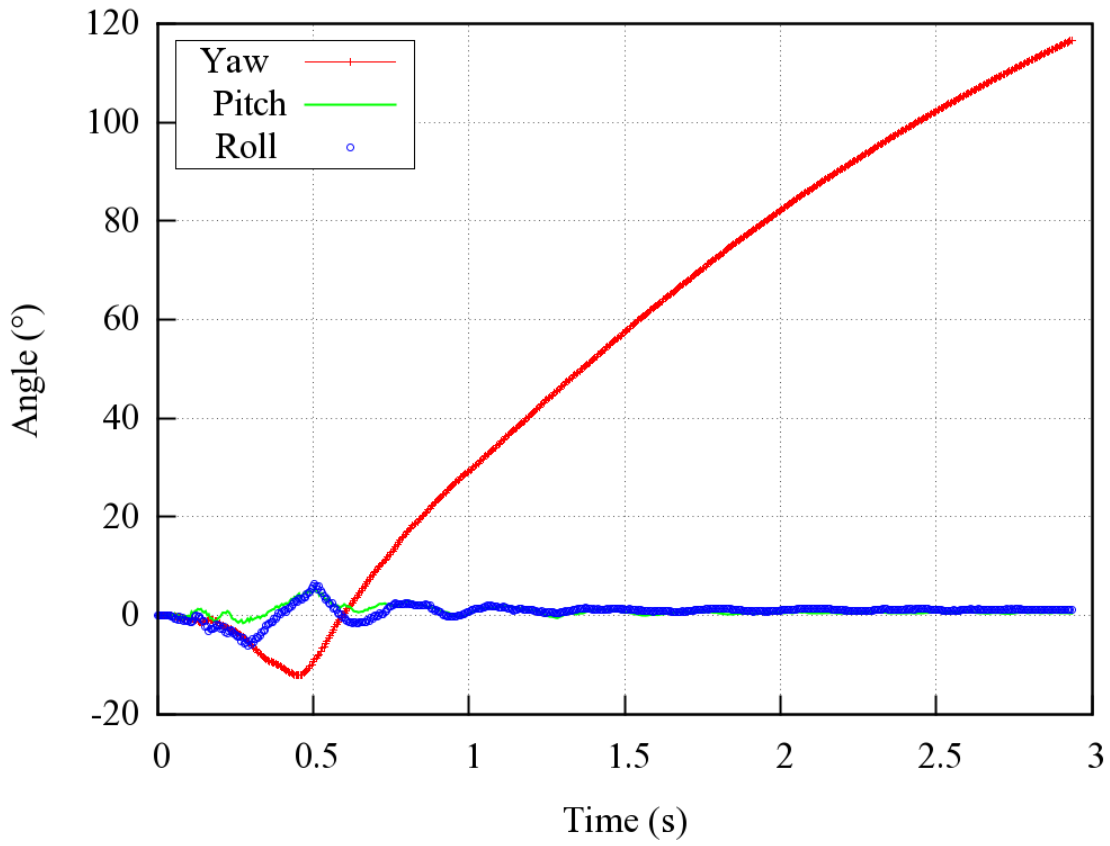

Figure 4.64: Yaw, pitch, and roll angles for F250 impacting front-side of 31-inch double-faced guardrail with lowered backside rail.

Figure 4.65 shows views of vehicle-barrier interaction at the time when the maximum deflection of the guardrail occurred. It can be seen that the damaged guardrail sections are small and localized as seen in the previous cases. The time histories of transverse displacements and speeds measured at the CG point of the vehicle are shown in Figure 4.66. The Ford F250 had a similar transverse displacement as seen with the 29-inch double-faced guardrail even with the increased barrier height. The transverse speed remained near 1 m/s towards the travel lane with spinning (i.e., loss of control of the vehicle), which was 3 m/s less than that with the 29-inch double-faced guardrail with the lowered backside rail. As seen in Figure 4.63, the vehicle has entered the travel lane, so the chance of getting involved in a secondary collision is relatively high.

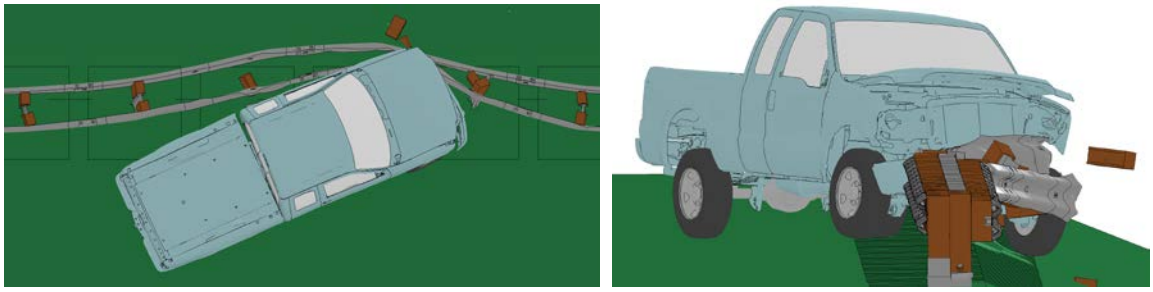

Top view Front view

Figure 4.65: Maximum deflection of W-beam for F250 impacting front-side of 31-inch double-faced guardrail with lowered backside rail.

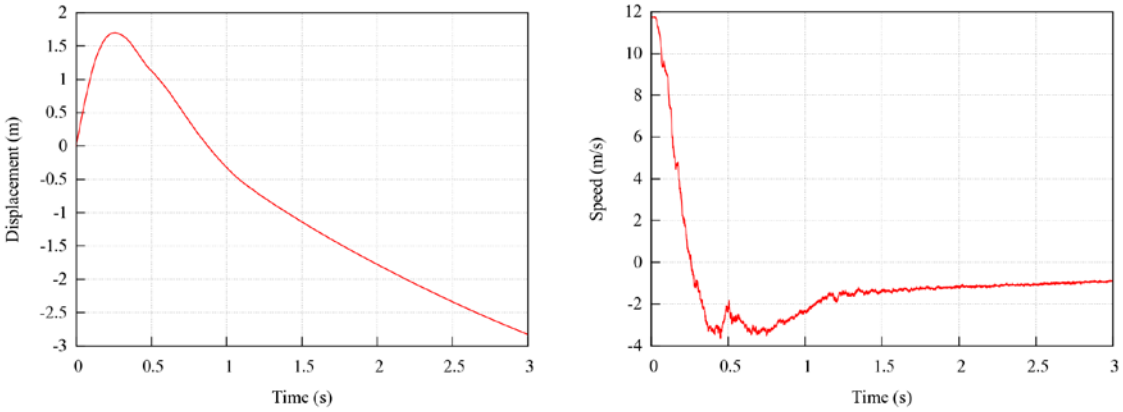

Transverse displacements Transverse speeds

Figure 4.66: Transverse displacements and speeds for F250 impacting front-side of 31-inch double-faced guardrail with lowered backside rail.

4.3.2 Backside Impacts on the Double-faced Guardrail with Lowered Backside Rails

Figure 4.67 shows the displacement path of the Dodge Neon impacting the backside of the 29-inch double-faced W-beam guardrail with lowered backside rail shown in its original shape. There is no exit box and resulting exit angle due to the vehicle overriding the barrier. The yaw, pitch, and roll angles of the Dodge Neon are shown in Figure 4.68. The roll angle was greater than 75° and thus failed the MASH evaluation criterion F.

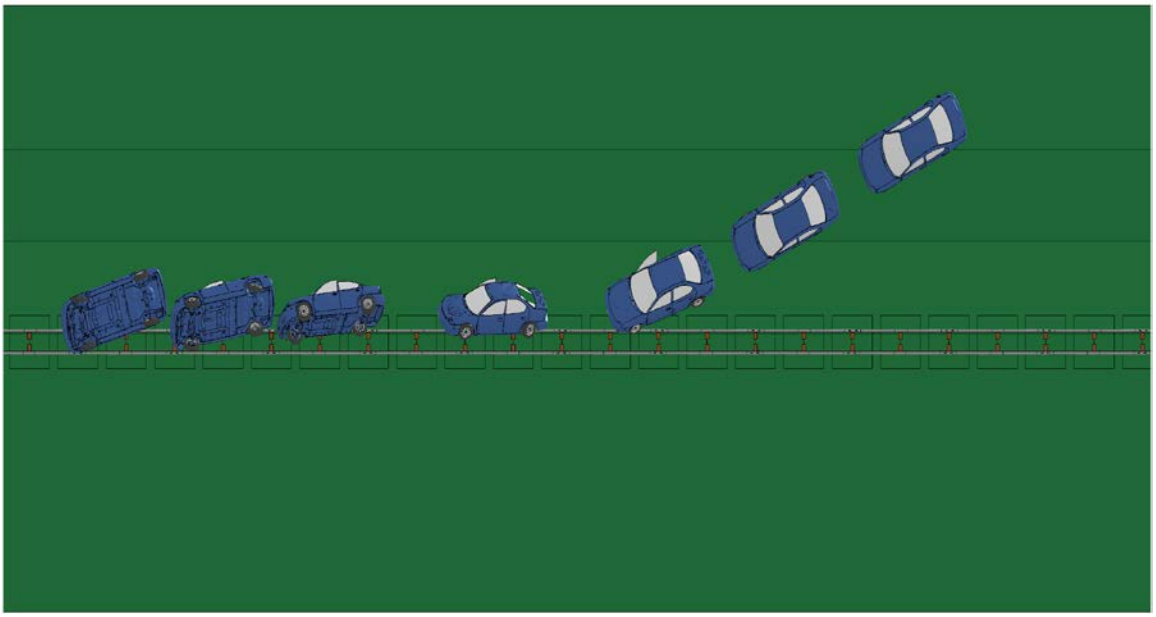

Figure 4.67: Displacement path and exit box for Neon impacting backside of 29-inch double-faced guardrail with lowered backside rail.

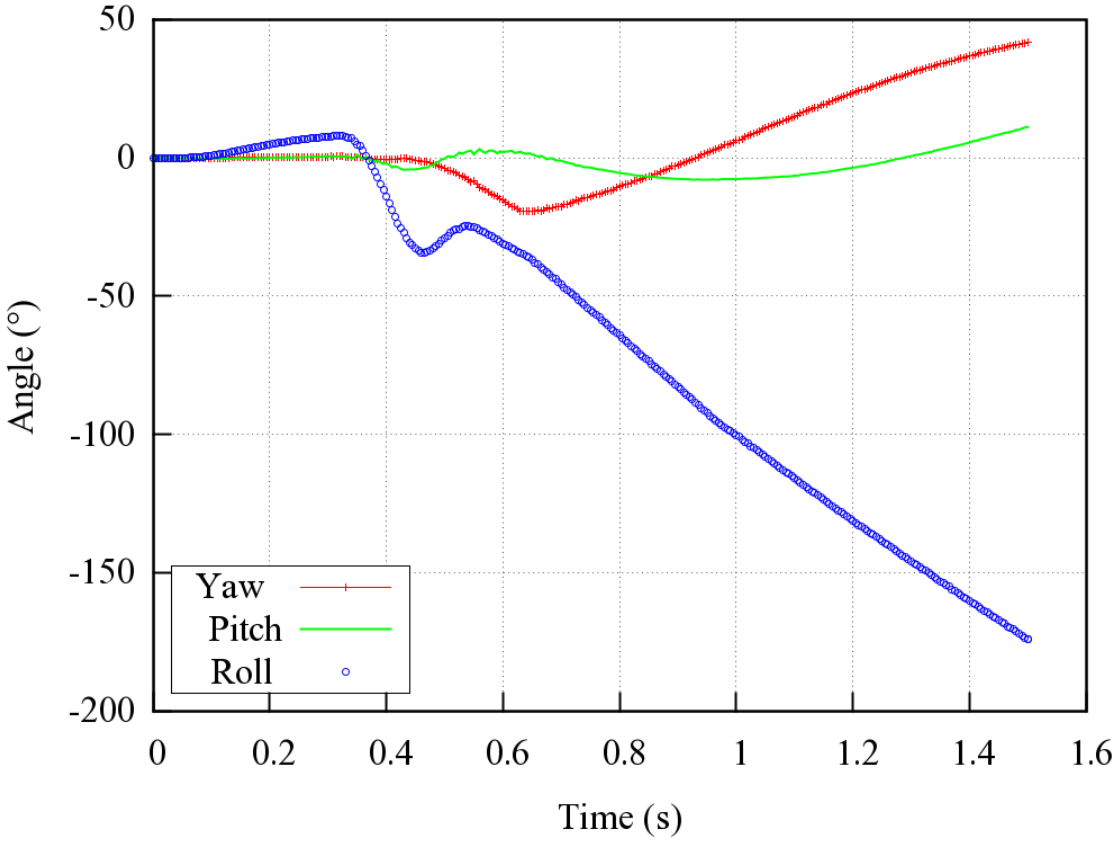

Figure 4.68: Yaw, pitch, and roll angles for Neon impacting backside of 29-inch double-faced guardrail with lowered backside rail.

Figure 4.69 shows views of vehicle-barrier interaction at the time when the maximum deflection of the guardrail occurred. It can be seen that the damaged guardrail sections are small and localized, which serves as an indication of a relatively low impact severity. The time histories of transverse displacements and speeds measured at the CG point of the vehicle are shown in Figure 4.70. The transverse speed was approximately zero, indicating no further displacement would occur. As seen in Figure 4.67, the vehicle overrode the guardrail due to vaulting and rolled over towards the median, which would result in significant risk of occupant injury/fatality.

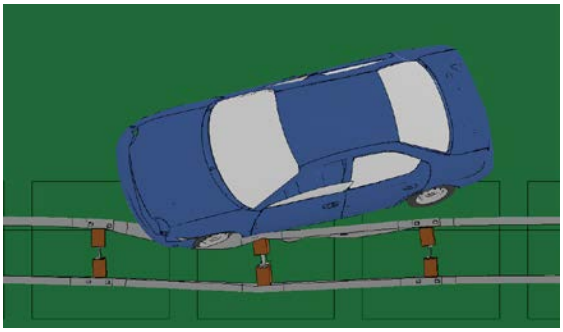

Top view

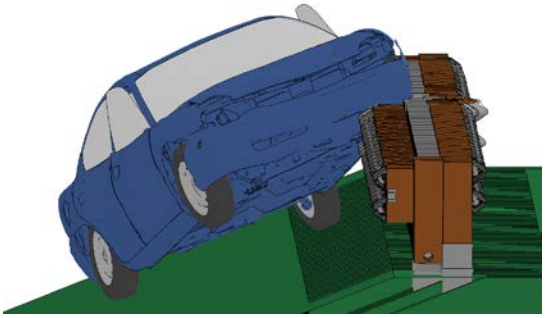

Front view

Figure 4.69: Maximum deflection of W-beam for Neon impacting backside of 29-inch double-faced guardrail with lowered backside rail.

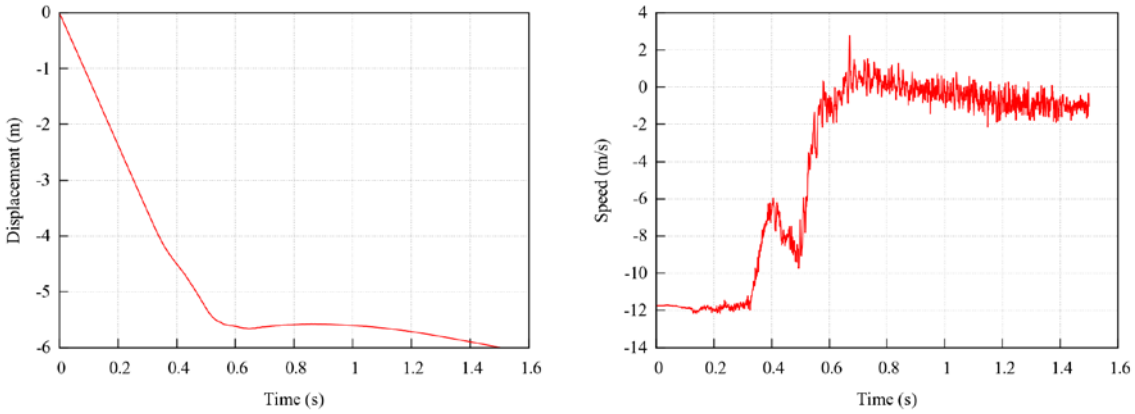

Transverse displacements Transverse speeds

Figure 4.70: Transverse displacements and speeds for Neon impacting backside of 29-inch double-faced guardrail with lowered backside rail.

Figure 4.71 shows the displacement path of the Ford F250 impacting the backside of the 29-inch double-faced W-beam guardrail with lowered backside rail. There is no exit box and resulting exit angle due to the vehicle overriding the barrier. The yaw, pitch, and roll angles of the Ford F250 are shown in Figure 4.72. The roll and pitch angles were less than fifty degrees in either positive or negative direction and thus passed the MASH evaluation criterion F.

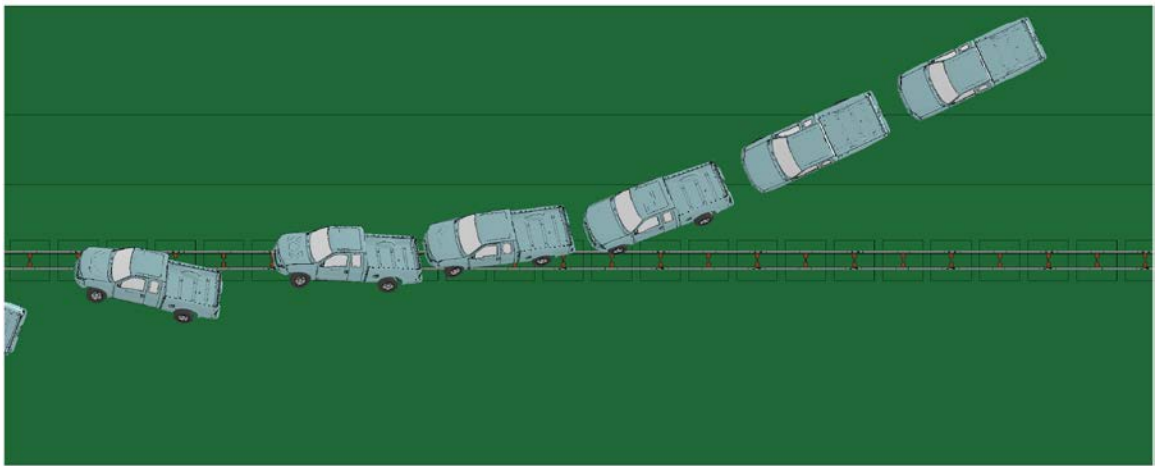

Figure 4.71: Displacement path for F250 impacting backside of 29-inch double-faced guardrail with lowered backside rail.

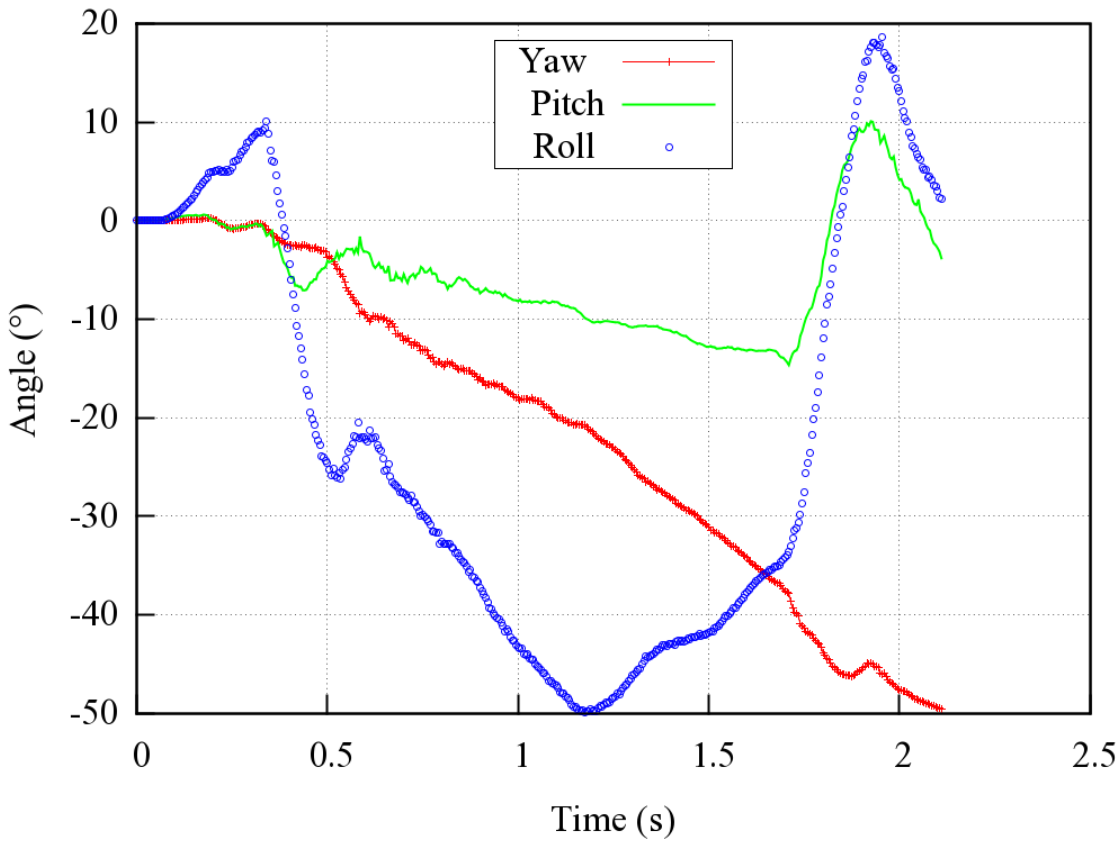

Figure 4.72: Yaw, pitch, and roll angles for F250 impacting backside of 29-inch double-faced guardrail with lowered backside rail.

Figure 4.73 shows views of vehicle-barrier interaction at the time when the maximum deflection of the guardrail occurred. It can be seen that the damaged guardrail sections are small and localized as seen in the previous cases. The time histories of transverse displacements and speeds measured at the CG point of the vehicle are shown in Figure 4.74. The transverse speed remained at 2 m/s over the barrier and towards the oncoming travel lane. As seen in Figure 4.71, the vehicle overrode the guardrail due to vaulting and entered the oncoming travel lane, so the chance of getting involved in a secondary collision is relatively high.

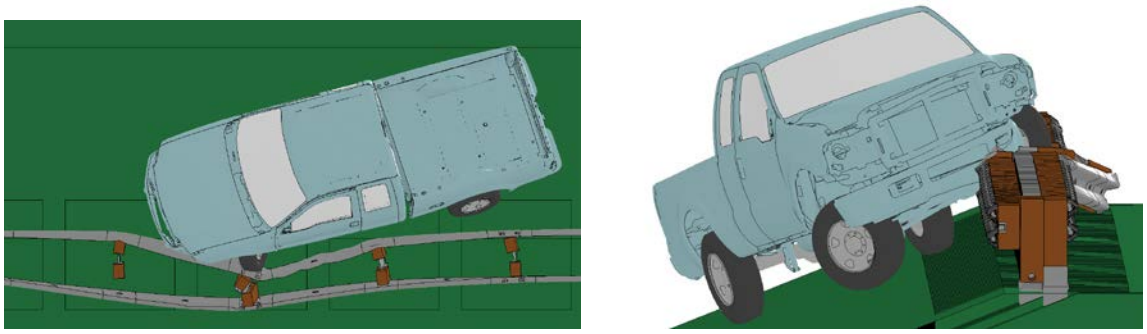

Top view Front view

Figure 4.73: Maximum deflection of W-beam for F250 impacting backside of 29-inch double-faced guardrail with lowered backside rail.

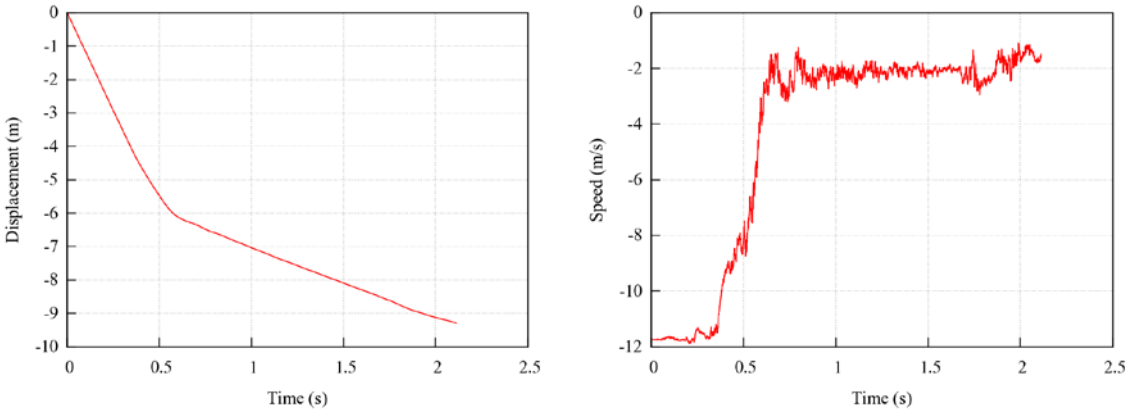

Transverse displacements Transverse speeds

Figure 4.74: Transverse displacements and speeds for F250 impacting backside of 29-inch double-faced guardrail with lowered backside rail.

Figure 4.75 shows the displacement path of the Dodge Neon impacting the backside of the 31-inch double-faced W-beam guardrail with lowered backside rail. Given the large distance from the guardrail to the travel lane where the vehicle ran off, the exit box (denoted by the yellow rectangle) for a backside impact was only used as a convenient indicator of the vehicle's relative post-impact positions. The yaw, pitch, and roll angles of the Dodge Neon are shown in Figure 4.76. Although the exit angle of the Dodge Neon was determined to be 13°, the roll angle was greater than 75°, indicating a rollover of the vehicle and thus failed the MASH evaluation criterion F.

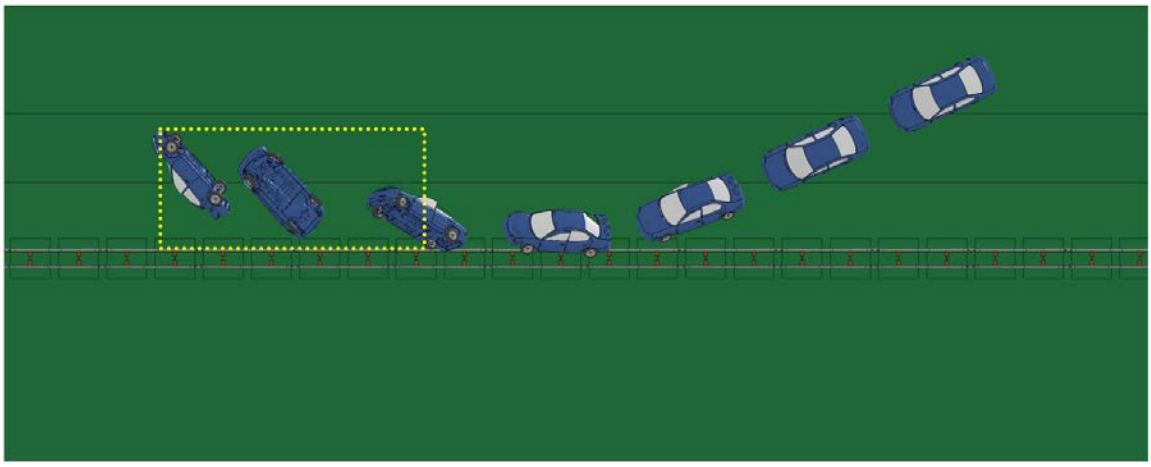

Figure 4.75: Displacement path and exit box for Neon impacting backside of 31-inch double-faced guardrail with lowered backside rail.

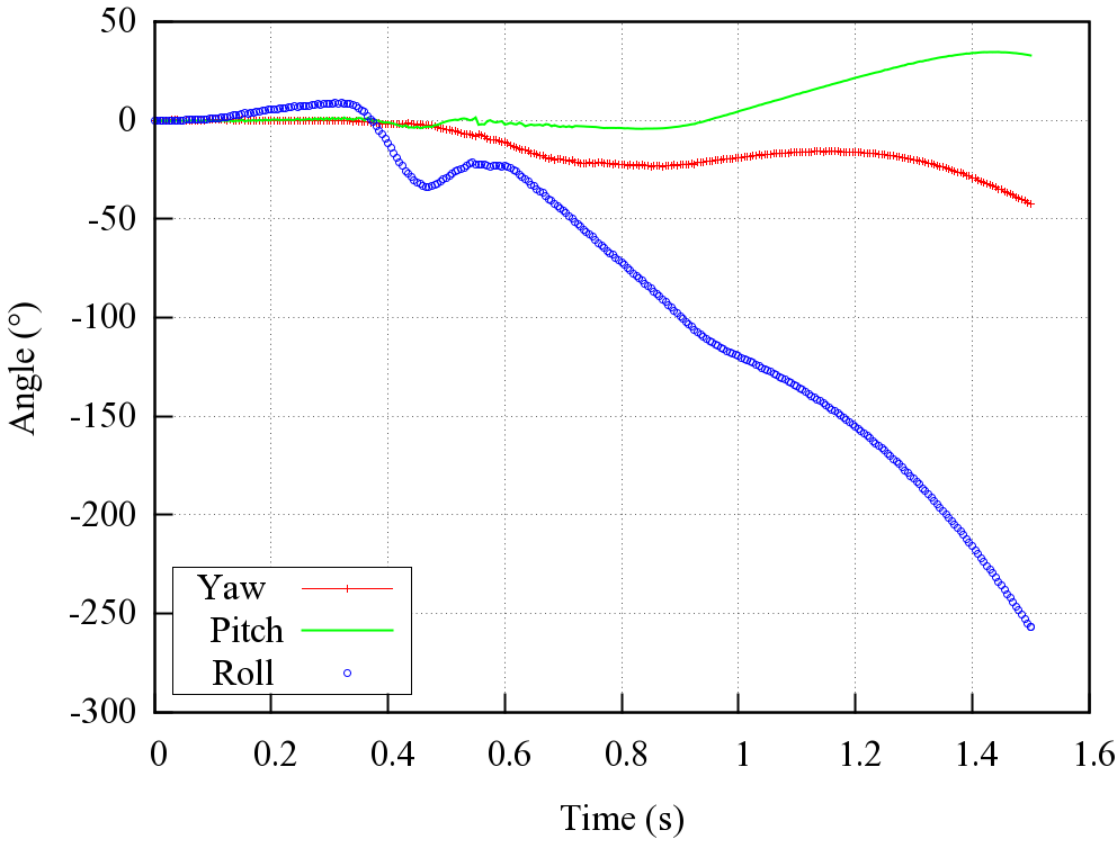

Figure 4.76: Yaw, pitch, and roll angles for Neon impacting backside of 31-inch double-faced guardrail with lowered backside rail.

Figure 4.77 shows views of vehicle-barrier interaction at the time when the maximum deflection of the guardrail occurred. It can be seen that the damaged guardrail

sections are small and localized, which serves as an indication of a relatively low impact severity. The time histories of transverse displacements and speeds measured at the CG point of the vehicle are shown in Figure 4.78. The Dodge Neon had a smaller transverse displacement than seen with the 29-inch double-faced guardrail with the lowered backside rail due to the vehicle being redirected by the guardrail instead of overriding it. The transverse speed remained at 3 m/s towards the median with rolling (i.e., loss of control of the vehicle). As seen in Figure 4.75, the vehicle rolled over towards the center of the median and would result in significant risk of occupant injury/fatality.

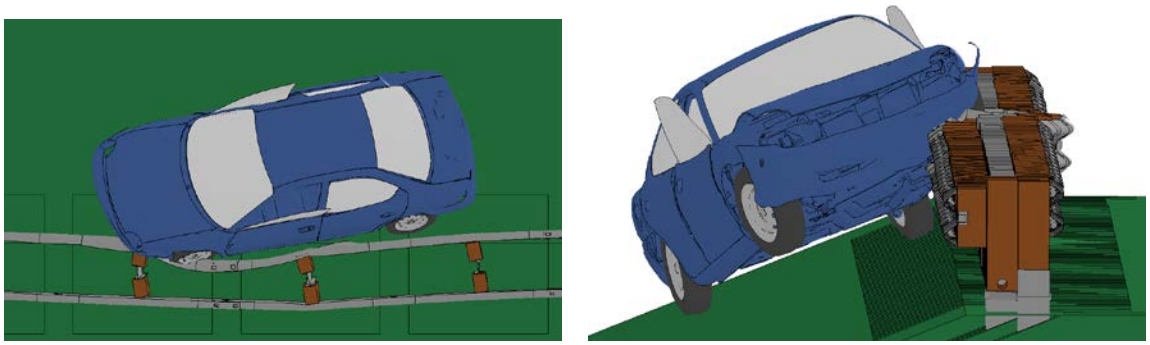

Top view Front view

Figure 4.77: Maximum deflection of W-beam for Neon impacting backside of 31-inch double-faced guardrail with lowered backside rail.

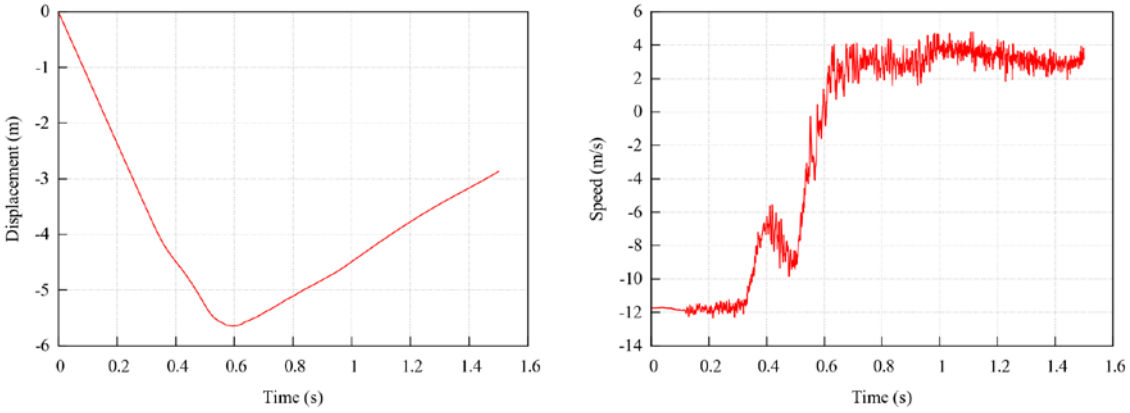

Transverse displacements Transverse speeds

Figure 4.78: Transverse displacements and speeds for Neon impacting backside of 31-inch double-faced guardrail with lowered backside rail.

Figure 4.79 shows the displacement path of the Ford F250 impacting the backside of the 31-inch double-faced W-beam guardrail with lowered backside rail. The yaw, pitch, and roll angles of the Ford F250 are shown in Figure 4.80. The roll and pitch angles were less than thirty degrees in either positive or negative direction and thus passed the MASH evaluation criterion F. However, the vehicle had a continuously increasing yaw angle after 0.6 seconds, indicating a continuous spinning of the vehicle. Similar to its responses impacting the backside of the double-faced guardrails, the Ford F250 snagged on the post, continuously spun counterclockwise, and consequently went outside the exit box.

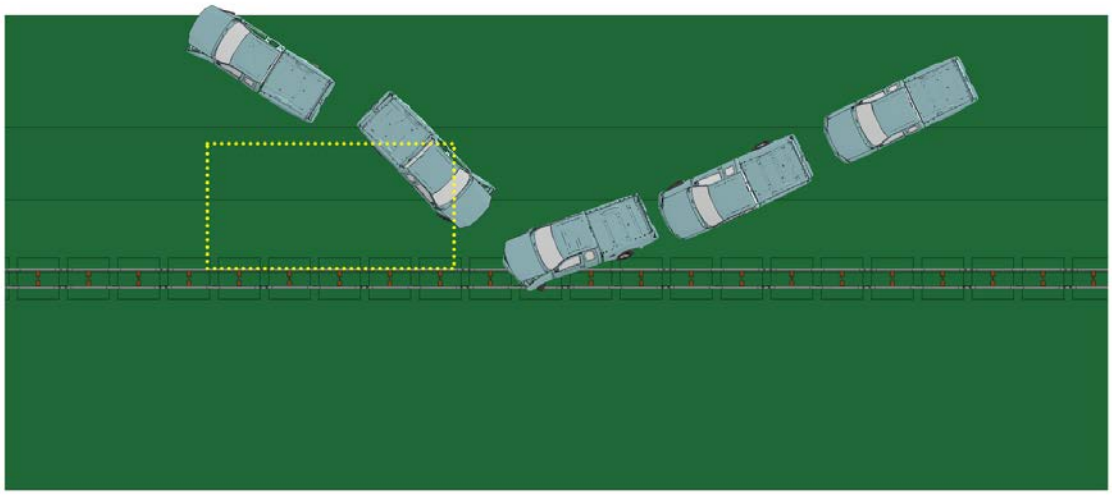

Figure 4.79: Displacement path for F250 impacting backside of 31-inch double-faced guardrail with lowered backside rail.

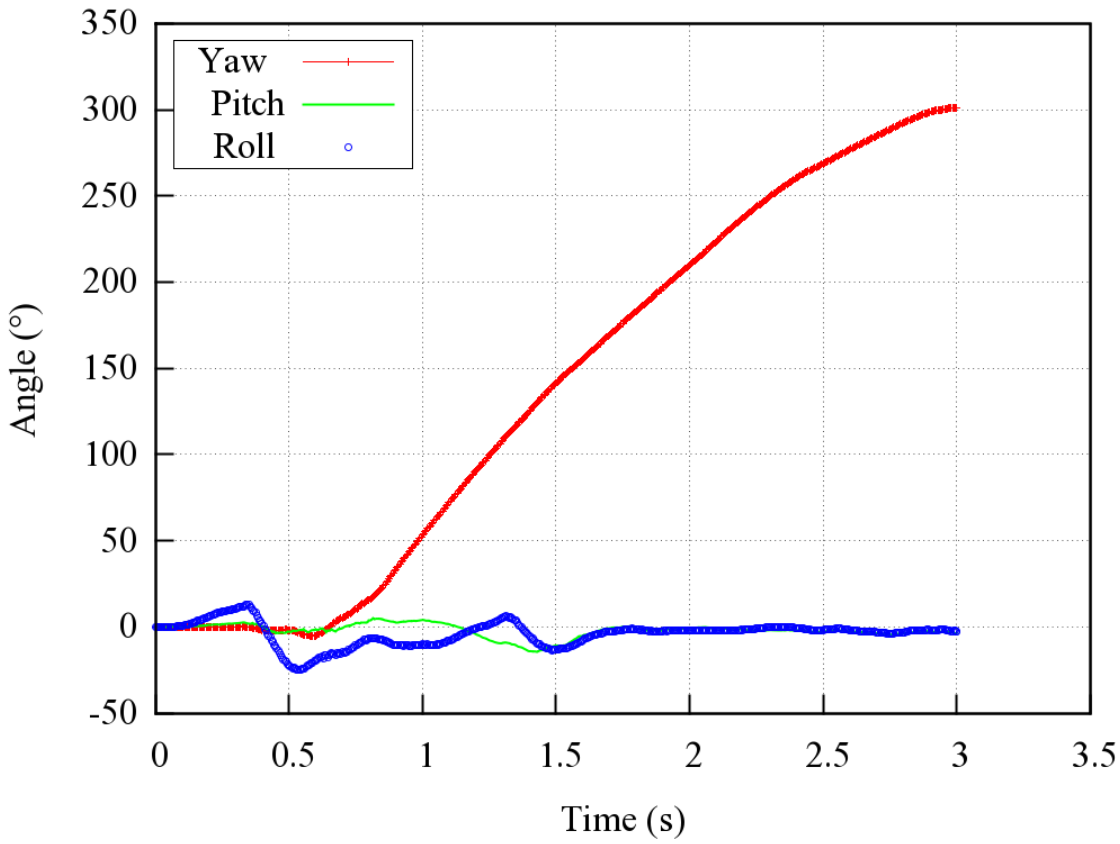

Figure 4.80: Yaw, pitch, and roll angles for F250 impacting backside of 31-inch double-faced guardrail with lowered backside rail.

Figure 4.81 shows views of vehicle-barrier interaction at the time when the maximum deflection of the guardrail occurred. It can be seen that the damaged guardrail sections are small and localized, which serves as an indication of a relatively low impact severity. The time histories of transverse displacements and speeds measured at the CG point of the vehicle are shown in Figure 4.82. The Ford F250 had a smaller transverse displacement than that with the 29-inch double-faced guardrail with the lowered backside rail due to the vehicle being redirected by the guardrail instead of overriding it. The transverse speed started at 6 m/s towards the median and then became approximately zero after impacting the median and stopping in the travel lane, all with spinning (i.e., loss of

control of the vehicle). As seen in Figure 4.79, the vehicle has entered the travel lane, so the chance of getting involved in a secondary collision is relatively high.

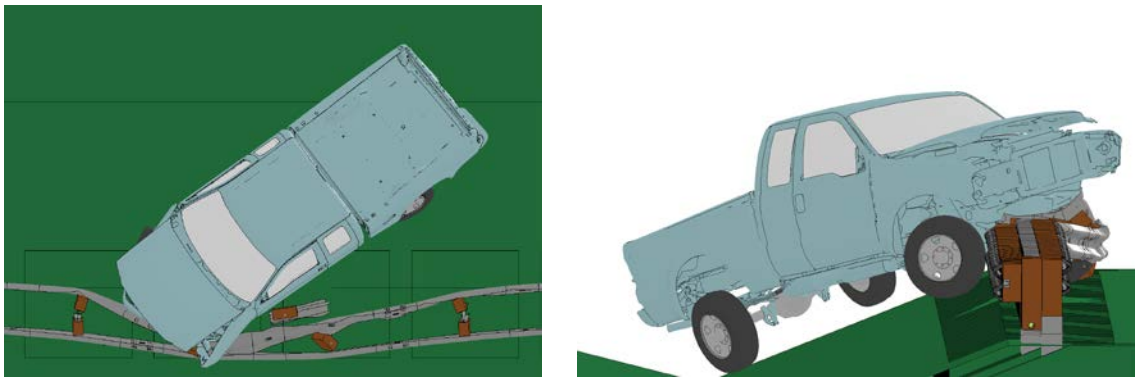

Top view Front view

Figure 4.81: Maximum deflection of W-beam for F250 impacting backside of 31-inch double-faced guardrail with lowered backside rail.

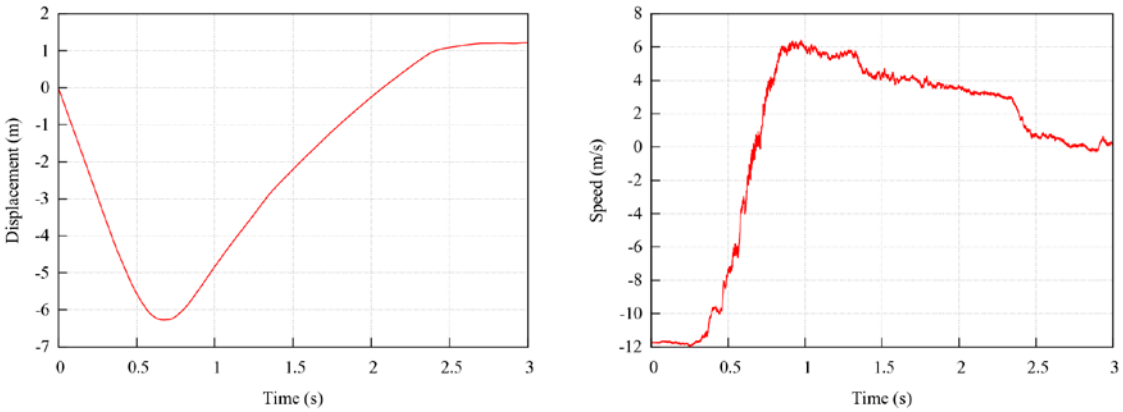

Transverse displacements Transverse speeds

Figure 4.82: Transverse displacements and speeds for F250 impacting backside of 31-inch double-faced guardrail with lowered backside rail.

CHAPTER 5: CONCLUSIONS

Finite element (FE) simulations were performed to study the performance of 29- and 31-inch W-beam guardrails that were single-faced, double-faced, and double-faced with a lowered backside rail under the impacts of a 1996 Dodge Neon passenger car and a 2006 Ford F250 pickup truck. The simulations were performed under MASH TL-3 impact conditions for all cases. The simulation results provided valuable information on how a vehicle will respond to different guardrail installations, as well as the guardrail's performance.

The 29- and 31-inch single-faced W-beam guardrails had similar results for both vehicles under MASH TL-3 conditions. Both the Dodge Neon and Ford F250 were snagged by the guardrail upon impacting the post and thus were not safely redirected. All of the simulations exhibited a spin-out of the vehicle, which resulted in large exit angles and the vehicle going out of the exit box.

The front-side impacts for the double-faced guardrail showed similar results to the single-faced guardrail when impacted by the Dodge Neon, but different results for impacts by the Ford F250. The Dodge Neon exhibited the same spin-out as it did for the single-faced guardrail for both the 29- and 31-inch double-faced W-beam guardrails. The Ford F250 was retained by the guardrail without redirection by the 29-inch double-faced guardrail because of tire snagging on the guardrail, while the 31-inch double-faced W-beam guardrail resulted in the F250 going outside of the exit box.

The backside impacts for the double-faced guardrails showed a major difference between the impact cases by the Dodge Neon and the Ford F250. The Dodge Neon was redirected by both the 29- and 31-inch double-faced guardrails, though it should be noted that the roll angle was greater than 75° for the 29-inch guardrail. The Ford F250 was not safely redirected by both the 29- and 31-inch double-faced guardrails due to vehicle spin-out, which caused the vehicle to enter the travel lane with a relatively high risk of getting involved in a secondary collision.

For the 29- and 31-inch double-faced guardrail with the lowered backside rail, the simulation results were similar for the front-side impacts by both vehicles under MASH TL-3 conditions. Both the Dodge Neon and Ford F250 were not safely redirected by the guardrail due to the vehicles being snagged on a guardrail post, causing a continuous spinning and consequently going outside the exit box. All of the simulations exhibited a spin-out of the vehicle, which resulted in large exit angles and the vehicle going out of the exit box.

The vehicular responses in the backside impacts on the double-faced guardrail with the lowered backside rail were shown to be different from those on the double-faced guardrail without the lowered rail. The Dodge Neon was not safely redirected by the 29-inch guardrail because of vehicle overriding. The Dodge Neon was also not safely redirected by the 31-inch guardrail due to the roll angle being greater than 75°, indicating a vehicle rollover with high risk of occupant injury. The Ford F250 was not safely redirected by either guardrail. The 29-inch guardrail caused the F250 to override the barrier, while the 31-inch guardrail caused a spin-out of the vehicle.

The simulation results suggested that almost all guardrail configurations were effective in retaining the test vehicles, but most exhibited undesirable post-impact trajectories occurring from vehicle spin-out. These undesirable responses could be related to the initial impact locations, which were chosen at a guardrail post in this study. It was observed from full-scale crash test of W-beam guardrails that impacting the post could lead to a high chance of vehicle wheel snagging during the impact. Therefore, the simulation results of this study could represent the worst-case scenarios of vehicular crashes on W-beam guardrails and thus should not be interpreted as the representative results. The simulation results also showed that there was a potential for the Dodge Neon to roll over in backside impacts and for the Ford F250 to have the tire snagged on the guardrail. Although the vehicle was redirected in these two scenarios, there could be a dramatically increased risk of occupant injury/fatality.

It should be noted that the simulation results of this research can be used to interpret the performance trends of W-beam guardrails. They should not be used to draw definitive conclusions about their performance for a specific crash event because some factors that could affect the performance were not considered in the simulations of this study. These factors included, but were not limited to, impact locations along the longitudinal axes of the barriers, soil conditions, and driver behaviors. Nevertheless, finite element analysis was demonstrated to be a useful tool in crash analysis and could be used in future investigations of other research issues.

Due to the deterministic nature of the simulation results, one possible area for future work includes creating a stochastic process for running simulations. The key variables that could be changed for this process include the impact angle, the point of

impact, and the impacting speed of the vehicle. Those results, combined with the evaluations performed in this thesis, would provide a more comprehensive interpretation of the performance of the different W-beam guardrail configurations. Another possible area for future work involves increasing the width of the wood blockout or adding a second blockout all together. The Midwest Guardrail System, which is very similar to the strong-post W-beam guardrail used for this research, recommends a 12 inch blockout to reduce the likelihood of vehicle snagging upon striking the guardrail. Also, the FHWA states that two blockouts (with a total width of 16 inches) may be used for the strong-post W-beam guardrail to further increase the distance between the W-beam and post so as to reduce the possibility of vehicle snagging and spin-out. Both of these areas of possible future work would further improve the design and performance of strong-post W-beam guardrails.

REFERENCES

AASHTO (2011). *Roadside Design Guide*, 4th edition, American Association of State Highway and Transportation Officials, Washington, D.C.

Abu-Odeh, A. Y., Albin R. B., and Olson, D. K. (2013). "A new MASH Compliant Guardrail System for Placement on Slope." *2013 TRB Annual Meeting*, Washington, D.C.

Alluri, P., Haleem, K., and Gan, A. (2012). "In-Service Performance Evaluation (ISPE) for G4 (1S) Type of Strong-Post W-Beam Guardrail System and Cable Median Barrier: Volume I." *Final Report FDOT BDK80 977-19*, State of Florida Department of Transportation, Tallahassee, FL.

Atahan, A. O. (2002). "Finite element simulation of a strong-post W-beam guardrail system." *Simulation*, 78(10), 587-599.

Atahan, A. O. (2003). "Impact behaviour of G2 steel weak-post W-beam guardrail on nonlevel terrain." *International Journal of Heavy Vehicle Systems*, 10(3), 209-223.

Bligh, R. P., Abu-Odeh, A. Y., Hamilton, M. E., and Seckinger, N. R. (2004). "Evaluation of roadside safety devices using finite element analysis." *Report 0-1816-1*, Texas Transportation Institute, College Station, TX.

Bligh, R., Miaou, S.-P., Lord, D., and Cooner, S. (2006). "Median barrier guidelines for Texas." *Report 0-4254-1*, Texas Transportation Institute, College Station, TX.

BMI-SG. (2004). "Improved guidelines for median safety." *NCHRP 17-14(2) Draft Report of Analysis Findings*, Transportation Research Board, National Research Council, Vienne, VA.

Donnell, E. T., Harwood, D. W., Bauer, K. M., Mason, J. M., and Pietrucha, M. T. (2002). "Cross-median collisions on Pennsylvania interstates and expressways." *Transportation Research Record*, 1784, 91-99.

Dorcely, J., and McKyes, E. (2010). "Post-Soil Interactions on Guardrails Near the Crown of a Slope." *Transportation Research Record: Journal of the Transportation Research Board*, 2186, 147-153.

Fang, H., Li, N., Tian, N., (2010). "Median barrier placement on six-lane, 46-foot median divided freeways." *Final Report NCDOT 2009-04*, North Carolina Department of Transportation, Raleigh, NC.

Fang, H., Gutowski, M., Li, N., DiSogra, M., (2013). "Performance Evaluation of NCDOT W-beam Guardrails under MASH TL-2 Conditions." *Final Report NCDOT 2012-11*, North Carolina Department of Transportation, Raleigh, NC.

Ferdous, M. R., Abu-Odeh, A., Bligh, R. P., Jones, H. L., Sheikh, N. M., (2011). "Performance limit analysis for common roadside and median barriers using LS-DYNA." *International Journal of Crashworthiness*, 16(6), 691-706.

Ferdous, M. R., Abu-Odeh, A., Bligh, R. P., Jones, H. L., (2013). "Placement of traffic barriers on roadside and median slopes – guidelines based on numerical simulations." *International Journal of Crashworthiness*, 18(2), 110-125.

Findley, D. J., Cunningham, C. M., Schroeder, B. J., Vaughan, C. L., Fowler, T. J., (2012). "Structural and safety investigation of statewide performance of weathered steel beam guardrail in North Carolina" *Transportation Research Record: Journal of the Transportation Research Board*, 2309, 63-72.

Gabauer, D. J., Kusano, K. D., Marzougui, D., Opiela, K., Hargrave, M., Gabler, H. C. (2010). "Pendulum testing as a means of assessing the crash performance of longitudinal barrier with minor damage." International Journal of Impact Engineering, 37(11), 1121-1137.

Gabler, H.C., Gabauer, D.J., and Bowen, D. (2005) "Evaluation of Cross Median Crashes, Final Report", *Final Report FHWA-NJ-2005-004*, Rowan University, Glassboror, NJ.

Gabler, H. C. and Gabauer, D. J. (2006). "Safety audit of fatalities and injuries involving guide rail." *Final Report FHWA-NJ-2007-001*, Virginia Tech, Blacksburg, VA.

Hallquist, J. O. (2006). "LS-DYNA Theory Manual." Livermore Software Technology Corporation. Livermore, CA.

Hampton, C. E., Gabauer, D. J., Gabler, H. C., (2010) "Limits of acceptable rail-and-post deflection in crash-damaged strong-post W-beam guardrail" *Transportation Research Record: Journal of the Transportation Research Board*, 2195, 95-105.

Hampton, C. and Gabler, H. (2013). "Development of a missing post repair guideline for longitudinal barrier crash safety." *Journal of Transportation Engineering*, 139(6), 549–555.

Hiser, N. R., and Reid, J. D. (2005). "Modeling slip base mechanisms." *International Journal of Crashworthiness*, 10(5), 463-472.

Hu, W., Donnell, E. T., (2010) "Median barrier crash severity: some new insights" *Accident Analysis & Prevention*, 42(6), 1697-1704.

Kan, C.-D., Marzougui, D., Bahouth, G. T., and Bedewi, N. E. (2001). "Crashworthiness evaluation using integrated vehicle and occupant finite element models." *International Journal of Crashworthiness*, 6, 387-398.

Lewis, B. A. (2004). “Manual for LS-DYNA soil material model 147.” *FHWA-HRT-04-095*, U.S. Department of Transportation, Federal Highway Administration, McLean, VA.

LSTC (2007). “LS-DYNA keyword user’s manual - version 971.” Livermore Software Technology Corporation (LSTC), Livermore, CA.

Lynch, J. M., Crowe, N. C., and Rosendahl, J. F. (1993). “Interstate across median accident study: a comprehensive study of traffic accidents involving errant vehicles which cross the median divider strips on North Carolina interstate highways.” *1993*

AASHTO Annual Meeting Proceedings, Publisher American Association of State Highway and Transportation Officials, 125-133.

Mackerle, J. (2003). “Finite element crash simulations and impact-induced injuries: an addendum. A bibliography (1998–2002).” *The Shock and Vibration Digest*, 35(4), 273-280.

Mak, K.K., and Bligh, R.P. (2002). “Assessment of NCHRP Report 350 test conditions.” *Transportation Research Record 1797*, 38-43.
Mak, K. K., and Sicking, D. L. (2003). “NCHRP Report 492 roadside safety analysis program (RSAP) – engineer’s manual.” *Transportation Research Board*, 7-28.

Marzougui, D., Bahouth, G., Eskandarian, A., Meczkowski, L., and Taylor, H. (2000). “Evaluation of portable concrete barriers using finite element simulation.” *Transportation Research Record*, 1720, 1-6.

Marzougui, D., Zink, M., Zaouk, A. K., Kan, C.-D., and Bedewi, N. E. (2004). “Development and validation of a vehicle suspension finite element model for use in crash simulations.” *International Journal of Crashworthiness*, 9(6), 565-576.

Marzougui, D., Mohan, P., Kan, C.-D., and Opiela, K. S. (2007). “Evaluation of rail height effects on the safety performance of W-beam barriers.” *2007 TRB Annual Meeting*, Washington, D.C.

Marzougui, D., Mohan, P., Kan, C.-D., and Opiela, K. S. (2012). “Assessing options for improving barrier crashworthiness using finite element models and crash simulations.” *Final Report NCAC-2012-W-008*, National Crash Analysis Center, George Washington University, Washington, D.C.

MASH (2009). “Manual for assessing safety hardware (MASH).” American Association of State Highway and Transportation Officials (AASHTO), Washington D.C.

Miaou, S.-P., Bligh, R. P., and Lord, D. (2005). “Developing guidelines for median barrier installation: benefit-cost analysis with Texas data.” *Transportation Research Record*, 1904, 3-19.

Mid-Park (web1). “Guardrail Information.” <*http://www.mid-park.com/rcp/guardrail/guardrail_info*>.

Mohan, P., Marzougui, D., and Kan, C.-D. (2007). “Validation of a single unit truck model for roadside hardware impact.” *International Journal of Vehicle Systems Modelling and Testing*, 2(1), 1-15.

Mongiardini, M., and Reid, J. D. (2013). “Investigation of a series of relevant phenomena for modeling the full-scale crash test of a small vehicle with a guardrail system.” *International Journal of Computer Aided Engineering and Technology*, 5(1), 58-75.

Murray, Y. D., Reid, J. D., Faller, R. K., Bielenberg, B. W., and Paulsen, T. J. (2005). “Evaluation of LS-DYNA wood material model 143.” *FHWA-HRT-04-096*, U.S. Department of Transportation, Federal Highway Administration, McLean, VA.

Murray, Y. D. (2007). “User manual for LS-DYNA concrete material model 159.” *FHWA-HRT-05-062*, U.S. Department of Transportation, Federal Highway Administration, McLean, VA.

NCAC (web1). “NCAC finite element models.” <*http://www.ncac.gwu.edu/vml/models.html*>.

NCAC (web2). “NCAC publications.” <*http://www.ncac.gwu.edu/filmlibrary/publications.html*>.

NCHRP 22-21 (2011). “Project 22-21: median cross-section design for rural divided highways.” <*http://apps.trb.org/cmsfeed/TRBNetProjectDisplay.asp?ProjectID=694*>.

NCHRP 22-22 (2010). “Project 22-22: placement of traffic barriers on roadside and median slopes.” <*http://apps.trb.org/cmsfeed/TRBNetProjectDisplay.asp?ProjectID=695*>.

NCHRP 22-27 (2012). “Project 22-27: roadside safety analysis program (RSAP) update.” <*http://apps.trb.org/cmsfeed/TRBNetProjectDisplay.asp?ProjectID=2517*>.

Nicol, D. A., (2010) “Roadside design: steel strong-post W-beam guardrail.” *Memorandum 051710*, U.S. Department of Transportation, Federal Highway Administration, McLean, VA.

Ochoa, C. M., Ochoa, T. A., (2011) “Guardrail optimization for rural roads.” *Transportation Research Board of the National Academies*, 2203, 71-78.

Orengo, F., Ray, M. H., and Plaxico, C. A. (2003). “Modeling tire blow-out in roadside hardware simulations using LS-DYNA.” *IMECE2003-55057*, 2003 ASME International Mechanical Engineering Congress & Exposition, Washington, D.C.

Patzner, G. S., Plaxico, C. A., and Ray, M. H. (1999). “Effects of post and soil strength on performance of modified eccentric loader breakaway cable terminal.” *Transportation Research Record,* 1690, 78-83.

Plaxico, C. A., Ray, M. H., and Hiranmayee, K. (2000). “Impact performance of the G4(1W) and G4(2W) guardrail systems: comparison under NCHRP Report 350 test 3-11 conditions.” *Transportation Research Record*, 1720, 7-18.

Plaxico, C. A., Mozzarelli, F., and Ray, M. H. (2003). “Tests and simulation of a w-beam rail-to-post connection.” *International Journal of Crashworthiness*, 8(6), 543-551.

Ray, M. H. (1996a). “Repeatability of full-scale crash tests and criteria for validating simulation results.” *Transportation Research Record*, 1528, 155-160.

Ray, M. H. (1996b). “Use of finite element analysis in roadside hardware design.” *Transportation Research Circular*, 453, 61-71.

Ray, M. H., and Patzner, G. S. (1997). “Finite element model of modified eccentric loader terminal (MELT).” *Transportation Research Record,* 1599, 11-21.

Ray, M. H., and Weir, J. A. (2001). “Unreported collisions with post-and-beam guardrails in Connecticut, Iowa, and North Carolina.” *Transportation Research Record*, 1743, 111-119.

Ray, M. H., Weir, J., and Hopp, J. (2003). “In-service performance of traffic barriers.” *NCHRP Report 490*, Transportation Research Board, National Research Council, Washington, D.C.

Ray, M. H., Oldani, E., and Plaxico, C. A. (2004). “Design and analysis of an aluminum F-shape bridge railing.” *International Journal of Crashworthiness*, 9(4), 349-363.

Reid, J. D. (1996). “Towards the understanding of material property influence on automotive crash structures.” *Thin-Walled Structures*, 24, 285-313.

Reid, J. D. (1998). “Admissible modeling errors or modeling simplifications?” *Finite Elements in Analysis and Design*, 29, 49-63.

Reid, J. D. (2004). “LS-DYNA simulation influence on roadside hardware.” *Transportation Research Record*, 1890, 34-41.

Reid, J. D., and Marzougui, D. (2002). “Improved truck model for roadside safety simulations: Part I - structural modeling.” *Transportation Research Record*, 1797, 53-62.

Reid, J. D., Coon, B. A., Lewis, B. A., Sutherland, S. H., and Murray, Y. D. (2004). “Evaluation of LS-DYNA soil material model 147.” *FHWA-HRT-04-094*, U.S. Department of Transportation, Federal Highway Administration, McLean, VA.

Reid, J. D., and Hiser, N. R. (2004). “Friction modelling between solid elements.” *International Journal of Crashworthiness*, 9(1), 65-72.

Reid, J. D., and Hiser, N. R. (2005). “Detailed modeling of bolted joints with slippage.” *Finite Elements in Analysis and Design*, 41, 547-562.

Reid, J. D., Kuipers, B. D., Sicking, D. L., and Faller, R. K. (2009). “Impact performance of W-beam guardrail installed at various flare rates.” *International Journal of Impact Engineering*, 36, 476-485.

Ross Jr, H. E., and Sicking, D. L. (1984). “Guidelines for placement of longitudinal barriers on slopes.” *Transportation Research Record*, 970, 3-9.

Ross, H. E., Jr., Sicking, D. L., Zimmer, R. A., and Michie, J. D. (1993). “Recommended procedures for the safety performance evaluation of highway features.” *NCHRP Report 350*, Transportation Research Board, National Research Council, Washington, D.C.

Schrum, K.D., Lechtenberg, K.A., Bielenberg, R.W., Rosenbaugh, S.K., Faller, R.K., Reid, J.D., and Sicking, D.L., (2013). “Safety performance evaluation of the non-blocked midwest guardrail system (MGS).” Midwest Roadside Safety Facility. TRP-03-262-12.

Tiso, P., Plaxico, C., and Ray, M. (2002). “Improved truck model for roadside safety simulations: Part II - suspension modeling.” *Transportation Research Record*, 1797, 63-71.

Whitworth, H. A., Bendidi, R., Marzougui, D., and Reiss, R. (2004). “Finite element modeling of the crash performance of roadside barriers.” *International Journal of Crashworthiness*, 9(1), 35-43.

Zaouk, A. K., Bedewi, N. E., Kan, C.-D., and Marzouigui, D. (1997). “Development and evaluation of a C-1500 pickup truck model for roadside hardware impact simulation.” *FHWA-RD-96-212*, Federal Highway Administration, Washington, D.C.

Zaouk, A. K., Marzougui, D., and Bedewi, N. E. (2000a). “Development of a detailed vehicle finite element model, Part I: methodology.” *International Journal of Crashworthiness*, 5(1), 25-36.

Zaouk, A. K., Marzougui, D., and Kan, C.-D. (2000b). “Development of a detailed vehicle finite element model, Part II: material characterization and component testing.” *International Journal of Crashworthiness*, 5(1), 37-50.

Zweden, J. V., and Bryden, J. E. (1977). “In-service performance of highway barriers.” *Report NYSDOT-ERD-77-RR51*, New York State Department of Transportation, Albany, NY.